Dynamical Hierarchy in Biological Regulatory Networks: Applications in Modeling the Cell Cycle

Dávid Deritei

Supervisor: János Kertész
Co-supervisor: Réka Albert

A Dissertation Submitted in Partial Fulfillment of the Requirements
for the Degree of Doctor of Philosophy in Network Science

Central European University
Budapest, Hungary
2020

RESEARCHER DECLARATION

I, Dávid Deritei, certify that I am the author of the work Dynamical Hierarchy in Biological Regulatory Networks: Applications in Modeling the Cell Cycle. I certify that this is solely my own original work, other than where I have clearly indicated, in this declaration and in the thesis, the contributions of others. The thesis contains no materials accepted for any other degree in any other institution. The copyright of this work rests with its author. Quotation from it is permitted, provided that full acknowledgement is made. This work may not be reproduced without my prior written consent.

Statement of inclusion of joint work

I confirm that Chapters 4 and 5 are based on a paper that was written in collaboration with Erzsébet Ravasz Regan, William B. Aird and Mária Ercsey-Ravasz. Dr. Ravasz Regan conceived the idea and designed the cell cycle model based on her extensive knowledge of the biology literature. My contributions to the paper and the included results are the following: validating the simulations independently of Dr. Ravasz Regan, designing the quantitative measures of dynamical modularity (detailed in Chapter 5). I also contributed to writing the paper. The figures of Chapters 4 and 5 are adapted to this thesis, with the exception of Figure 5.1 that is reproduced from the paper. Figure 4.6 is reproduced form from our 2019 followup paper.

I confirm that Chapter 6 is based on a paper that was written in collaboration with Réka Albert, Jordan Rozum and Erzsébet Ravasz Regan. My contributions to the paper and the included results are the following: I discovered the capacity of the Phase Switch model to oscillate under certain conditions. Together with Dr. Albert we conceived the concept of conditionally stable motifs. I wrote and performed the majority of the simulations with support from Jordan Rozum and Dr. Albert. The analyses and visualisations presented in the chapter are the result of the close collaboration between Dr. Albert, Jordan Rozum and myself. The figures of Chapter 6 are reproduced from the paper. The example network of Figure 3.1 is also reproduced from the paper. The validation of the biological

implications and the biological literature review was done by Dr. Ravasz Regan. Writing the paper was a close collaboration of all four authors.

I confirm that Chapter 8 is based on a paper that was written in collaboration with Herbert Sizek, Andrew Hamel, Sarah Campbell, Erzsébet Ravasz Regan and myself, with acknowledged contribution and guidance from Réka Albert. My own contribution was comparing the results of synchronous and asynchronous update schemes and verifying which of the predictions hold under stochastic timing. Together with Dr. Ravasz Regan we conceived the biased asynchronous update specific to the model. I also implemented some of the simulations and developed the code that constitutes the accompanying notebook for the paper. The figures of Chapter 8 are reproduced from the paper (with slight modifications).

Signature of PhD Candidate:

April, 2020

Signature of Dr. Erzsébet Ravasz Regan, endorsing statement of joint work:

April, 2020

Signature of Dr. Réka Albert, endorsing statement of joint work:

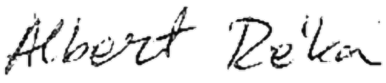

April, 2020

ABSTRACT

Life is an infinitely complex symphony of physical, chemical, biological processes composed by billions of years of evolution and maintained by its most elementary units: cells. Life is driven by a deep and also widespread hierarchy of self-organizing systems and mechanisms: from the most basic atomic interactions, through the biochemistry of folding proteins, the networks of protein-protein interactions, the different cell organelles, to the large organs in our bodies. Understanding all levels of this hierarchy, how the levels relate to each other, and how the behaviors at one level emerge from the interactions at a lower level is a major scientific challenge. Complex diseases such as cancer infiltrate multiple facets of this complex hierarchy and thus curing them requires its profound understanding. This thesis makes a case for a holistic, systems approach aimed at a better understanding of biology. Most other approaches have brought only limited results to a general understanding, despite technological advances with large amounts of resources dedicated to the life sciences and developing treatments. I argue that network models, specifically Boolean dynamic systems offer a fruitful abstraction of complicated biochemical mechanisms into logical circuits and make useful, non-trivial and experimentally validated predictions. Here we focus on the cell cycle: the process of growth and duplication of cells.

We present a Boolean model for the mammalian cell cycle as the interaction of two decision-making modules. We argue that the same way as complex biochemical entities such as genes can be abstracted into simple switch-like binary nodes of a logical network (in a useful way), there are functional network modules that also act as simple decision-makers at a higher level of the dynamic hierarchy. These decision-making modules (switches) are integrated into a network of coupled modules without losing their functionality (i.e. their stable states). As a step towards a general understanding of how the dynamic hierarchy in nature emerges, we formulate three principles for dynamical modularity and propose three corresponding measures that quantify the degree to which the conditions posed by the principles are true in any system. We demonstrate that they hold for the cell cycle model but not for its randomized counterparts.

We show that cell cycle progression is halted at its checkpoints by generalized positive feedback loops called stable motifs. Conversely, the checkpoint-free cell is an autonomous oscillator that robustly toggles through the cell cycle phases. We introduce the concept of a conditionally stable motif, a positive feedback loop that can maintain an associated state as long as one or more nodes external to the motif have a sustained state. The conditionally stable motifs in the cell cycle are organized into a sequence, such that they channel the dynamics by reducing degrees of freedom in the system, lending robustness to the oscillation. Conditionally stable motifs that destabilize themselves suggest a general negative feedback mechanism leading to robustly sustained oscillations. We reinforce this argument by showing that conditionally stable motifs are key to the robustness of the oscillation of the full cell cycle model.

Finally, we present a more recent, larger Boolean model that includes three additional dynamical modules dealing with programmed cell death (apoptosis), checking DNA origin (origin licensing) and growth stimulation (PI3K pathway). This model makes a number of valid biological predictions and we demonstrate that many of its dynamic behaviors are preserved despite stochastic variability in timing.

ACKNOWLEDGEMENTS

I would like to thank and acknowledge several people who whether directly or indirectly but contributed to this work.

First and foremost, I would like to express my gratitude to my advisor Réka Albert for her tireless, caring support and for teaching me the humble thoroughness that she has shown in everything we did during our collaboration. I thank János Kertész for his confidence in me and his continued support of this project. I thank my co-author and mentor, Erzsébet Ravasz Regan, for introducing me to the magical world of biological regulation and taking me on her projects that eventually formed the basis for this thesis.

I thank my other co-authors, without whom the research presented in this thesis wouldn't be a reality: Jordan Rozum, Mária Ercsey-Ravasz, William B. Aird, Herbert Sizek, Andrew Hamel, Sarah Campbell.

I would like to thank my closest colleagues and friends from CEU: Johannes Wachs, Orsolya Vásárhelyi, Tamer Khraisha, Luis Guillermo Natera Orozco, Júlia Perczel, Milan Janosov, Rebeka O. Szabó and the rest of the Department of Network and Data Science, including our coordinator Olga Peredi and the truly diverse and wonderful team of Ph.D. students and faculty. Special thanks to Éva Ajkay-Nagy from the Center for Academic Writing for her insightful comments.

I would also like to acknowledge the brilliant team of the Albert Lab at Penn State for their contributions to my research through the many discussions we had: Jordan Rozum, Jorge G. T. Zañudo, Xiao Gan, David Wooten, Parul Maheshwari, and Fatemeh Sadat Fatemi. My gratitude to the Pennsylvania State University for hosting me for a very productive year as a visiting scholar.

My appreciation goes to the colleagues and mentors who set me on this path of science: my first ever scientific collaborator, Fodor Norbert, my physics teacher from Apáczai Csere János High School, Vörös Alpár, who convinced me physics is a good idea and my two principal mentors from the Babes-Bolyai University, Faculty of Physics, Zsolt Lázár and Mária Ercsey-Ravasz.

I thank András Incze and Chris Shilling for their mentorship from the non-academic side of professional life and their support for my academic aspira-

tions.

There is a long list of friends and mentors whose presence in my life had had a profound effect on it and as such on this work. I cannot possibly do all of them justice but I list those whom I cannot skip: Balázs Szabó, Eszter Szabó-Reznek, Zsoly Vatány, Előd Székely, and Noémi Éltető. Special thanks to Nóra Makai and Csaba Kondor.

My eternal gratitude goes to my roots and family: to my mother Katalin Debreczeni-Kovács and my brother Kristóf. On the other branch, to Edit "Nénnyus" Deritei, György "Bákka" Deritei, Attila Deritei, Áron Deritei, Éva Horváth, and their respective families. I also thank my paternal grandmother Ilona Deritei, "Ilona Mama".

I dedicate my thesis to three people. To my maternal grandparents, Katalin and Ferenc Kovács; "Mama" and "Tata", to whom I am forever grateful for their endless care and loving sacrifices in raising me and supporting my education for so many years. Finally, to my stepfather, István Debreczeni-Kovács, "Pika", whom we unexpectedly lost, shortly after the submission of this thesis. We carry his memory and the fruits of his tireless work with us for the rest of our lives.

CONTENTS

CHAPTER 1

INTRODUCTION

1.1 Problems in life sciences and drug development – Eroom's law

The technological and scientific advancements of the 20th century have brought an unprecedented expansion of knowledge and innovation into human civilization. Yet in the last 70 years, developing effective treatments to the most prevalent diseases has become increasingly more difficult and expensive [1]. This trend is quantified by Eroom's law [2], which states that the number of new drugs approved by the United States Food and Drug Administration (FDA) for 1 billion dollars of research and development is halved every 9 years. This is a stark exponential decline that has been steady since the 1950s, and is still so, despite giant leaps in technological advancements in molecular biology and medicine. For instance, DNA sequencing has become a billion times faster and much more cost-effective since its discovery [3]. The engineering and synthetization of molecules with specific structure i.e. drug candidates has become orders of magnitude more efficient [4], which in principle allows researchers to interact with distinct targets in the cell. High Throughput Screening (HTS) technologies make it possible to automate many experiments and significantly decrease the cost of testing drug candidates against treatment targets [5]. All this leads to the accumulation of large amounts of biological data on the microscopic mechanisms within cells.

Curing complex diseases, such as cancer or Alzheimer's disease is the aim of both the multi-billion dollar pharmaceutical industry and of the largest portion of publicly funded research grants. In 1970 US President Richard Nixon declared the "War on Cancer", an ambitious commitment (he compared to the development of the atomic bomb and the Moon landing) that aimed for a gen-

eral cure by 1976 [6]. Today, almost fifty years after the National Cancer Act, although major milestones have been reached in the treatment of cancer, there is still no general cure in sight. In 2016 more than half of the total funds of the US National Academic Research & Development spending was distributed to life sciences [7]. It does seem like throwing more and more resources at the problem did not lead to any breakthrough, nor did it stop the decline of effective drug development in general. Moreover, the field has been observing a grave reproducibility crisis of published research [8, 9, 10].

Eroom's law is a clever wordplay on Moore's law with which it stands in stark contrast. Moore's law quantifies the advancement in computing power, specifically the number of transistors in microprocessors – that was doubling every 18 months up until the 2010s. Scannell and co-authors point out the principal difference between the two laws:

"Part of the contrast between Moore's Law and Eroom's Law is related to the complexity and limited current understanding of biological systems versus the relative simplicity and higher level of understanding of solid-state physics."[2]

I find this parallel both insightful and useful, mainly because it highlights a key difference: what made physics so successful we lack in biology. Namely, a more general, systems-level understanding of the complex interactions that give rise to the emergent behaviors we observe. Physics (especially statistical physics) has a more holistic approach to explain the macroscopic behavior of a system as emergent from its small scale (microscopic) interactions. Like predicting the temperature or pressure of a gas from the collisions of its atoms. Biology, on the other hand, is more reductionist and generally focuses on studying specific biochemical mechanisms and pathways of interaction. Naturally, the reductionist approach is very much justified by the incredible complexity of the molecular biochemistry of cells and *necessary* to understand the small scale interactions. Yet, as our knowledge grows and more and more experimental data is available, integrating it into more holistic models gradually becomes feasible. Thus we can turn many small pieces of knowledge into an understanding of the more fundamental systemic principles. With such understanding, we can create models that make more accurate, non-intuitive predictions. The models presented in this thesis in Chapters 4, 6 and 8 follow this systemic approach and have the potential to be useful tools in combating diseases by explaining their complex effects and by making predictions about their potential cures.

1.2 Capturing complexity – Networks

The 20th century brought extraordinary scientific leaps in unraveling the laws of nature and the fundamental building blocks of our universe. The branching

fields of physics from quantum mechanics through solid-state physics to astrophysics model the interactions between entities from as small as quarks to as large as clusters of galaxies. One thing shared by most of the models is that the interactions are almost always dependent on physical proximity. In most models the span of interactions can be one of two kinds: it is either assumed that everything interacts with everything else (e.g. mean-field models), or the interactions are only local, i.e. they range to other agents in close physical proximity (e.g. atoms in a grid).

Towards the second half of the century, as physics was slowing down in producing paradigm-shifting breakthroughs, some turned towards a third kind of interaction. In complex systems, especially if they are dynamic, the concept of interaction can be much more intricate. The idea of graphs (or networks) presents a paradigm that interaction patterns can be complex and not necessarily tied to physical dimensions. Every introduction to network theory starts with Euler's famous "bridges of Königsberg" problem that is accepted as the first documented case where a real-world problem has been abstracted into a set of vertices connected by a nontrivial pattern of edges. Social scientists have also been utilizing the concept rather early [11, 12], having recognized that interactions within society are rather heterogeneous. It is clear however that the network approach is not an obscure scientific intuition, as even pieces of literature have recognized some of its consequences [13].

The first mathematical model aimed at understanding the general principles of graphs was published by the iconic Paul Erdős and Alfréd Rényi [14]. Erdős and Rényi made the simple assumption that edges emerge randomly with a constant probability between pairs of vertices. Although their model has become a fundamental building-block of network theory, it made few empirically verifiable predictions. The breakthrough models that brought network theory into the forefront of attention at the end of the century were the small-world model of Watts and Strogatz [15] and the scale-free model of Barabási and Albert [16, 17]. These were the first models to make strong, testable empirical predictions on how networks organize.

The advances in network theory have profound effects on the global economy and modern life in general. A relatively simple network measure, the PageRank [18], developed by Larry Page and Sergey Brin has catapulted Google, a small garage startup at the time, into being one of the wealthiest and most powerful companies on Earth. Some of the other current tech giants like Facebook and Amazon have similar business models, all intertwined with exploiting the power of knowledge extracted from the networks that make up our society, economy [19] and even cognition [20]. However, once again, the theoretical advancements are less straightforward to apply to biological systems,

where the landscape of variables is more complex and unpredictable. Still, as data is becoming increasingly abundant it is much more difficult to synthesize it into predictive models. A cautionary tale reflecting this difficulty is the controversy of Theranos, the Silicon Valley company that promised to solve a host of medical problems by running diagnostics on very small quantities of blood. The Silicon Valley business model works in engineering and software development but does not necessarily work in medicine. Theranos, even after raising four hundred million dollars (reaching a net worth of nine billion) failed to deliver any workable product and its fraudulent way to hide this fact lead to its spectacular downfall [21]. In this thesis, I argue that to have meaningful models in life sciences one has to have a profound understanding of biology itself coupled with the systemic approach that is offered by the science of networks and complex systems.

1.3 Early network models in biology

The earliest network models that had biologically relevant predictions were the NK models of Stuart Kauffman [22], also known as Kauffman networks. In these models, N stands for the number of nodes and K for the in-degree of each node that is constant across all nodes. The innovation of the NK models was that they have a dynamical aspect, namely that each node has a time-dependent state. The configuration of all the node-states makes up the state of the system. A trajectory of the system is the sequence of states it visits from an initial state to some final state. Kauffman used simple binary variables for nodes states, and Boolean logic to determine how the states change in time. This was inspired by gene-regulation where genes regulate each other in a self-organizing way, such that a gene is either expressed in one point in time or not i.e., it is *on* or *off*. By a gene being expressed we mean that the molecule (usually a protein) coded by a gene is present in the cell in higher than the basal concentration. The changes in concentration usually occur suddenly in a step-like manner, due to strong feedback mechanisms, and thus the Boolean formalism of treating these variables as binary (on or off) is often justified. The state of a node in the next time-step is determined by the state of nodes regulating it (nodes with directed edges pointing towards a node) and the node's regulatory function. A node's regulatory function (also called rule or gate) encodes how a node reacts to the different states of its regulators. For example, if node X is regulated by nodes Y and Z, with the logical regulatory rule $f(X) = Y\ AND\ Z$, X will turn on in the next time-step if both Y and Z are on, otherwise, it will stay off. All the models presented in this work are generalized Kauffman networks, we refer to as Boolean models or Boolean dynamical systems. The exact formalism

of the models with detailed examples is presented later in Section 3.1. Kauffman studied randomly generated *NK* models and found that these networks have states of convergence, so-called attractors. Attractors are states of "attraction" which once are approached by the dynamical trajectory, the system can get stuck in them (for definitions and examples see Section 3.1.4). Kauffman correctly concluded that attractors could correspond to stable biological phenotypes (functions) in an empirical gene-regulatory network. He has also shown that the number of attractors grows proportionally with the square root of N – which is also a correct prediction of how the number of phenotypes relates to the number of genes. The Boolean approach has been adapted into a formal mathematical framework by René Thomas in 1973 [23]. These papers lay the foundation to the field that has become today's *systems biology*.

Aaron Novick, Jacques Monod, and colleagues introduced the earliest models of coupled ordinary differential equations (ODEs) to explain the regulatory mechanisms and continuous changes in the concentration of regulatory molecules. Their models explained simple feedback mechanisms that they observed in experiments done on bacterial cultures [24, 25]. Since then ODEs have become a standard tool in systems biology. ODE models offer a more nuanced, quantitative modeling framework, as compared to Boolean models. They can encode more complex kinetic interactions and dependencies as well. However, the large number of parameters makes ODE models more difficult to scale for larger systems. It is also very difficult to estimate many of the parameters, where there is no real data available.

Boolean models by definition do not have numerical parameters whose value has to be continuously tuned to fit experimental data. The main challenge is determining the regulatory links and the logical regulatory rules between the biological agents. Considering alternative assumptions, e.g. considering an "and" relationship instead of "or" between certain regulators, has similarities with tuning discrete parameters. On the other hand, once a model is established and is validated by reliable predictions, there are virtually no parameters that one has to explicitly tune to get new predictions.

1.4 The rise of Boolean models in systems biology

The Boolean modeling framework was developing slowly during, the late 20th century, but it started to attract more attention together with (or as a consequence of) the rise of general network theory at the turn of the millennium.

The major advantage of Boolean models is a *compromise in complexity*: they offer a comprehensive representation of the complex interactions of biological agents, through the network structure and the logical activation rules, but also

involve a drastic simplification of the continuous space of kinetic parameters, concentrations, chemical interactions, etc. As more and more abundant information about system-level interactions in the cell has become available, scientists were able to construct various empirical networks and adapt them into the Boolean modeling framework, which then produced various testable predictions.

There are several relevant and successful models explaining a large spectrum of biological phenomena, such as explaining and predicting the embryonic segmentation of the *Drosophila melanogaster* also known as the fruit-fly [26], the abscisic acid induced stomatal closure in plants [27], signal transduction in mammalian cells [28], T-cell large granular lymphocyte (T-LGL) leukemia [29, 30], the heterogeneity of endothelial cells (a cell type on the inside surface of blood vessels) [31], epithelial-to-mesenchymal transition (EMT) of cells (a process by which epithelial cells become migratory mesenchymal stem cells – an extremely harmful transition in the case of cancer) [32, 33]. The main predictive feature of these models is the fact that their attractors correspond to known and experimentally measurable biological states. The models are also capable of making predictions based on *in silico* experiments (computer simulations) from different initial conditions, involving random or observed mutations as well as external manipulations to the networks' states – simulating potential treatments to diseases. Some of the works mentioned above, together with the applications of various methods form control theory, predict combinatorial interventions (combinations of multiple targets) that can drive the biological system from unhealthy states to healthy ones. Many of the predictions were confirmed experimentally. It is also possible to iteratively improve existing models based on a feedback loop of experimental validation or biology literature and adjustments made to the models as discussed in [34].

I am going to discuss the Boolean models of the cell division cycle – the focus of this work – in Section 2.2 and our own models in Chapters 4, 6 and 8.

1.5 Modularity - Macroscopic and functional organization of networks

To better understand the principles that govern biological systems we turn to the main organizational principles of networks. One of the most fundamental principles of collective behavior observed in networks is that the nodes that share some common set of features tend to self-organize into groups or communities. This most often manifests in the topology of the network as the nodes are more densely connected within their respective groups than with the rest of

the network. This has been observed early in studies of social networks [35, 36] – which is also supported by intuition – we organize our daily lives in often overlapping, but distinct communities, from groups as small as families to as large as nations. What is less intuitive is that most networks have similar mesoscopic structures as the ones we observe in our social environment. For instance, biological networks have been shown to have modular organization just as societies [37]. Ravasz et al. have shown on a multitude of biological networks that the modular structure also has an *internal hierarchy* of groups nested within groups [38]. These discoveries sprang an entire new sub-field of network science into motion for finding more efficient ways of mapping the community structure of networks [39]. The idea that molecules in cells organize into functional modules has been proposed by Hartwell el al. [40] – already suggesting a new paradigm in biology that we have to shift focus from single molecules to functional groups or modules. This insight is reinforced by our results discussed throughout this thesis.

Milo et al. proposed that certain elementary connective patterns called *network motifs* are statistically over-represented in biological networks and they can have specific functional roles [41]. An explanation for *how* functional units emerge in biological networks has been proposed by Kashtan et al. [42]. The authors developed a genetic algorithm where they mutated the network structure, mimicking the natural progress of evolution, in which both Boolean regulatory and neural networks had to adapt to a "task" representing a challenge by the environment. They discovered that regularly switching between two different environments not only causes the adaptation to happen in much fewer generations, but specialized modules emerge in the networks for dealing with the alternating environments. This is strong evidence that evolution tends to "delegate" different adaptive behaviors by creating functional modules.

In this thesis, I present our work where we build on these ideas but propose that modularity is not necessarily just structural in nature. We propose a kind of modularity that is dynamical and thus it is not detectable from network topology by any conventional means. Dynamical modularity is a property of systems where the diverse functionalities of the network are expressed in the dynamical evolution of their states. I discuss dynamical modularity in detail in Chapters 4 and 5.

1.6 Thesis outline

The two main statements of this thesis are the following: first, systems-level approaches, more specifically Boolean dynamic systems, are capable of predicting the emergent behaviors of the cell cycle from a network of molecular interac-

tions derived from the literature. Second, we can identify general principles of dynamical self-organization, which are true on all scales of the dynamical hierarchy that governs living organisms. We do this by bringing together multiple strands of knowledge from biology and applying methods from dynamic systems theory and network science.

In Chapter 2 I introduce the basic biological background of the cell cycle. Most importantly the key genes and molecules, the phases of the cell cycle and the checkpoints separating the phases. I also discuss the relevant milestones in understanding and modeling it.

Chapter 3 introduces the essential methodological tools and concepts that we use throughout the study. We define Boolean models, their dynamical properties, what are attractors, and what the different update schemes mean. I also introduce some of the tools, such as the logic expanded network and its different motifs (stable, conditionally stable, oscillating), which help us handle and interpret the often large dynamical landscape of Boolean models.

In Chapter 4 I present our Boolean model for the mammalian cell cycle as the interaction of two decision-making modules: the Restriction Switch and the Phase Switch. The two switches have biologically relevant steady states corresponding to before/after restriction point passage and the three major cell cycle checkpoints respectively. The coupled model gives rise to a cyclic attractor with states corresponding to events of the biological cell cycle. The cyclic attractor matches the biological sequence by toggling through the steady state combinations of its modules. We call this behavior – the modular dynamics preserved in the global dynamics in a meaningful way – dynamical modularity. The decision-making modules (switches) are integrated into a network of modules without losing their functionality (i.e., their stable states).

In Chapter 5 we formulate the three principles for dynamical modularity and propose three corresponding measures that quantify the degree to which the conditions posed by the principles hold in any modular Boolean model. We show that the principles hold for the cell cycle model but not for its randomized counterparts.

In Chapter 6 I present our work on the Phase Switch module of the cell cycle and its intrinsic oscillator. We show that the stable states of the Phase Switch are contingent on the state of four nodes through which it receives input from the rest of the network. Biologically, these conditions correspond to cell cycle checkpoints. Holding these nodes locked (akin to a checkpoint-free cell) transforms the Phase Switch into an autonomous oscillator that robustly toggles through the cell cycle phases. We introduce the concept of a conditionally stable motif, a generalized positive feedback loop that can maintain an associated state as long as one or more nodes external to the motif have a sustained state. The

conditionally stable motifs of the Phase Switch Oscillator are organized into an ordered sequence, such that they serially stabilize each other but also cause their destabilization. Along the way, they channel the dynamics of the module onto a narrow path in state space, lending robustness to the oscillation. Self-destabilizing conditionally stable motifs suggest a general negative feedback mechanism leading to sustained oscillations. We perform a coarse-graining of the Phase Switch Oscillator based on the interaction of the conditionally stable motifs and reduce the 8 node model into a higher level 3 node model that still maintains the relevant features of the original model.

Returning to the cell cycle model in Chapter 7 we analyze the robustness of the model-simulated cell cycle under timing variability. A comparison with the biological cell cycle allows us to identify the model's strengths and shortcomings. We identify the conditionally stable motif structure of the Restriction Switch module and further analyze the interplay between the Phase Switch, the Phase Switch Oscillator, and the Restriction Switch in the full cell cycle model.

In Chapter 8 I present the latest Boolean model of the cell cycle from our collaboration. This model includes three additional dynamical modules dealing with apoptosis, origin licensing, and growth factor stimulation. This model makes useful biological predictions and we demonstrate that many of its emergent dynamic behaviors are preserved despite stochastic variability in timing.

Finally in Chapter 9 I summarize our results, propose directions in going forward with future research, and conclude the thesis.

CHAPTER 2

MODELING THE CELL CYCLE

2.1 Basic concepts and biological background

The main purpose of the cell cycle is to replicate the DNA and produce two identical daughter cells. This process happens in every living organism that we know and thus it is one of the most fundamental building blocks of life. Billions of years of evolution accumulated a multitude of checks and balances to make sure this process is robust internally yet it is adaptive in a multitude of different environments. Balancing robustness and adaptive behavior is a difficult task that is accomplished by a vastly complex procedure. In the progression of the cell cycle, we can identify distinct phases that are separated by checkpoints. Every checkpoint makes sure that everything is going according to the intricate "plan" of dividing the cell, which gradually evolved to its current level of complexity through the eons. The checkpoints evaluate both external signals (e.g. is there enough nutrition for further growth) and internal checks (e.g. was the DNA replicated accurately) to either halt the division process or let it proceed. All of this is executed and coordinated by an interaction network of various proteins and molecules driving the cycle, managing checkpoints, transmitting signals, etc. Unfolding this network and understanding the nature of interactions as well as the dynamic processes lying beneath is a difficult task. For example, studying the biochemistry of how various proteins can fold in three dimensions and change their function based on what shapes they take is an entire field of its own. Our goal is to keep a more systemic view in mind to understand this complex process.

2.1.1 The phases of the cell cycle

The cell cycle process, besides the optional quiescent phase, can be divided into four main phases, which are separated by three main checkpoints; illustrated in Figure 2.1.

- G_0 – Quiescent phase, where the cell executes its basic functions, but there is no active growth, nor progression along the cell cycle. For example, neurons are in the G_0 phase during most of their lifetime.

- G_1 – The first growth phase when the cell is gathering the necessary nutrients to divide and evaluates if the environment is favorable for proliferation. If so the cell generates so-called *growth factors* that stimulate the procedure. The first growth phase is guarded by the first checkpoint the **restriction point** that makes sure it is safe to start the replication of the DNA. Passing the restriction point also represents an irreversible commitment to the division cycle.

- S – The *synthesis* phase when the DNA is replicated

- G_2 – A second growth phase following the replication. During this phase, the cell evaluates the quality of the replicated DNA and repairs all damage if it is possible. If the damage is irreparable the cell commits to *apoptosis* or programmed cell death. Until the DNA is fully checked the cell cycle is halted. This is called the **DNA damage checkpoint**.

- M – Mitotic phase. This is the most complex and eventful phase that in itself can be divided into several sub-phases. First is the *Prophase*, where the *mitotic spindle* starts to form, the nuclear envelope breaks down and the chromosomes start to condense. The mitotic spindle is a sort of ”scaffolding” attached to the pairs of replicated chromosomes still sticking to each other (sister chromatids). Next is *Metaphase*, where the sister chromatids line up in the middle of the cell, getting ready to be pulled apart by the spindle. Here, the cell has to make sure that the spindle is perfectly attached to the sister chromatids and the pulling will not damage either of them. This is called the **spindle assembly checkpoint** (SAC). In the third sub-phase, the Anaphase, the sister chromatids are pulled apart by the spindle towards opposite poles of the cell. In the following *Telophase* the spindle disintegrates, the chromosomes start to de-condense and the new nucleoli start to form around them. The final phase is the *Cytokinesis* (which can partially overlap with preceding phases), when the cytoplasm is split into two and two identical daughter cells form, both re-entering G_1 or entering G_0.

In Chapters 4 and 7 we discuss a case that is predicted by our cell cycle model, in which the two forming daughter cells in the presence of constant growth factors pre-commit to the next cycle and pass the restriction point of the next division before cytokinesis.

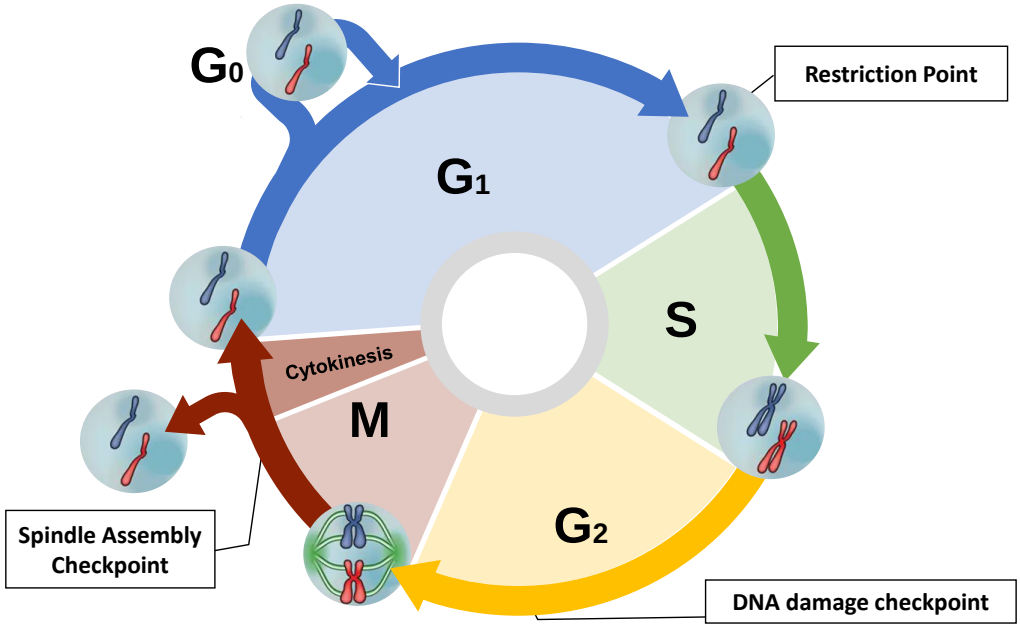

Figure 2.1. *Illustration of the cell cycle phases. The sections of different colors represent the distinct phases of the cell cycle, with their corresponding labels. The arrows indicate the direction of the process. The M (mitosis) phase can be divided into five subsegments: Prophase, Metaphase, Anaphase, Telophase (not shown on the figure) and finally Cytokinesis, where the two cells split, indicated by the bifurcating brown arrow. After Cytokinesis the cell cycle restarts in both daughter cells, with optionally entering the quiescent phase (G_0), indicated by the blue parallel path. Image credit for chromosome drawings: [43]*

2.1.2 The cell cycle control system

The cell cycle control system is a network of regulators that makes sure that the events necessary for the progression of the cycle are started in the correct sequence and everything is completed before the next process starts. This same control system has to make sure that the cycle halts (arrests) if the conditions of certain checkpoints are not fulfilled.

In this work we mostly focus on the cell cycle of mammalian cells, however, the control system is virtually the same in almost all eukaryotic cells. Many of

these mechanisms are so ancient that certain core molecules when transferred from a yeast cell to a human cell still work properly [44].

The key molecules driving the cell cycle are a family of proteins that activate and deactivate in different phases of the cell cycle called **Cyclin**s and the **Cyclin dependent protein kinases** or **Cdk**s. The discovery and understanding of these molecules and other key regulators was pioneered by Leland Hartwell, Paul Nurse and Timothy Hunt, who were jointly awarded the Nobel Prize in Physiology and Medicine in 2001 for this work [45]. The main mechanism of regulation of proteins is the **phosphorylation** and **de-phosphorylation**, which is the attachment of a phosphate group to a molecule. For instance, a Cdk to be active it needs to be phosphorylated at one site and dephosphorylated at two other sites. The activity of Cyclins and Cdks changes abruptly, due to various feedback mechanisms that accelerate their regulation. This is one of the reasons why the Boolean approximation is justified in modeling the cell cycle.

There are different kinds of Cyclins and Cdks responsible for triggering different phases of the cell cycle. The proteins that are "guarding" the checkpoints between phases can inhibit the Cdks at the specific checkpoints. Also, if certain actions are not completed in time, the control system delays the next step until the previous step is completed.

This fact is a good justification for the *synchronous update* process of nodes (defined in 3.1.2) when simulating our Boolean cell cycle models that incorporate many of the above molecules and mechanisms introduced in Chapters 4 and 8. The randomly updating *general asynchronous* update scheme has no regard for the synchronicity of events, and it can help us understand, how the cell makes sure that even in the presence of stochastic timing, the sequence of events is robust – or which parts are vulnerable for such noise. We derive an analysis and propose explanations for the robustness of the cell cycle process in Chapter 6.

2.2 Regulatory models of the cell cycle

One of the earliest network models had already recognized the essential role of negative and positive feedback loops in cell cycle regulation. Novák and Tyson introduced a mathematical model for the M-phase control by studying the M-phase promoting factor (MPF) based on data from *Xenopus* oocyte embryos [46]. They proposed that the MPF complex consisting of Cyclin B and the Cdc2 molecule is part of a positive feedback loop with Cdc25 and Wee1 that promotes the production of MPF, and a negative feedback loop, involving a ubiquitin-conjugating enzyme (UbE) and an enzyme dubbed intermediary enzyme (IE), which start the delayed degradation of the MPF. They predicted that

the positive feedback loop creates a *bistable switch* as well as the fact the hysteresis in the concentration of molecules is an important mechanism in regulating the cell cycle. However, many of the specific molecules involved were still not known. Most predictions of the model were later confirmed experimentally [47]. Our models make similar predictions involving a more comprehensive set of regulators, discussed in Chapters 4 and 6.

Li et al. proposed a cell cycle model for the budding yeast, where they have shown that the emerging dynamic pathway matching the cell cycle is extremely robust against perturbations [48]. The model involved a more comprehensive set of cyclins (Cln1,2,3; Clb1,2,5,6), inhibitor complexes (Cdc20; Cdc14; Cdh1; Sic1) and transcription factors (SBF; MBF; Mcm1; SFF) found in yeast. The cell cycle checkpoints were represented by *abstract nodes* (not actual biological agents) interacting with the molecules. Our model discussed in Chapter 4 also utilizes abstract nodes to simplify cellular processes that are not part of the model in mechanistic detail, but contrary to Li et al.'s model in our case some of the checkpoints are already represented by actual molecular interactions. In Li et al.'s model, the attractor representing the cell cycle is not a closed limit cycle but a linear pathway that nonetheless accurately corresponded to biological trajectory executed by yeast cells during their division.

In the same year, Chen et al. published a kinetic network model for the budding yeast, based on the biological *consensus model* of the cell cycle control mechanisms. The model included all agents used by Li et al. in [48] with the addition of several other key molecules such as Mad2, APC, Net1, PPX, Tem1, etc. The model was able to accurately predict most (more than 100) experimental results in mutant cells, but it also produced some inconsistencies with experiments that were useful in identifying what parts of the biological consensus model had to be revised [49].

Based on the skeleton provided by the yeast control network Novák et al. proposed a model for the restriction point in *mammalian cells* working with the assumption that most of the core control system is inherited from much simpler eucaryotic ancestors. The model was supplemented with the mammalian equivalent of regulatory agents found in yeast such as the core cyclins (Cyclin E; Cyclin A; Cyclin D), cyclin-dependent kinases (Cdk1; Cdk2), Cdk inhibitor (Kip1) and transcription factors (Rb; E2F). Table 2.1 is instructive of the corresponding molecules from yeast and mammals together with their roles, reproduced from the paper. The model also made predictions matching experimental results [50].

A problem of the kinetic equation models, such as the one proposed by Novák et al. is that the methods and results are extremely reliant on fine-tuning specific parameter sets that become more and more difficult to establish as the

Budding yeast	Mammalian Cell	Role
Cdc28	Cdk1	Cyclin-dependent kinase
Cln3/Cdc28	CyclinD/Cdk4	Growth-factor sensor
Cln2/Cdc28	CyclinE/Cdk2	Starter kinase
Clb5/Cdc28	CylcinA/Cdk2	Initiate DNA synthesis
Sic1	Kip1	Cdk inhibitor in G1
SBF,MBF	Rb, E2F	Regulate transciption at G1/S
Clb2/Cdc28	CyclinB/Cdk1	Mitosis promoting factor
Cdh1	Cdh1	Degradation of B-type cyclins
Cdc20	p55cdc	Proteollysis at anaphase

Table 2.1. *Corresponding core cell cycle molecules and their roles in yeast and mammalian cells, reproduced from [50]*

models grow.

Fauré et al. built on the model of Novák and Tyson, but adapted the compromise of the more qualitative Boolean approach [51]. Fauré's paper is imperative from the perspective of our work as the model presented in Chapter 4 builds on the Fauré model. Virtually all regulatory nodes proposed by Fauré et al. (CyclinE; CyclinD; E2F; Rb; p27(Kip1); CyclinA; CyclinB; Cdh1; Cdc20; UbcH10) are also present in our larger model. They also investigated the different ways of updating the node-states to establish temporal dependencies of the cell cycle. Neither of the two extremes - synchronous or asynchronous update (see Section 3.1.2) produced a convincing emergent behavior, so the authors also introduced a mixed update that improved the qualitative match between the emerging attractors and the biological reality. Throughout this thesis comparing the predictions of models under different update schemes is a major topic, as the timing of events is a key factor in biological systems.

Novák et al. also proposed that the irreversibility of cell cycle transitions is also a regulatory network phenomenon, which can be attributed to systems-level feedback [52]. Our results discussed in Chapter 6 confirm this hypothesis within the framework of generalized positive feedback loops we call *stable motifs*.

Gérard and Golbeter proposed a very detailed 39 node model where they have shown the importance of the Cdk oscillations in driving the cell cycle, as well as ways the cell can leave the quiescent (G0) phase and initiate the cell cycle. They also introduce a reduced version of the network, consisting of only 5 nodes that still maintains the key features of the larger detailed model [53]. This way of reducing complexity by coarse gaining a more detailed model into a smaller one is a key feature of our results discussed in Chapter 6.

CHAPTER 3

KEY METHODOLOGICAL CONCEPTS

Boolean regulatory models or Boolean dynamical systems introduced in Section 1.4 offer a compromise in complexity. By reducing the intricate biochemical interaction and concentration levels into simple logical interactions between binary variables we make much more tractable but qualitatively still valuable analysis of biological systems possible. In this chapter, I am going to introduce the mathematical framework with the basic concepts and terminology essential to understand our methods and interpret our results. Then we introduce some of the tools to better understand and simplify the dynamical landscape of Boolean regulatory networks, through the so called *logic expanded network* and the special strongly connected components or motifs in it.

3.1 Boolean Regulatory Models

Boolean regulatory networks can be represented by a graph $G = (V, E)$ consisting of $V = (v_1, v_2, ..., v_n)$ vertices (nodes) and E edges. The edges are directed, representing a one-way, signed interaction between the vertices of the network. The sign of an edge represents the activation or inhibition of the target node. Each node has a binary state, σ_v equal to 1 or 0, often referred to as *on* or *off*. The state of the model is the collective state configuration of all of its nodes. Overall, the model can have 2^N different states, where N is the number of vertices. The state of each node v is determined by the state if its incoming neighbors (parents, regulators) through a logical function assigned to each node, $F = (f_1, f_2, ..., f_n)$. We also call these functions Boolean regulatory functions or Boolean rules. The logical function encodes how every node responds to the different states of its regulators. The value of a node σ_{v_i} in time-step $t + 1$

is calculated as:

$$\sigma_{v_i}(t+1) = f_i(\sigma_{Par(v_i)}(t)) \tag{3.1}$$

where $Par(v_i)$ is the set of *parents* or in-neighbors of node v_i and $\sigma_{Par(v_i)}(t)$ is their state configuration at time t. If a node has k incoming neighbors, this means 2^k different possible inputs with 2^{2^k} possible output functions. This allows an incredibly large variety of possible dynamics that a Boolean network can manifest.

In Figure 3.1 I present a toy Boolean regulatory model that I am going to use consistently in this chapter as an example to illustrate the discussed concepts.

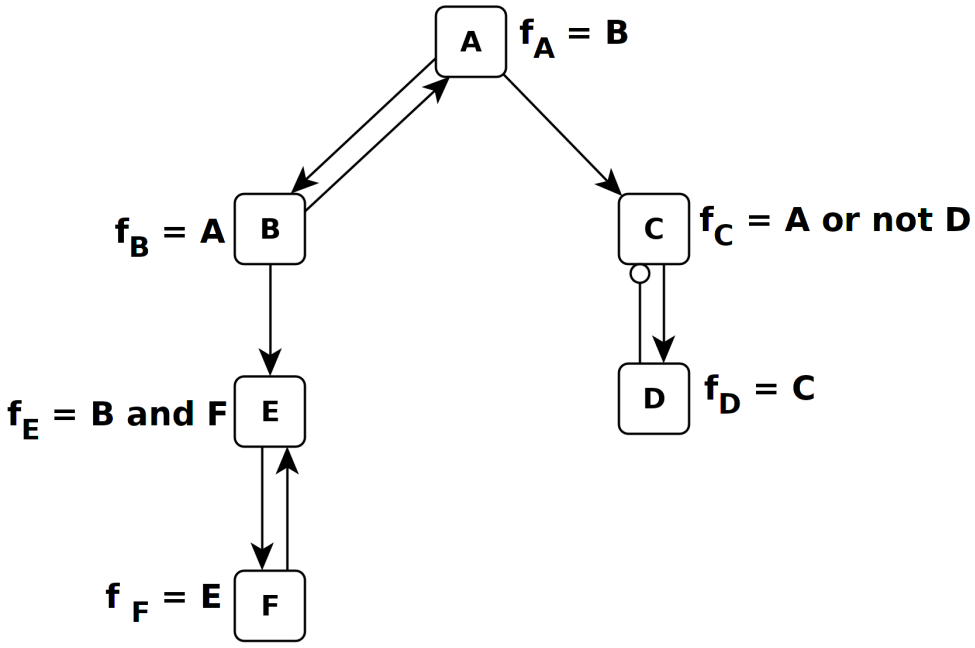

Figure 3.1. *A toy Boolean regulatory model. The Boolean regulatory functions (rules) that determine the state of each node are shown next to the nodes. Edges ending in arrows represent positive regulation, while the edge terminating in a white circle represents negative regulation (inhibition)*

3.1.1 Truth Tables and Boolean Rules

Regulatory functions have two common ways of representation – truth tables and Boolean rules. The two representations are fully *equivalent* but useful in different ways. The set of truth tables (or Boolean rules) are sufficient in fully

determining the Boolean model, as they encode both the dynamical and the relational interactions.

Truth Tables

Truth tables, as their name suggests, are tables that tell for each variable in which configuration of their inputs they return 1 (or 0). A main advantage of the truth table representation is that as logical interactions can get very complicated it allows the encoding of more complex interactions, which are difficult to express as logical rules straightforwardly (e.g. activation patterns based on gene expression data). With truth tables, we explicitly encode what input state configuration activates every node. It is also more machine-readable (many simulation algorithms turn rule inputs into truth tables first). The equivalent truth tables for all the variables based on the logical rules in Figure 3.1 are shown below:

B	A^*
0	0
1	1

A	B^*
0	0
1	1

A	D	C^*
0	0	1
0	1	0
1	0	1
1	1	1

C	D^*
0	0
1	1

E	F	E^*
0	0	0
0	1	0
1	0	0
1	1	1

E	F^*
0	0
1	1

Each variable in the model has a truth table, where the columns (except the rightmost) are the inputs, the rows represent the possible input combinations. The rightmost column of each table represents the output variable signed with an $*$ representing the state of the node in the next time step (if updated) given the different inputs.

Boolean Rules

The Boolean rules are a compact way of defining a Boolean model, they are more "human readable" and in that sense are also more intuitive. A set of Boolean rules is basically a system of logical equations. This way of representation is often useful to interpret and evaluate the actual mechanistic interactions between biological agents. The regulatory network shown in Figure 3.1 has the following Boolean rules (also shown on the figure):

$$\begin{aligned} A^* &= B \\ B^* &= A \\ C^* &= A \vee \neg D \\ D^* &= C \\ E^* &= E \wedge F \\ F^* &= E, \end{aligned} \tag{3.2}$$

where the $*$ represents the next temporal value of the given variable, $\vee$ is the logical **or**, $\wedge$ is the logical **and** and $\neg$ is the logical **not**.

3.1.2 Update Schemes

An update scheme refers to the order in which the state of the nodes in a Boolean model is updated. This is important if we are interested in not just the long-term steady state behavior of the system but the trajectories and pathways of convergence from different initial conditions. Any update scheme makes strong assumptions about the timing of events in a biological system. These assumptions always have to be taken into account when interpreting the emergent behavior of a model. It is common practice to analyze a model using multiple different update schemes simultaneously to see what features are dependent or independent of timing. In our research, we are mostly utilizing two update schemes representing to extremes of the temporal spectrum: synchronous and general asynchronous updates.

Synchronous Update

The synchronous update scheme assumes that all events encoded by the logical rules happen in synchrony, meaning that every node is updated at the same time. Because of this, the next state of the dynamical system is fully determined by its previous state. Using the notation of equation (3.1) the synchronous update is defined as:

$$\sigma_{\mathbf{v}}(t+1) = f(\sigma_{Par(\mathbf{v})}(t)),$$

where $\mathbf{v}$ represents the vector of all N nodes and $\sigma_{\mathbf{v}}$ represents the corresponding vector of all node states. Since every state of the system is *exactly* determined by the previous state the trajectories from all initial conditions are *deterministic* when using synchronous update. This means that every state has one and only one next state it can transition into.
This update scheme is very restrictive, but it can be very useful for simulating biological systems where exact timing and sequence of events is critical as it enforces that events happen in a deterministic order. One such system is the cell cycle, the empirical focus of this work.

General Asynchronous Update

General asynchronous update assumes that events encoded by the logical rules are temporally independent. The nodes are updated asynchronously (one at a

time), and they are picked randomly *with* repetition. This is the largest degree of sequential stochasticity we can apply to a Boolean model. Because of this, the trajectory of a model can be also very stochastic. In Chapter 6 I am going to discuss the network mechanisms that make a system's trajectory robust even with general asynchronous update.

Random Order Asynchronous Update

In the case of random order asynchronous update, a time step constitutes from updating all nodes asynchronously, but only once, in a randomly generated order. The random order is regenerated in every time-step. This type of asynchronous update introduces a smaller degree of timing variability to a system than general asynchronous update, but it is still not deterministic like the synchronous update. We only use random order asynchronous update in some cases with the model introduced in Chapter 8.

3.1.3 State Transition Graph

The state of a Boolean model is discrete – a configuration of N ones and zeros, where N is the number of nodes. The dynamical changes in a Boolean model are transitions between these discrete states. Because of the discrete nature of the dynamics, it is convenient to represent the states and transitions in a graph format, where nodes are states of the model and edges are transitions between the states. Such a representation is called a *state transition graph* (STG).

An STG can have 2^N nodes. The number of edges is determined by the update scheme. For synchronous update, since the emergent dynamics is deterministic every node has a single outgoing edge (self-loops included), thus the number of edges is equal to the number of states (STG nodes). With general asynchronous update a state can have transitions into up to N other states, in the case where every node's update leads to some different state. This means that STGs have an upper bound of having $N \times 2^N$ edges. In Figures 3.2 and 3.3 two STGs of the regulatory model introduced in Figure 3.1 are presented generated with synchronous and general asynchronous update respectively. Both STGs have the same set of nodes, the 2^6 possible configurations of the toy network, but the edge wiring is radically different, due to the nature of the two update schemes.

A fully mapped out STG gives full information on the dynamical landscape of a Boolean model; however, as the size of the STG grows exponentially with the size of the regulatory network, this quickly becomes intractable in larger models. Yet, as the figures also suggest, most models have only a few states of convergence, and any system quickly merges into pathways that lead into

the "sinks" of such graphs. What we are usually looking for when studying a model are these states of convergence that we call attractors.

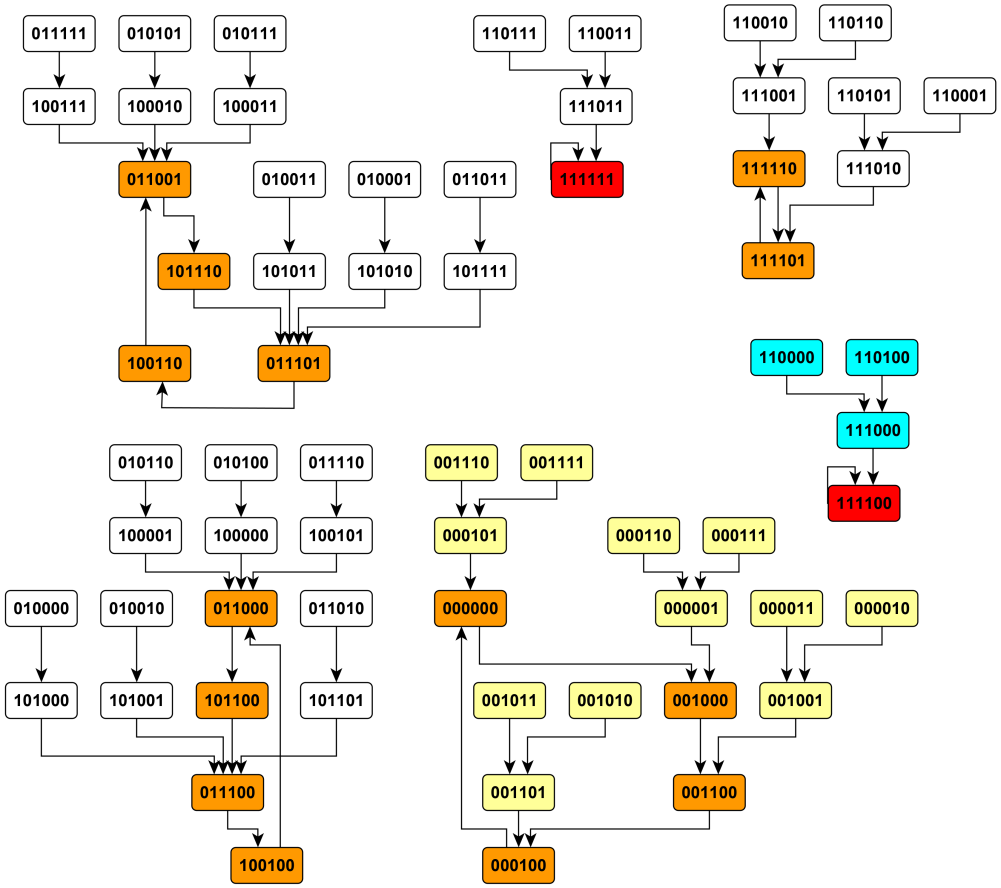

Figure 3.2. *The STG of the regulatory model from Figure 3.1 when using synchronous update. The nodes represent states, where the labels correspond to the node configuration following the alphabetical order of the regulatory node labels (ABCDEF). Every node has a deterministic transition from it represented as a single out-going edge. The red and orange nodes represent the attractors. The red nodes are single steady state attractors, while the orange nodes are representing cyclic attractors (or limit cycles) consisting of multiple states. Light blue nodes represent the basin of attraction of the attractor state (111100), while the yellow states represent the basin of attraction of the cyclic attractor looping through the states* $(000000) \rightarrow (001000) \rightarrow (001100) \rightarrow (000100)$.

3.1.4 Attractors

Generally, attractors are states or a set of states toward which a system tends to evolve, for a wide variety of initial conditions of the system. As the name sug-

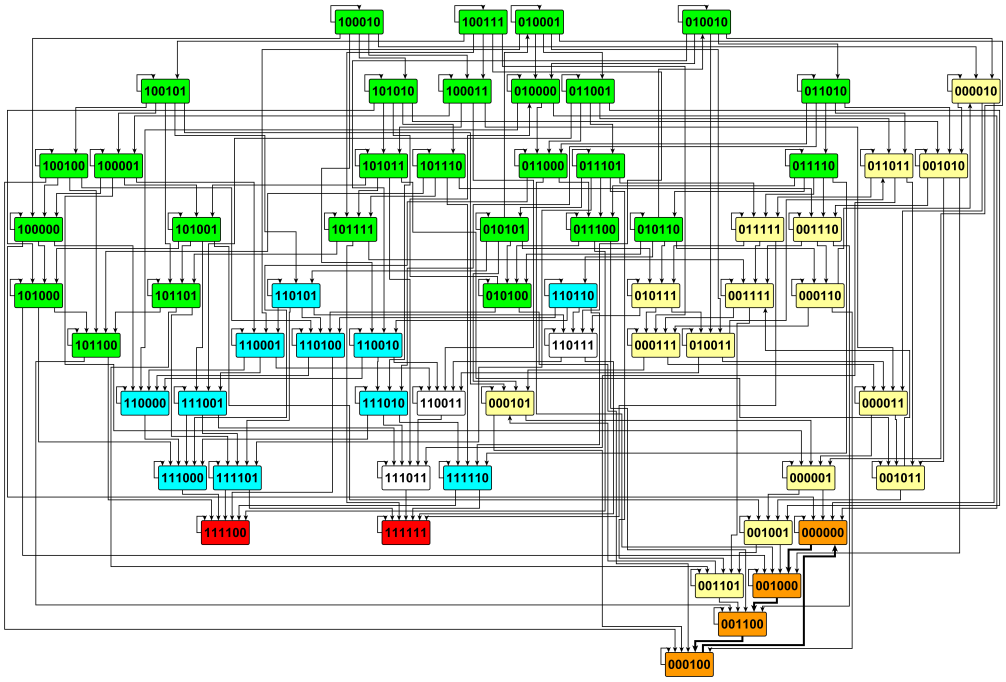

Figure 3.3. *The STG of the regulatory model from Figure 3.1 when using general asynchronous update. The nodes represent states, where the labels correspond to the node configuration following the alphabetical order of the regulatory node labels (ABCDEF). Most nodes have multiple transitions from them which are picked randomly during simulations. The red and orange nodes represent the attractors. The red nodes are single steady state attractors, while the orange nodes represent the complex attractors of the system. Light blue and green nodes represent the basin of attraction of the attractor state (111100), while the yellow and green states represent the basin of attraction of the complex attractor looping through the states* $(000000) \rightarrow (001000) \rightarrow (001100) \rightarrow (000100)$. *The green states represent the overlap of the two basins.*

gests, attractors "attract" the dynamic trajectory of the system towards themselves. Attractors of Boolean models with deterministic regulatory rules are defined as states or sets of states that a dynamical model converges into and keeps visiting indefinitely. Attractors represent the long term behavior of a system – and as such are the most relevant features of a model. As explained in Section 1.4 in the case of accurate empirical Boolean models attractors correspond to stable biological states (phenotypes). A dynamical model can have multiple different attractors. The red and orange nodes in Figures 3.2 and 3.3 represent the attractors on the state transition graph. Initial conditions, noise, external perturbation, or combinations of these determine in which of its attractors a system converges into. The states that inevitably converge into an attractor but

do not make part of the attractor are called the *basin* of the attractor. Once the system is in the basin of an attractor it cannot leave it, except due to external perturbation. When using synchronous update the basin of each attractor is unique - due to the deterministic dynamics. These appear as disjoint connected components of the STG as shown in Figure 3.2. On the same figure two basins are colored - one light blue and one yellow. The asynchronous update makes the basins fuzzy, thus stochasticity becomes an important factor in which will be the final attractor. In Figure 3.3 we colored the corresponding basins of the same two attractors as on the synchronous STG shown in Figure 3.2 blue and yellow. The green states in Figure 3.3 represent the overlap of the two basins. From any of the green states, update noise can lead the system in either of the two attractors. The fact that a significant portion of the basins is overlapping highlights how much stochasticity affects the long term behavior in the case of general asynchronous update.

There are different kinds of attractors depending on the update scheme and the type of noise one introduces to the system. Here I introduce three major types of attractors: fixed-point attractors (steady states), cyclic attractors (limit cycles) and complex attractors (a.k.a. loose attractors).

Steady states

A steady state or a fixed point attractor is a single state that once a system converges into, it permanently maintains. In Figures 3.2 and 3.3 the nodes highlighted in red are steady states - they have no out-edges (except a self loop). Steady states are *invariant to different update schemes* – as the two figures also suggest. Mathematically the steady states are the solutions of the system of logical equations that one can turn a Boolean model into.

In biological models, the steady states usually represent the gene expression of differentiated cells or states that are sustained for longer periods (e. g. the G_0 quiescent state or locked checkpoints in the cell cycle).

Limit cycles

A limit cycle is an attractor consisting of a *deterministically* repeating sequence of states. The deterministic nature of such cycles is only guaranteed when using the synchronous update scheme. Such cyclic behavior is due to some sort of negative feedback in the regulatory model. In Figure 3.2 four different emergent limit cycles are shown, consisting of states highlighted by orange. Each connected subgraph made up of orange states is a different limit cycle. A very important empirical limit cycle is the emergent cell cycle of our model discussed in Chapter 4.

Complex attractors

Complex attractors are akin to limit cycles in the sense that they are made up of multiple states that are indefinitely visited by the system, however, the key exception is that the paths (or sequence of states) are not necessarily deterministic. Complex attractors can emerge when using general asynchronous update. In network terms, complex attractors are strongly connected components of the general asynchronous STG with no edges point out from the component. The orange states in Figure 3.3 represent a complex attractor. We will discuss in detail some empirical complex attractors in Chapters 6, 7 and 8.

3.1.5 Sampling complex attractors

When the full mapping of a model's state transition graph becomes intractable due to its size we often need to use different methods to sample it. This is especially important in the case of larger complex attractors, whose states can all bear biological significance. Here I present a method for sampling complex attractors we used during our research.

The trajectories generated by general asynchronous update can be interpreted as a random walk on the state transition graph. During a random walk on a directed network, a walker on node i at time step t randomly chooses one of the edges going out of i and traverses that edge in one time-step. Using general asynchronous update every node has the same probability of being updated, thus every outgoing edge (i.e. every state transition that yields a different state than the starting state) has the same probability. An extended simulation of the model trajectory starting from any node in the basin of attraction of the complex attractor (i.e. the states that are starting points of trajectories that reach the complex attractor) gives us a reliable sample of the most probable states and transitions. For example, performing a random walk of n steps can give us convergent visitation probabilities of states and transitions. We can validate the visitation probabilities emerging from our sampling process by using the PageRank algorithm [18] on the full complex attractor. Mapping of the full state transition graph of relatively small models is tractable; this is not the case for larger networks.

3.1.6 Biological noise with synchronous update and the attractor barriers of Boolean models

Here I present a method of adding noise to synchronously updated dynamics, by assuming a nonzero probability that nodes can return the wrong output for the given inputs at any given time-step. This is used in Chapter 5 to determine

the probability of states when calculating the measures of dynamical modularity.

Biological noise can occasionally lead to transitions between attractor basins. In the presence of noise, the models' trajectory also explores the connections and barriers between individual attractors [54, 55]. Assuming that a small amount of noise affects each logical rule in each time-step offers an elegant way to estimate the long-term probability that the system spontaneously visits *any state* (not just the attractors. It also mitigates some of the drawbacks of synchronous node update [56, 57, 58]. In this case, we follow the method of Zhang et al. [59], who used a Markov chain approach to calculate the stationary probability $\Pi(s)$ of finding the ergodic system in any state s (not just the attractors). To this end, we first calculate the probability matrix M_{ij} of every state transition $s_i \rightarrow s_j$ the system can have in a single time-step. Given a nonzero probability p_E that any Boolean function returns the wrong output in every time-step, the system's dynamics is a Markov process and all M_{ij} transitions take place with a nonzero probability. From each state s_i (each row of M_{ij}) there will be a single transition with probability $(1 - p_E)^N$ corresponding to the deterministic, synchronous state transition observed in the noise-free system. In addition, there will be N transitions with probability $p_E(1 - p_E)^{N-1}$ where one of the N gates was affected by error, $\binom{N}{2}$ further transitions with probability $p_E^2(1 - p_E)^{N-2}$ and so on.

In stationary state, the overall probability of the system transitioning into state s_i must be balanced by the probability of it leaving s_i:

$$\Sigma_j \Pi(s_j) M_{ji} = \Pi(s_i) \Sigma_j M_{ij}, \tag{3.3}$$

where $\Sigma_j M_{ij} = 1$. In matrix form: $(M - \mathbb{I})\Pi = 0$ ($\mathbb{I}$ is the identity matrix), an underdetermined system of 2^N linear equations. Adding the additional constraint that the stationary probabilities across the *entire* state space add up to 1, $\Sigma_i \Pi(s_i) = 1$, renders the system of equations determined with a single solution. The exact calculation, however, is only feasible on very small Boolean networks (it is a system of $2^N + 1$ equations). For larger networks we estimate $\Pi(s)$ as the visitation probability of state s, sampled by long runs of noisy dynamics (for further details Deritei et al. [60] Supplementary Methods 1). Using $\Pi(s)$, an energy-like quantity can be defined, which is associated with each network state during noisy Boolean dynamics: $E(s) = -\log[\Pi(s)]/\beta$, where $\beta = \log(1/p_E - 1)/2$ is a function of rule error probability p_E [59].

The stability of an individual attractor (and thus, biological phenotype) may be characterized as the overall probability of finding the system within its basin of attraction:

$$P(a) = \sum_{i \in B(a)} \Pi(s_i), \tag{3.4}$$

where s_i is an initial condition from which the system's noise-free dynamics leads to attractor a. $B(a)$, the basin of a, denotes the set of all such states. Using a similar logic, we can compute the overall probability of spontaneous transitions between attractor basins as:

$$T(a \to b) = \sum_{i \in B(a)} \sum_{j \in B(b)} \frac{\Pi(s_i)}{P(a)} M_{ij}. \tag{3.5}$$

3.2 The dynamic repertoire of Boolean models

Analyzing a Boolean model by mapping out the state transition graph (STG) with different update schemes gives us a complete map of the dynamic landscape of the model as well as potentially profound insights into the empirical system it represents. However, as the models grow in size doing a full analysis of the STG becomes intractable. In this section we are going to discuss a set of tools introduced by Zañudo et al. in [61] that offer an efficient way to map out the main dynamical features of a Boolean model. These methods are imperative in the analysis of our empirical models. Here we also introduce a methodological innovation, which makes part of this framework and emerged from our research, the *conditionally stable motif* discussed in detail in 3.2.3, published in [62].

3.2.1 The Logic Expanded Network

The signed interaction network of a Boolean model encodes only partial information about the model since there can be nontrivial logical rules that determine the next state of a node (see Figure 3.1). The logic expanded network (often referred to as just the expanded network) offers a way to *encode the logical rules into network structure*. This representation then allows finding key dynamical features in a model doing structural analysis.

The expanded network consists of two **virtual nodes** for each node (one for each of the two possible states) and **composite nodes** that embody AND gates among two or more node states. In Figure 3.4 we present the toy regulatory model, already introduced in Figure 3.1 and its expanded network conversion.

The expanded network (right panel) of the regulatory model (left panel) includes two virtual nodes for each node: the virtual node marked by the node name indicates the *on* (1) state of the node while the virtual node marked by the node name preceded by $\sim$ indicates the *off* (0) state of the node. The expanded network represents each AND gate with a composite node (small filled circle), e.g. the composite node with light blue background indicates the AND gate

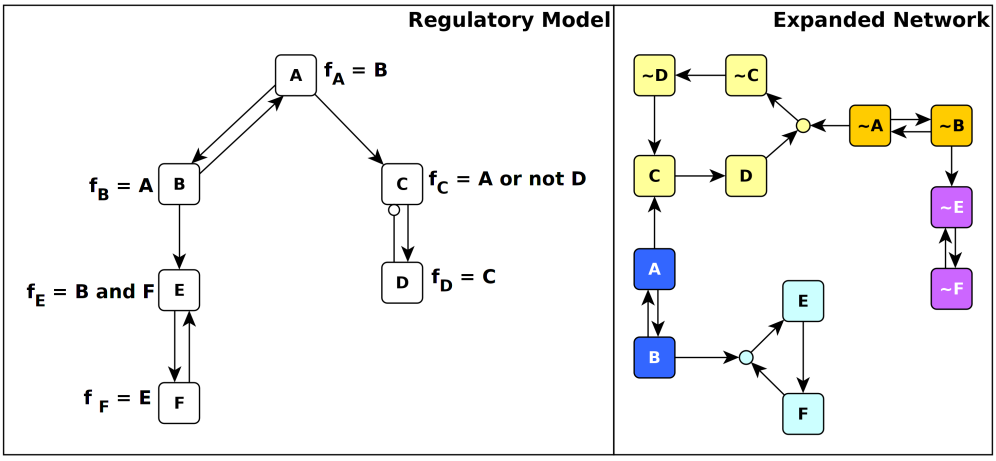

Figure 3.4. *The expanded network (right panel) of the regulatory model (left panel) includes two virtual nodes for each node: the virtual node marked by the node name indicates the on (1) state of the node while the virtual node marked by the node name preceded by ∼ indicates the off (0) state of the node. The expanded network represents each AND gate with a composite node (small filled circle), e.g. the composite node with light blue background indicates the AND gate in the regulatory function of node E. (Recall that an OR gate in a Boolean rule corresponds to an AND gate in its negation, as seen in the case of the other, yellow composite node). The positive feedback loop between A and B yields two stable motifs, one corresponding to the on state of both nodes (shown in blue) and one corresponding to the off state of both nodes (shown in orange). The positive feedback between E and F can sustain their off state (stable motif shown in purple) but the on state of E and F can only be sustained if B is on. Thus, the virtual nodes E and F form a conditionally stable motif conditioned on B (light blue). The negative feedback between C and D leads to sustained oscillation of these two nodes (indicated by the cycle in yellow) if A=0. If A=1 C will also converge to 1 (see the edge from A to C in the expanded network)*

in the regulatory function of node E (E*=B and F) with inputs from the virtual nodes representing the *on* states of B and F and an outgoing edge pointing to the virtual node representing the *on* state of E. The negation of the rule of E (not E*= not B or not F) is also represented by the virtual nodes ∼B and ∼F pointing to ∼E. (Recall that an AND in a Boolean rule corresponds to an OR in its negation, and vice-versa).

An edge from a virtual node to a composite node indicates that the virtual node is a *necessary* condition for states described by the composite node. An edge from any node to a virtual node indicates that the parent node is a *sufficient* condition for the state represented by the child node. Special *strongly connected*

subgraphs of the expanded network have strong dynamical implications. In this section, we are going to discuss these special subgraphs and how they can help us explore the dynamic repertoire of Boolean models.

3.2.2 Stable and Oscillating Motifs

Stable motifs are generalized *positive feedback loops* in a regulatory model, which have a pivotal influence on the dynamical evolution of a model and can be identified in the expanded network formalism. A stable motif is a subgraph of an expanded network that satisfies four properties:

1. it is strongly connected – there is a directed path within all pairs of nodes within the subgraph

2. it is consistent – there are no virtual nodes in the subgraph that also have their negated pair in the subgraph. E.g. if virtual node A is in the subgraph $\bar{A}$ cannot be for the subgraph to be consistent.

3. it is composite-closed – if a composite node is in the subgraph, so too are all its virtual node parents

4. it is minimal – it contains no nontrivial subgraphs satisfying the first three properties

On our toy network in Figure 3.4 the positive feedback loop between A and B yields two stable motifs, one corresponding to the on state of both nodes (shown in blue) and one corresponding to the off state of both nodes (shown in orange). The positive feedback between E and F forms a stable motif of their off states (stable motif shown in purple). The identification of stable motifs is useful because of one important reason – they are (as their name suggests) parts of the regulatory network that can sustain their stability independent of the rest of the network. If the node states represented by the virtual nodes are established (by the naturally evolving dynamics, as the initial condition or by external intervention), these states lock-in and will not change, regardless of what happens in the rest of the network. In other words, stable motifs create trap-spaces: once the dynamical trajectory enters it can no longer leave, and thus the degrees of freedom in the system are permanently reduced. On the STG this means that once the model reaches a state where a stable motif is stabilized (e.g. A=B=0 on the toy network) in every state downstream from that state the nodes of the stable motif will be in the same configuration.

An oscillating motif is a subgraph of an expanded network that satisfies five properties, some shared with the properties of stable motifs:

1. it is strongly connected,

2. it is composite-closed,

3. each of its virtual nodes is contradicted by another one of its virtual nodes,

4. it contains no stable motifs

5. it is minimal

The difference between oscillating and stable motifs is in condition number 3, which means that oscillating motifs are not consistent, but the opposite – oscillating motifs have both virtual nodes of each variable in the subgraph fitting the conditions listed above. Oscillating motifs create trap-spaces as well but the nodes represented by the motif will not stabilize but oscillate indefinitely. The yellow subgraph in Figure 3.4 right panel is not a perfectly realized oscillating motif (it is not composite closed – i.e. the yellow composite node's parents are outside the motif) but it becomes one if the stable motif A=B=0 stabilizes. If that happens, the nodes C and D will oscillate indefinitely (see the orange attractor in Figure 3.3). However, the oscillation is *conditioned* on the stabilization of another motif or node. In the next section, I am introducing a generalization of stable and oscillating motifs: the conditionally stable (oscillating) motif.

3.2.3 Conditionally Stable Motifs

Conditionally stable motifs (CSM) are strongly connected subgraphs of the expanded network that have the same structural conditions as stable (or oscillating) motifs, except for the condition of the motif being composite closed, i.e. all parents of a composite node in the motif are not necessarily in the motif. The parents of the composite nodes in the CSM that are *not part of the subgraph* are the **conditions** of the conditionally stable motif. If the conditions of a CSM are held fixed, the CSM becomes a stable (or oscillating) motif. In our example in Figure 3.4 the positive feedback between E and F can sustain their off state (stable motif shown in purple) but the on state of E and F can only be sustained if B is on. The negative feedback between C and D leads to sustained oscillation of these two nodes if A is off. In Chapter 6 I am going to discuss how conditionally stable motifs are key in creating checkpoints in the cell cycle (that are intuitively conditionally stable states) as well as how do they make sure that the dynamic evolution of the cell cycle is robust to update noise.

3.2.4 Stable Motif Succession Diagram

As stated in the introduction of this section, the identification of different motifs in the expanded network can help us map out the dynamic repertoire of a Boolean model, without the need to explore the full state space (STG). The subsequent stabilization of stable, conditionally stable, and oscillating motifs will create different paths that then converge into one of the attractors of the system. By mapping out the possible sequences of stable motif stabilization we can create a much more simplified picture of the dynamical landscape of a model. We call such a map a **stable motif succession diagram**. In Figure 3.5 we show such a succession diagram for the toy network we've been using so far. Comparing Figure 3.5 to the state transition graphs of the same model on Figures 3.2 and 3.3 one can see that using this framework one can drastically simplify the dynamical landscape of a model.

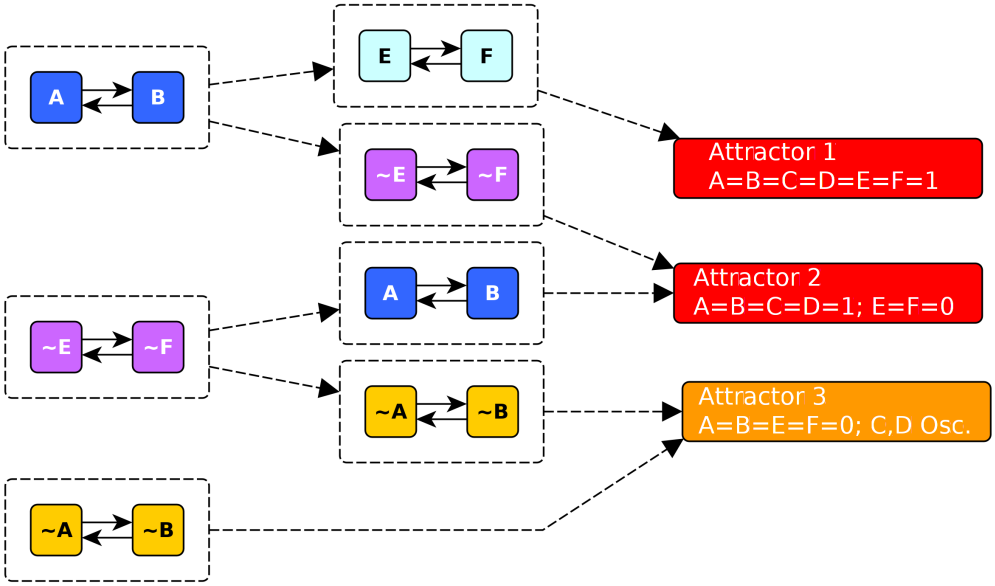

Figure 3.5. *The stable motif succession diagram indicates the possible sequences of successive stabilization of the three stable motifs and of the conditionally stable motif as well as the resulting attractor repertoire of the system.)*

CHAPTER 4

A Boolean model for the Cell Cycle with two interacting dynamical modules

The cell cycle is one of the most fundamental processes of life. Understanding its intricacies not only has tremendous scientific value but it can help us better understand and alleviate complex diseases such as cancer. In this chapter we are going to present and discuss the cell cycle model, published in the paper titled *Principles of dynamical modularity in biological regulatory networks* published in Scientific Reports in 2016 [60]. This paper is the result of a collaboration between Erzsébet Ravasz Regan, William B. Aird, Mária Ercsey Ravasz and myself. My contribution to this paper was validating the simulation results and coming up with the generalized quantitative measures of the principles of dynamical modularity discussed in the next chapter, as well as writing the paper. The distillation of the vast experimental literature into the Boolean regulatory interactions presented in this chapter is the work of Dr. Ravasz Regan. My work focused on the analysis of the already constructed Boolean models. The tables explaining the detailed biological mechanisms referencing the experimental literature can be found in our paper [60] Supplementary Tables S1 to S3. I believe it is more appropriate to not include those details in this thesis.

The Boolean cell cycle model in the paper is composed of two semi-autonomous modules that are the two essential empirical models of focus in this thesis. The first module called the **Restriction Switch**, models the irreversible switching cells undergo when they pass the restriction point and commit to a full division cycle irrespective of further growth stimulation. The second module called the **Phase Switch** models the switch-like transitions from G2

into mitosis, as well as spindle assembly checkpoint passage from metaphase to anaphase. The two modules are coupled to each other, as well as to the main processes driven by the cell cycle control machinery; namely DNA Replication and assembly of the mitotic spindle. Cell cycle progression in this model is dependent on a single **Growth Factor** input (GF). GF represents an extracellular environment with saturating mitogen levels, leading to full activation of growth signaling pathways that activate the transcription factors and G1 cyclins responsible for starting the cell cycle. Thus, when GF is on the model settles into a limit cycle and mimics continuously cycling cells. In contrast, GF = 0 leads to a stable state that corresponds to quiescent cells in G_0.

4.1 The Restriction Switch – a bistable model of the restriction point

4.1.1 Biological background

The mammalian restriction point marks a commitment in late G_1, before which cells require ongoing mitogenic (growth) stimulation to initiate the cell cycle. Past the restriction point, division proceeds regardless of the presence of growth signals. In cells entering the cell cycle from quiescence (G0 state), growth factors stimulate the activation of Myc, a transcription factor responsible for early G1 induction of Cyclin D1, as well as its partner kinase Cdk 4 (the active complex is modeled by CyclinD1 = ON). As active Cyclin D1 / Cdk complexes accumulate, they block the activity of the cyclin-dependent kinase inhibitor p27Kip1 and phosphorylate the retinoblastoma protein RB. This blocks RB's ability to inhibit E2F1-mediated transcription. E2F1 then orchestrates the production of a wide array of proteins required for cell cycle progression and DNA replication, including Cyclin E. As Cyclin E / Cdk2 complexes are also potent inhibitors of RB, the presence of Cyclin E guarantees that E2F1 remains active, keeping Cyclin E levels high regardless of mitogenic stimulation. At this point, cells are committed to replication. In this respect, the Restriction Switch is similar to previously published models of cell cycle commitment [63, 64, 65, 66]. Besides, the switch also includes experimentally documented feedback from E2F1 to Cyclin D1 and Myc, which allow the Restriction Switch to switch into its committed state early in metaphase (following Cyclin A degradation in pro-metaphase) and drive an additional cell cycle in the absence of growth factors.

4.1.2 The Boolean model of the Restriction Switch

The Boolean model of the Restriction Switch (from this point only referred to as Restriction Switch) encapsulates the biological mechanisms described above and its emergent dynamics reflects an irreversible switch: it has two distinct steady states.

in Table 4.1 we provide the description of individual nodes of the Restriction Switch. In Figure 4.1 we show the regulatory network representation of the Restriction Switch. The regulatory interactions (Boolean rules) are listed in Table 4.2. A detailed description of the regulatory interactions included in this model, supported by references from the experimental literature can be found in [60] Supplementary Table S1.

node	description
CyclinD1	active complex of Cyclin D1 and cyclin-dependent kinases 4 or 6
CyclinE	active complex of Cyclin E and cyclin-dependent kinase 2
E2F1	E2F family transcription factor 1
Myc	Myc transcription factor
p27Kip1	cyclin-dependent kinase inhibitor 1B
RB	hypho-phosphorylated Retinoblastoma protein

Table 4.1. *Nodes of the Restriction Switch and their descriptions.*

node	regulatory function
CyclinD1*	= (Myc and E2F1) or (CyclinD1 and (Myc or E2F1))
CyclinE*	= E2F1 and (not RB) and (not p27Kip1)
E2F1*	= (not RB) and (E2F1 or Myc)
Myc*	= E2F1
p27Kip1*	= not (CyclinD1 or CyclinE)
RB*	= (not CyclinD1) and ((not CyclinE) or p27Kip1)

Table 4.2. *Regulatory functions (Boolean rules) of the Restriction Switch model*

The two steady states (point attractors) of the Restriction Switch, are shown in Figure 4.2 – one corresponding to the biological state *before* restriction point passage while the other represents mitogen-independent commitment to the next division (*past* restriction point). All unstable states of this circuit follow trajectories into one of these two states, partitioning the system's state space into two attractor basins.

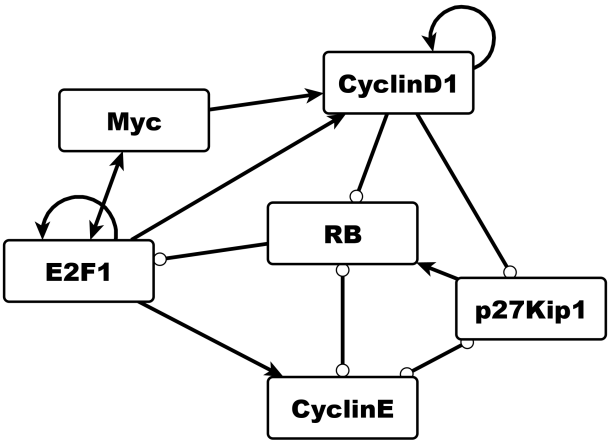

Figure 4.1. *The regulatory network representation of the Restriction Switch model. Edges with terminal arrows indicate positive regulation, edges that end in open circles indicate negative regulation, and edges that have endings on both sides (i.e., bidirectional edges) indicate the superposition of two edges with opposite directions.*

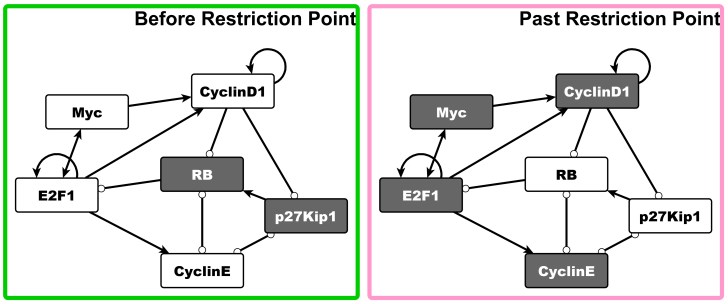

Figure 4.2. *The two steady states of the Restriction Switch in the regulatory network representation of Figure 4.1. The dark grey color background represents the ON state of a node and the white background represents the OFF state. The color of the two boxes is the color code of the respective steady states we are going to use on later figures.*

4.2 The Phase Switch – a tri–stable model of the phase defining checkpoints

4.2.1 Biological background

Once cells finish DNA replication and repair all DNA damage, they undergo another irreversible switch-like transition that commits them to mitosis. Mechanistically, this commitment involves full activation of M-phase Cyclin B / Cdk1 complexes. The process starts with Cyclin B accumulation in G2 when the activity of the APC/C – Cdh1 ubiquitin ligase complex is blocked by Cyclin A / Cdk2 activity. Once the checkpoint proteins sensing ongoing DNA replication and/or DNA damage turn OFF and Wee1 activity decreases, the inhibition of Cdk1 kinase by Wee1 is lifted. Once active, Cyclin B / Cdk1 can keep Wee1 suppressed even if DNA damage signals reappear [67], making the commitment to Cyclin B / Cdk1 a switch-like transition. Cyclin B / Cdk1 activity initiates the processes of mitosis, including chromosome condensation, dissolution of the nuclear membrane and the assembly of the mitotic spindle.

In the coupled cell cycle model shown in Figure 4.5 and further discussed in Section 4.3 this complex choreography of biological events is simplified into the Metaphase node outside of the Phase Switch. The Metaphase node is activated by Cyclin B and Cdk1 in cells with 4N DNA content; its ON state represents the completion of spindle assembly. As long as Metaphase is OFF, the Phase Switch maintains a robust Cyclin B and Cdk1-high state where the anaphase-promoting complex is phosphorylated (pAPC) but inactive. This is the spindle assembly checkpoint. Its passage requires Metaphase = ON (a signal external to the Phase Switch) and the subsequent inhibition of Mad2. Mad2 is a highly sensitive signaling molecule that remains active as long as even a single kinetochore (and thus chromosome) remains unattached to the mitotic spindle. Once Mad2 is inactive, the Cdc20-bound and phosphorylated APC/C complex, modeled as pAPC = ON and Cdc20 = ON, degrades Cyclin B and thus inactivates mitotic cyclin / cyclin-dependent kinase activity. In addition, the complex tags the protein securin for degradation, releasing a protease (separase) that cleaves the cohesin rings that keep sister chromatids together. This marks the start of anaphase when sister chromatids begin their movement to opposite poles of the mitotic spindle. The activity of the Cdc20-bound and phosphorylated APC/C complex is short-lived, however, as APC/C loses its Cdk1/Cyclin B-mediated phosphorylation and Cdh1 replaces Cdc20 in the complex. This leads to Cdc20 degradation, following which the Phase Switch locks into a stable state that matches that of G0/G1 cells. At this point, further external input from a committed Restriction Switch as well as the Replication node is required to toggle it

back into G2 [68].

4.2.2 The Boolean model of the Phase Switch

The Phase Switch is a Boolean model incorporating the above mechanisms that together with other key regulators are the core driving interactions of the cell cycle phases. in Table 4.3 we list the nodes of the Phase Switch with their descriptions. Regulatory functions of the Phase Switch module are listed in Table 4.4. A detailed description of the regulatory interactions included in the Phase Switch model, supported by references from the experimental literature can be found in [60] Supplementary Table S2.

node	description
Cdc20	cell-division cycle protein 20
Cdc25A	cell-division cycle protein 25A
Cdc25C	cell-division cycle protein 25C
Cdh1	complex of Cdh1 and anaphase-promoting complex
Cdk1	cyclin-dependent kinase 1
CyclinA	Cyclin A
CyclinB	Cyclin B
Mad2	mitotic arrest deficient 2
pAPC	phosphorylated anaphase-promoting complex
UbcH10	ubiquitin conjugating enzyme UbcH10
Wee1	nuclear kinase Wee1

Table 4.3. *Nodes of the Phase Switch and their descriptions.*

The Phase Switch module when isolated from external interactions has three unique steady states, shown in Figure 4.4 that each correspond to states locked into the three major checkpoints in the cell. More precisely this isolation is a special configuration of external signals where no checkpoint gets "green light". Without external intervention, the final stabilization of the Phase Switch depends on the initial condition of the model and/or noise. Naturally, this is not the case in the actual cell. Yet it is an important feature that the Phase Switch can capture the locked-in states into the checkpoints, which we further explore in Chapter 6.

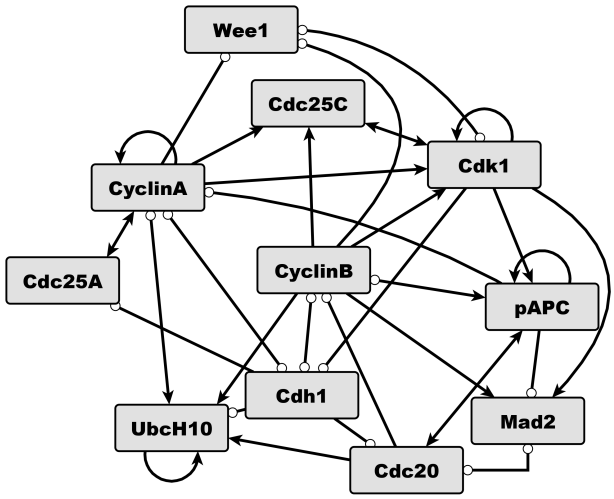

Figure 4.3. *The regulatory network representation of the Phase Switch model. Edges with terminal arrows indicate positive regulation, edges that end in open circles indicate negative regulation, and edges that have endings on both sides (i.e., bidirectional edges) indicate the superposition of two edges with opposite directions.*

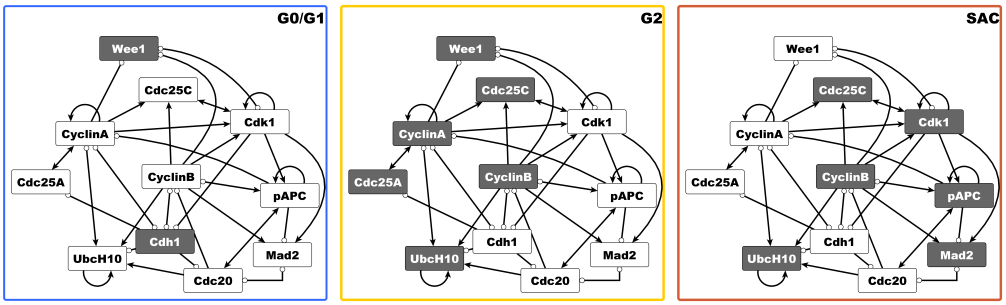

Figure 4.4. *The three steady states of the Phase Switch in the regulatory network representation of Figure 4.3. The dark grey color background represents the ON state of a node and the white background represents the OFF state. The color of the two boxes is the color code of the respective steady states we are going to use on later figures.*

node	regulatory function
Cdc20*	= pAPC and (not Cdh1) and (not Mad2)
Cdc25A*	= CyclinA and (not Cdh1)
Cdc25C*	= CyclinA or (CyclinB and Cdk1)
Cdh1*	= (not CyclinA) and (not (CyclinB and Cdk1))
Cdk1*	= Cdc25C and (CyclinA or CyclinB) and (Cdk1 or (not Wee1))
CyclinA*	= (Cdc25A or CyclinA) and (not (pAPC or (Cdh1 and UbcH10)))
CyclinB*	= not (pAPC and Cdc20) and (not Cdh1)
Mad2*	= not (pAPC and Cdc20) and CyclinB and Cdk1
pAPC*	= (pAPC and Cdc20) or (CyclinB and Cdk1)
UbcH10*	= (not Cdh1) or (UbcH10 and (Cdc20 or CyclinA or CyclinB))
Wee1*	= not ((CyclinA or CyclinB) and Cdk1)

Table 4.4. *Regulatory functions (Boolean rules) of the Phase Switch model*

4.3 The cell cycle model – two switches toggle each other to generate cyclic dynamics

The full cell cycle model of our study is a coupling of the two modules introduced above, the Restriction Switch and the Phase Switch with interactions between the two modules. We extend the model with four additional nodes, we refer to as abstract nodes – since they represent simplifications of processes that themselves are complex decision-making modules. The additional nodes and their descriptions are listed in Table 4.5.

node	description
Replication	The ON state represents the ongoing process of DNA replication and it turns OFF when cells double their DNA content.
Metaphase	The Metaphase abstract node turns ON when spindle assembly is completed, and none of the kinetochores are left unattached.
4N_DNA	The 4N_DNA abstract node represents the completed duplication of a cell's DNA. It also represents the mechanisms that prevent the initiation of a new replication process.
GF	Growth factors in the cell's external environment

Table 4.5. *Nodes of the Phase Switch and their descriptions.*

The full cell cycle model is defined in Table 4.6, with the network representation shown in Figure 4.5. We discuss the biological details of the coupling interactions between the Restriction Switch and the Phase Switch in another

context in Section 7.4. The detailed description of the regulatory interactions of the full coupled model, with references from the experimental literature, can be found in [60] Supplementary Table S3.

node	regulatory function
GF*	= GF
CyclinD1*	= (not Replication) and ((GF and (Myc or E2F1)) or (Myc and E2F1))
CyclinE*	= (Cdh1 or (not Metaphase)) and (E2F1 and (not (p27Kip1 or RB)))
E2F1*	= not (CyclinA or RB) and (E2F1 or Myc)
Myc*	= GF or E2F1
p27Kip1*	= (not (CyclinB and Cdk1)) and (not (CyclinD1 or (CyclinA and CyclinE)))
RB*	= not (CyclinB and Cdk1) and (not CyclinD1) and (p27Kip1 or not (CyclinA or CyclinE))
Cdc20*	= pAPC and (not Cdh1) and (not Mad2)
Cdc25A*	= (E2F1 and (CyclinE or CyclinA)) or ((not Cdh1) and CyclinE and CyclinA)
Cdc25C*	= CyclinA or (CyclinB and Cdk1)
Cdh1*	= (not (CyclinB and Cdk1)) and (not CyclinA)
Cdk1*	= Cdc25C and (CyclinA or CyclinB) and (Cdk1 or (not Wee1))
CyclinA*	= ((E2F1 and Cdc25A) or CyclinA) and (not (pAPC or (Cdh1 and UbcH10)))
CyclinB*	= not (pAPC and Cdc20) and (not Cdh1)
Mad2*	= n4N_DNA and (CyclinB and Cdk1 and not ((pAPC and Cdc20) or Metaphase))
pAPC*	= (pAPC and Cdc20) or (CyclinB and Cdk1)
UbcH10*	= (not Cdh1) or (UbcH10 and (Cdc20 or CyclinA or CyclinB))
Wee1*	= Replication and (not ((CyclinA or CyclinB) and Cdk1))
Metaphase*	= n4N_DNA and CyclinB and Cdk1 and (not(pAPC and Cdc20))
Replication*	= CyclinE and Cdc25A and (not n4N_DNA)
n4N_DNA*	= (not Cdh1) and (n4N_DNA or (CyclinA and Replication))

Table 4.6. *Regulatory functions (Boolean rules) of the cell cycle model*

The cell cycle model has two attractors: a steady state attractor and a limit cycle, both corresponding to actual stable biological phenotypes.
In the absence of growth factors cells enter into the so-called quiescent state, G0, where they keep functioning (e.g. neurons fire) but are not engaged in growth

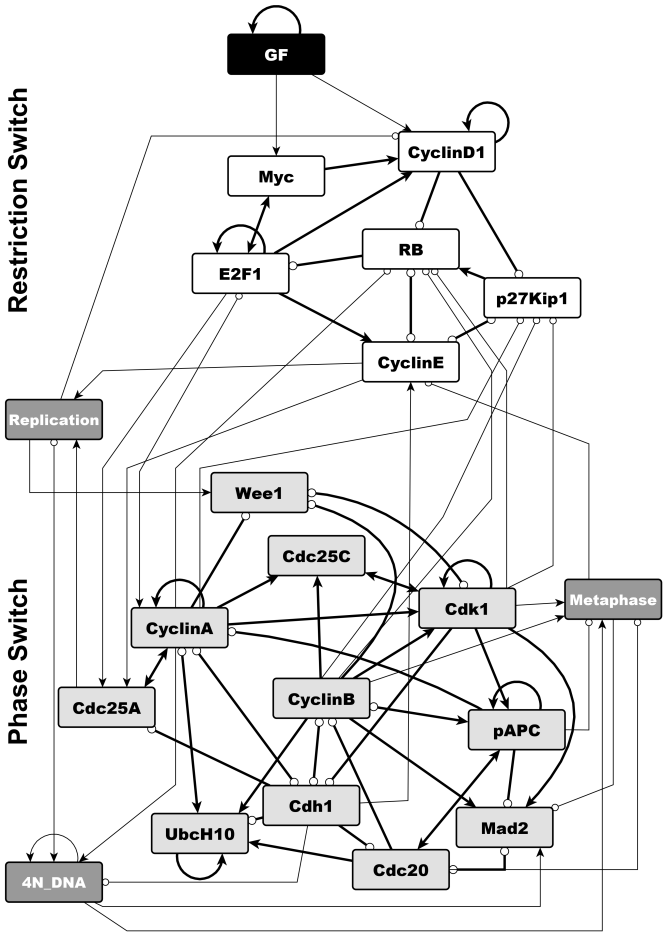

Figure 4.5. *Illustration of the coupled cell cycle model from its two modules, the Restriction Switch (shown with white node background) and the Phase Switch (nodes with light grey background). The network also contains a Growth Factor input node (black), and three abstract nodes (dark grey) that stand for cell cycle processes (Replication, Metaphase) or global cell states (4N_DNA) that are triggered, monitored and terminated by the two controller switches. Edges with terminal arrows indicate positive regulation, edges that end in open circles indicate negative regulation, and edges that have endings on both sides (i.e., bidirectional edges) indicate the superposition of two edges with opposite directions.*

and the subsequent division. In the case of our model if the GF input node is set to 0 the model converges to a steady state that corresponds to a quiescent cell. All the core molecules responsible for driving the cell cycles are off, only three nodes are active: RB, p27Kip1 and Cdh1. All three are strong inhibitors of Cyclins and Cdks and thus are responsible for blocking the cell cycle. This state

also corresponds almost perfectly to a combination of two module-attractors - the before restriction point attractor of the Restriction Switch (this lock-in is its main role) and G0/G1 attractor of the Phase Switch.

In the constant presence of growth factors (GF=1), under synchronous update, the model enters a **limit cycle** that has two important features: first, its 13 repeating states correspond to actual biological states emerging from by the sequence of events in the cell cycle – making the different phases of the cell cycle identifiable, in the correct order. In short, the limit cycle corresponds to the actual cell cycle. Second, the cell cycle states approach the attractors of the two modules and toggle between them. The states are shown in detail in Table 4.7 and the illustration of the limit cycle from the perspective of the two modules is shown in Figure 4.6.

This property of the global attractor toggling the attractors of its constituent modules is a feature we call *dynamical modularity*. We believe that dynamical modularity could be a general property of natural decision-making systems where decision making functional modules coordinate in intricate ways to exhibit robust but adaptive behavior.

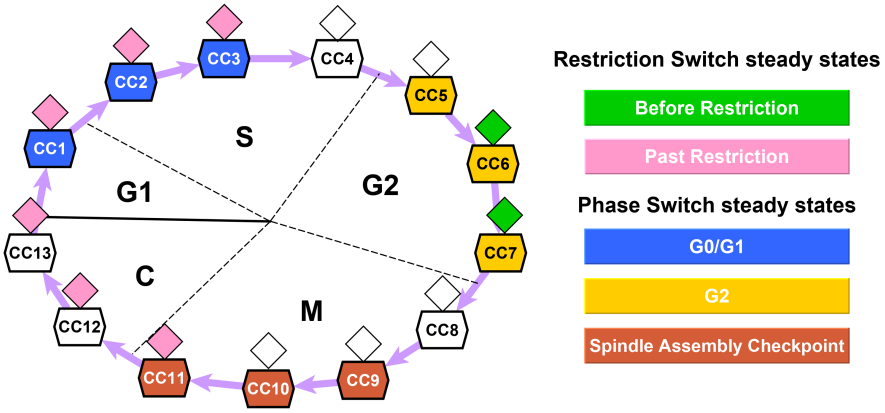

Figure 4.6. *In the presence of growth factors the model's states form a limit cycle that progresses through the phases of the cell cycle while toggling the steady states of the two modules. Each symbol represents a model state and separately encodes the state of the Restriction Switch (diamond) and the Phase Switch (hexagon). The color of each shape indicates that the corresponding state is close to one of the steady states indicated in the legend and Figures 4.2 and 4.4. The divided sections of the cycle represent the cell cycle phases accurately reproduced by the states of the limit cycle. For the detailed states see Table 4.7 and Figure 2 of Deritei et al. [60]*

	Phase	G1	S			G2			M				C		G1
	State label	CC1	CC2	CC3	CC4	CC5	CC6	CC7	CC8	CC9	CC10	CC11	CC12	CC13	CC1
Restriction Switch	E2F1	1	1	1	0	0	0	0	0	0	0	1	1	1	1
	CyclinE	1	1	1	1	0	0	0	0	0	0	0	0	1	1
	CyclinD1	1	1	0	0	0	0	1	1	1	1	1	1	1	1
	RB	0	0	0	0	0	0	1	0	0	0	0	0	0	0
	p27Kip1	0	0	0	0	0	1	1	0	0	0	0	0	0	0
	Myc	1	1	1	1	1	1	1	1	1	1	1	1	1	1
Phase Switch	CyclinA	0	0	1	1	1	1	1	1	1	0	0	0	0	0
	Cdc25C	0	0	0	1	1	1	1	1	1	1	1	1	0	0
	Cdc25A	1	1	1	1	1	0	0	0	0	0	0	0	0	1
	CyclinB	0	0	0	0	1	1	1	1	1	1	1	0	0	0
	Cdh1	1	1	1	0	0	0	0	0	0	0	0	0	1	1
	Cdk1	0	0	0	0	0	0	0	1	1	1	1	1	0	0
	Wee1	0	0	1	1	1	1	0	0	0	0	0	0	0	0
	UbcH10	1	0	0	0	1	1	1	1	1	1	1	1	1	1
	pAPC	1	0	0	0	0	0	0	0	0	1	1	1	1	1
	Cdc20	0	0	0	0	0	0	0	0	0	0	1	1	1	0
	Mad2	0	0	0	0	0	0	0	0	1	0	0	0	0	0
abstract nodes	Replication	0	1	1	1	1	0	0	0	0	0	0	0	0	0
	4N DNA	0	0	0	0	1	1	1	1	1	1	1	1	1	0
	Metaphase	0	0	0	0	0	0	0	0	1	1	1	0	0	0

Table 4.7. *States of the cyclic attractor of the synchronous cell cycle model. This limit cycle is obtained in the sustained presence of growth factors (GF=1). The columns of the table represent the 13 states of the limit cycle, while the rows denoted by node names represent the states of individual nodes in each state. We group the states according to the cell cycle phases, indicated in the topmost row. The state labels correspond to the labels shown in Figure 4.6. We group the nodes into three categories, namely the Phase Switch, the Restriction Switch and three abstract nodes. We highlight the states of the Restriction Switch or Phase Switch that are closest to a respective attractor with the colors corresponding to the attractors.*

CHAPTER 5

THE PRINCIPLES OF DYNAMICAL MODULARITY

5.1 Dynamical Modularity – attractors of multi-module systems are nontrivial combinations of module-attractors

Our modular description of the cell cycle builds on the hypothesis that a biological regulatory system's global attractors (phenotypes) are combinations of the attractors of its modules (switches), a property we call dynamical modularity. To test this hypothesis by measuring whether it holds in biological versus randomized multi-module networks we have to find a way to quantify to what degree is a biological model dynamically modular. To this end, we formulate *three principles* that have to be true for a system to be dynamically modular together with three quantitative measures of "how true" the given principle is for a Boolean model.

In this chapter I am using the terms *switch* and *module*, as well as *attractor* and *phenotype*, interchangeably, depending on whether the biological or the mathematical context is relevant. To clarify – a switch is a Boolean model that has very few distinct (preferably steady state) attractors i.e. it behaves as a switch between a few stable states. A phenotype in this context is an attractor of such a model that corresponds to some stable biological behavior.

The three principles of dynamical modularity are illustrated intuitively in Figure 5.1.

The first principle, the *principle of modular dynamics* (Figure 5.1 A) states that the phenotypes of a larger biological system (α, β, γ) are combinations of the

phenotypes of its constituent switches (a,b,c,d, etc.). In other terms, the attractors of the coupled system are combinations of the module attractors.

The second principle, the *principle of phenotype conservation* (Figure 5.1 B) states that all switch-phenotypes are present in at least one phenotype of the larger system, i.e. no switch loses any of its functions in the multi-switch model. This in terms of Boolean dynamics means that all attractors of the isolated modules are represented in at least one attractor of the coupled system.

The third principle, the *principle of robust coordination* (Figure 5.1 C) encapsulates two constraints. First, the phenotypes of the global system have to be radically different from each other (otherwise biological noise can easily switch between them, and they don't constitute distinct decisions). Second, they have to be nontrivial couplings of the underlying switch-phenotypes. When there is no coupling whatsoever between the switches, the first two principles are perfectly satisfied, but in that case, the global phenotypes are just trivial recombinations of the switch-phenotypes. This principle states that the coupling *constrains* the number of possible global phenotypes and *coordinates* the decisions of the switches. The second and third principles formulate an optimization problem: they require enough attractor-combinations to accommodate every module-attractor (second principle), but not more (third principle).

The third principle requires that the global phenotypes are radically different from each other, however, phenotypes similar to each other do exist in the cell. Our work is mostly focused on modules that make distinct, discrete decisions resulting in radically different phenotypes. This is a probable limitation of the generalizability of the principles described in the thesis. There is also a limitation coming from simplifications of the Boolean framework, as it ignores many details of biochemistry. Theoretically, proteins can create energy barriers on a biochemical level such that, while the phenotypes are similar, there is a low probability of noise-induced transition between them. It can be difficult to encode this in a Boolean model. The forces of evolution work gradually; besides, there are changes at shorter time-scales that show adaptation by fine-tuning, instead of radical decisions. On the other hand, I believe that at least at the core level of the control system of the cell, functional modules evolved to make radical decisions that can still give adaptive responses to the environment when they are well coordinated. The three principles express the amazing difficulty of such a task, that nature still managed to resolve.

In Figure 5.2 we illustrate the consequences of dynamical modularity on the cell cycle model introduced in the previous chapter. When the switches are uncoupled (A) the model has 12 disjoint basins of attraction with 12 steady state attractors. The 12 steady states are all the possible combinations of the module steady states that we plot on a 3D grid of dimensions 2 x 2 x 3 corresponding

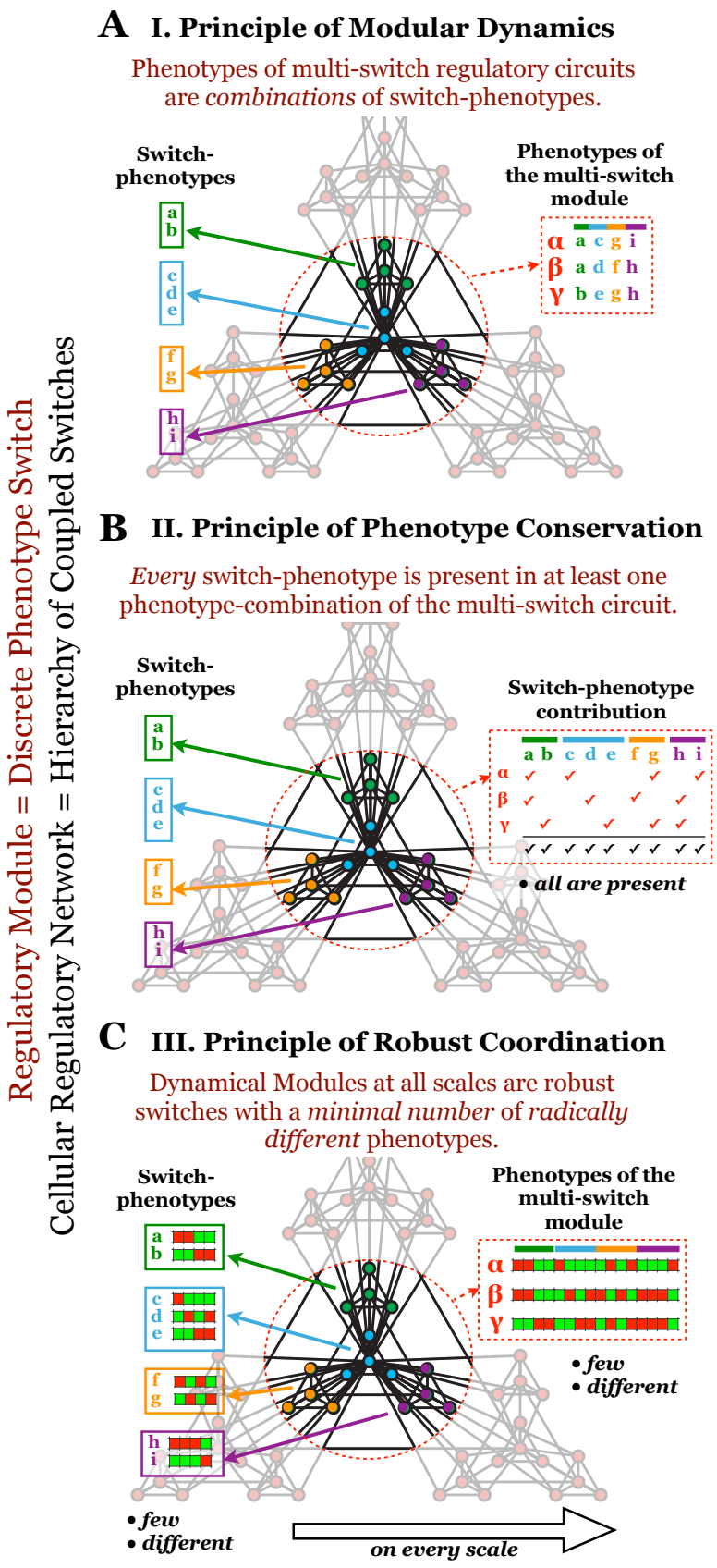

Figure 5.1. *Illustration of the three principles of dynamical modularity*

the two possible steady states of the Restrictions Switch (x-axis), the three possible steady states of the Phase Switch (y-axis) and the two possible states of the Growth Factor node (z-axis). Once we couple the switches Figure 5.2 (B) the 12 basins merge into 2 basins of two attractors: a steady state (G0) and a cyclic attractor (cell cycle) – depending on the presence or absence of growth factors. Keeping the basin layout of the decoupled system reveals that the trajectory of the limit cycle (red arrows) visits the basins of the decoupled attractor combinations, and approaches the attractor combinations to a large extent (this point is also illustrated in Figure 4.6 and Table 4.7).

In the following sections, I am going to explain the three principles in detail, along with their respective measures.

5.2 The Principle of Modular Dynamics and the Attractor Modularity Measure

The Principle of Modular Dynamics states that attractors of multi-module regulatory circuits are combinations of module-attractors (switch-phenotypes) (Figure 5.1 A). Even though arbitrary connections between modules can easily produce global attractors that are not combinations of module-attractors, this principle states that biological interactions connecting regulatory switches do not destroy the function of these switch-level cell states. Instead, they influence which module-attractors are selected under different circumstances, without creating new ones. The coordination between switches, however, is an emergent property of multi-switch systems. This phenomenon has been observed in Boolean regulatory models and leveraged to reduce computational complexity [69, 70, 71]. This principle does not imply that continuously tunable regulatory components (with no multi-stability) are completely absent from cells. It does, however, posit that tunable signal-processing layers feed into core decision-making circuits.

To measure to what degree is this principle true we introduce the ***Attractor Modularity Measure*** (AMM), designed to quantify the extent to which attractors of a multi-switch system are combinations of the attractors of its modules. To calculate AMM, we first map each global attractor of the multi-module system onto the most similar combination of individual module-attractors. In a model that conforms to our dynamical modularity premise, we expect all global attractors to fall onto (or toggle through) precise combinations of switch-level phenotypes, resulting in $AMM = 1$. On the other hand, the existence of even one global attractor that is significantly different from *all* module-attractors carries a penalty, resulting in a low overall AMM.

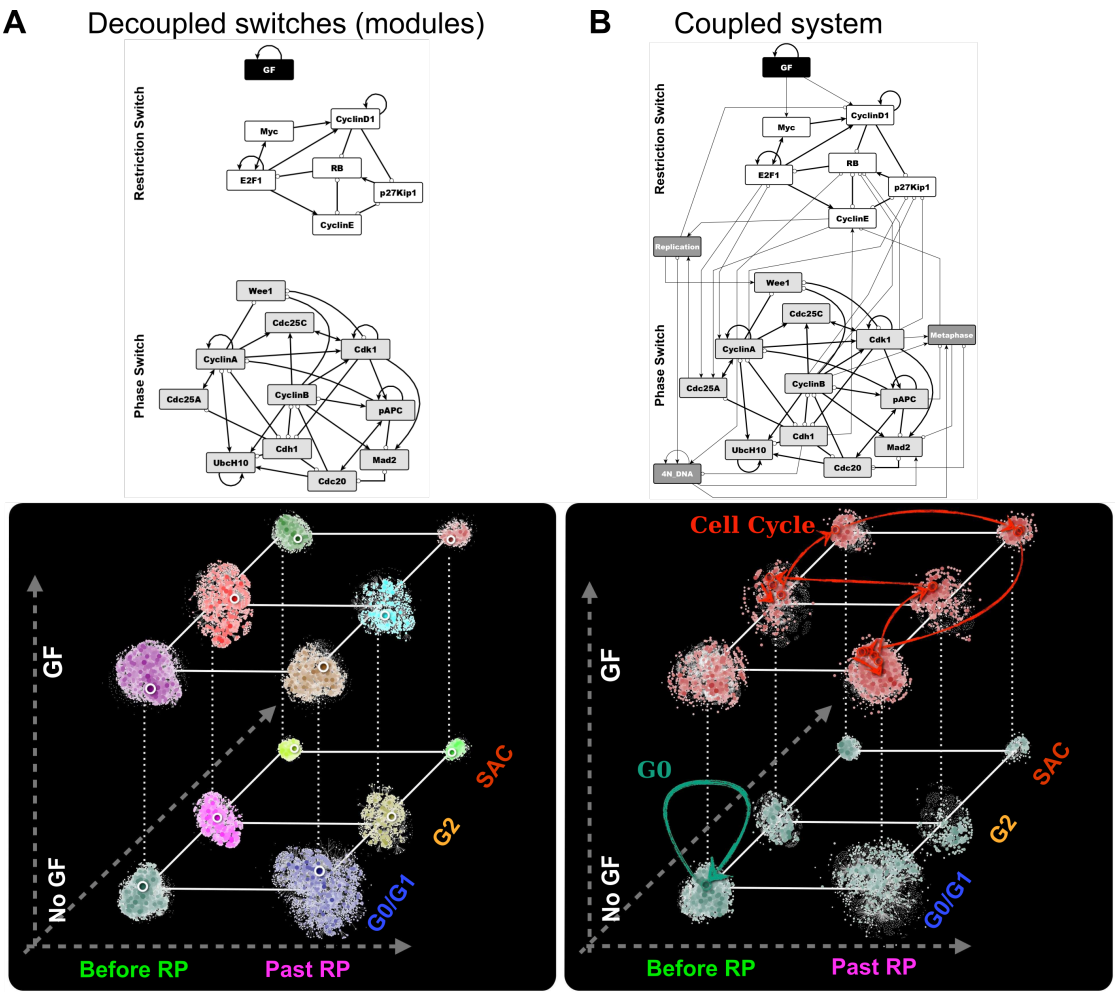

Figure 5.2. *Comparing the dynamics of the coupled cell cycle model to that of its decoupled switches reveals the sequence of discrete switch-level phenotypes as they follow each other during division. (A) Decoupled, the Restriction Switch, Phase Switch, and Growth Factor switch create a dynamical system with 12 fixed-point attractors, representing all switch-phenotype combinations. The 12 attractor-basins are laid out on a 3D grid, where switch-level attractors are organized along individual axes (Restriction Switch: x-axis; Phase Switch: y-axis; Growth Factors: z-axis; node colors of the state transition graph (STG): attractor basin membership; node size & color saturation: visitation probability with noisy synchronous update. (B) Coupled, the three switches give rise to the cell cycle model (top graph). This coupled system's STG is represented using the same 3D state-node position as in (A), with each state-node re-colored (and resized) to indicate its attractor membership dictated by the dynamics of the coupled network (we omitted most STG links from this figure for clarity, the green and red graphs each form a connected graph). This procedure reveals a single basin on the No Growth Factors plane with the fixed-point attractor G0 (dark green basin) and another basin on the Growth Factors plane with a limit cycle attractor, the cell cycle (red arrows and basin).*

To claim that a global attractor is a module-attractor combination, the global attractor has to have a high overlap with the attractor states of each module m. If the global attractor is a cyclic behavior (that is the case with the cell cycle model), we expect it to either avoid the basin of certain module-attractors altogether or implement them precisely at some point along the cyclic trajectory. We quantify this via the *Attractor Modularity* $AM_{i,m}$ of global attractor i with respect to module m. $AM_{i,m}$ is defined as:

$$AM_{i,m} = 2 \cdot \left[\max \left(O(Q_i^c, Q_j^m), \frac{1}{2} \right) - \frac{1}{2} \right], \tag{5.1}$$

where Q_i^c represents the i^{th} global attractor, and Q_j^m represents the j^{th} attractor of module m. Their overlap, $O(Q_i^c, Q_j^m)$, is based on the similarity of node states between Q_i^c and Q_j^m, generalized to cover comparisons between arbitrary global and module-level attractors. The generalization to be able to measure the overlap between all kinds of attractors (steady state with steady state, limit cycle with steady state, limit cycle with limit cycle) is a complicated method and explaining it is beyond the scope of this section (and the thesis). It is defined and explained in detail in Supplementary Methods 3 of the 2016 Deritei et al. paper [60].

$AM_{i,m}$ severely penalizes global states that are significantly different from all module-attractors of m. Thus, its lowest value 0 is reached when the overlap between Q_i^c and Q_j^m is $1/2$, representing a global attractor i in which the switch m is poised halfway between two completely different phenotypes; the opposite of dynamical modularity. The $\max(AM_{i,m}, 1/2)$ is necessary because of the way we defined overlap between limit cycle module-attractors and global cycles. If, for example, a global cycle executes the steps of a switch limit cycle with relatively high pairwise state-overlap but in a scrambled order, it is possible for $O(Q_i^c, Q_j^m)$ to be nonzero but below $1/2$. We consider these situations far from dynamically modular and treat them as worst-case scenarios with $AM_{i,m} = 0$. Conversely, perfect overlap results in $AM_{i,m} = 1$.

The attractor modularity of the entire coupled system with respect to the switch m is defined as:

$$AM_m = \left[\prod_i AM_{i,m} \right]^{1/q_c}, \tag{5.2}$$

where q_c is the number of global (coupled) attractors. Thus, AM_m is constructed to be very low if *any* of the global attractors are significantly different from all phenotypes of switch m.

Lastly, we define the global ***Attractor Modularity Measure*** as the geometric mean of attractor modularity across the modules, $AMM = \left(\prod_m AM_m \right)^{1/M}$ (M = number of modules). High AMM requires simultaneously high AM_m for every module.

5.3 The Principle of Phenotype Conservation and the Switch Stability Measure

The Principle of Phenotype Conservation guarantees that each module (switch) has a biological "decision making" function that is kept in the larger cellular context as well. It states that every module-attractor is present in at least one global attractor of the multi-module model (Figure 5.1 B). Thus, no switch's functionality is unconditionally locked out from the states of the global system.

This property is quantified by the ***Switch Stability Measure*** (SSM). SSM is built in three steps: first, measuring the prevalence of each individual module-attractor (switch-phenotype) ($PS_{m\to p}$) of each module (SS_m) in the dynamics of the multi-switch (coupled) system. To claim that the coupled system's dynamics replicates a module-attractor, two conditions have to be met. First, there needs to be at least one global attractor that maps onto this module-attractor. We test this while calculating AMM (Section 5.2), in that we compute the generalized overlap $O(Q_i^c, Q_j^m)$ between every coupled attractor i and module-m attractor j. Second, it is important that even if a coupled Q_i^c attractor exists that overlaps with module-m attractor j, its basin (and thus the overall stability of this global phenotype) is not overly small. To quantify this, we leverage noisy Boolean dynamics and calculate (or sample) the long-term probability $\Pi(s)$ of finding the coupled system in any state s in the presence of gate error p_E (see Section 3.1.6). Next, we estimate the size of the state space region (in terms of visitation probability) from which the system's dynamics flows into each attractor state. For fixed-point attractors, this equals the overall probability of finding the system somewhere in their basin. To generalize it to limit-cycles, we map each state s of the coupled system onto individual attractor states $s_k^{c\to i}$ by starting the coupled system in initial state s, and updating it in the absence of noise until an attractor state of i is reached for the first time: $s_k^{c\to i}$ being the k^{th} state of attractor i, of the coupled model c. For each global attractor state $s_k^{c\to i}$ we then sum up the probability $\Pi(s)$ of all states that map to $s_k^{c\to i}$: $W_i(k) = \sum_{s\to\cdots\to s_k^{c\to i}} \Pi(s)$. As we wish to approximate the overall probability of finding the coupled system in a state that maps onto module-m attractor j, we go through each global attractor i for which $O(Q_i^c, Q_j^m) > 0$ and sum up the $W_i(k)$ probabilities along the segment $S_j^{D\to m}$ mapped into switch-m attractor j (for the definition of $S_j^{D\to m}$, and mapping matrix $\Im^{D\to m}$ see Deritei et al. [60] Supplementary Methods 3). Stated differently, we sum all $W_i(k)$ probabilities for all rows k of the attractor mapping matrix $\Im^{D\to m}$ for which there are nonzero elements in *any* of the columns that correspond to module-m attractor j (a mapping exists). This gives us the probability of finding the coupled system

in a state that corresponds (is mapped) to the module level attractor j of module m.

$$PS^{C}_{m\to j} = \sum_{\{i \mid O(Q^{c}_{i},Q^{m}_{j})>0\}} \sum_{\{k \mid \Im^{D\to m}\neq 0\}} W_i(k). \tag{5.3}$$

To put it more simply, $PS^{C}_{m\to j}$ is a general probabilistic measure that quantifies the degree to which a module attractor j (of module m) is represented in the dynamical landscape of the global, coupled system. Lastly, we do not expect this overall probability, $PS^{C}_{m\to j}$, to be larger than the stability of attractor j in the isolated module m. Consequently, we compute a similar overall probability $PS^{U}_{m\to j}$ for the coupled system made of all M modules, but in which none of the inter-module links are present (U - uncoupled system). The final value of $PS_{m\to j}$ is then computed as

$$PS_{m\to j} = \min\left(\frac{PS^{C}_{m\to j}}{PS^{U}_{m\to j}}, 1\right). \tag{5.4}$$

The module level switch stability will be the geometric mean across all attractors $PS_{m\to j}$:

$$SS_m = \left(\prod_j PS_{m\to j}\right)^{1/q_m}$$

Finally, the switch stability measure of the whole model is the geometric average of SS_m across all modules:

$$SSM = \left(\prod_m SS_m\right)^{1/M} \tag{5.5}$$

5.4 The Principle of Robust Coordination and the Switch Quality and Coordination Measure

The Principle of Robust Coordination addresses the hierarchical nature of modularity. It states that the regulatory system is a hierarchy of dynamical modules, each a robust switch *with a minimal number of radically different* attractors (phenotypes) (Figure 5.1 C). Thus, dynamical modules at higher levels of the hierarchy, themselves composed of lower-scale modules, act as robust switches between small numbers of complex phenotypes. Within the lowest-scale modules, dense regulatory interactions create a small number of robust attractors. Similarly,

inter-module connections within the modules severely restrict the number of global attractors.

We define the ***Switch-Quality*** SQ_m of module m as the normalized average Hamming distance between each pair of its attractors (0 for mono-stable circuits). To assure that even a single low-quality switch in a dynamically modular network leads to a low network-wide ***Switch Quality Measure***, we define SQM as a geometric average over the switches:

$$SQM = (\prod_m SQ_m)^{1/M}.$$

We also want to distinguish higher-level dynamical modules made of tightly interacting switches from those that are distant in the cell-wide regulatory network and barely influence each other. Loosely coupled modules give rise to dynamics that generate a variety of similar phenotype combinations (many similar global attractors). In contrast, higher-level dynamical modules govern tightly coordinated phenotype-rearrangements among all constituent modules (few, very dissimilar global attractors). To track how well the inter-switch links restrict the trivial phenotype-combinations $\prod_m q_m$ that could, in theory, coexist in the dynamical landscape, we define a ***Switch Coordination Measure***

$$SCM = [(\prod_m q_m) - q_c] / (\prod_m q_m).$$

SCM is highest in systems in which the number of global attractors, q_c, is minimal. If q_c is equal to the number of module-attractor combinations (there is no effective coupling) SCM is 0. Combining SCM, SQM, and the Switch-Quality SQ_c of the coupled system itself, we define the ***Switch Quality & Coordination Measure***,

$$SQC = SQM \cdot SQ_c \cdot SCM$$

.

5.5 Requirements of measuring AMM, SSM and SQC in arbitrary Boolean models

To summarize, calculating AMM, SSM and SQC in arbitrary Boolean networks with arbitrary switch-assignments requires four components:

1) A method to cut the network into individual switches by automatically generating reduced Boolean rules that dictate the *internal* dynamics of an arbitrary subgraph. Whenever we sever a regulatory link in a Boolean model we

have to choose which state of the severed regulator do we choose as the constant influence, as the remaining internal dynamics are not independent of the regulator's influence. An intuitive way to understand this problem is with the truth table formalism. When we sever a regulating link form a node we remove the input column of that regulator from the truth table. However, because of this, we are left with two instances for each remaining input value combination, with contradicting outputs (if we have no contradictions the remaining influences are independent of the severed regulator). Thus we have to choose, which outputs we keep for each input combination. When isolating switches the main principle is that we wish to preserve as many of the intra-module regulatory influences as possible. The implementation we chose in the case of the randomized severing of links is twofold: (i) we keep output set with the highest entropy, defined as $H_G = -p \cdot log(p) - (1-p) \cdot log(1-p)$, where p is the fraction of input combinations for which the output is 0 (ii) the remaining inputs of the node have to be functional, i.e., there exists at least one value combination among the other intra-module links for which the input in question dictates the output.

For example in the cell cycle model the Boolean rule of E2F1 (see Table 4.6) is:

E2F1* = not (CyclinA or RB) and (E2F1 or Myc).

To isolate E2F1 as part of isolating the Restriction Switch we need to sever the link coming from CyclinA, which is part of the Phase Switch. We have to choose between fixing the value of CyclinA to 0 or 1. If we choose CyclinA=1 the rule becomes trivially E2F1*= 0 and all the other regulations lose their functionality. Conversely, if we choose CyclinA=0 the rule becomes E2F1* = not RB and (E2F1 or Myc). All other regulations maintain their functionality in this rule. E2F1 is 0 in 5 out of the 8 cases, thus $p = 5/8$; the entropy of the set of possible E2F1 outputs is $H_G = 0.661$. This is greater than for the first choice, where the entropy is 0.

2) a full list of attractors for each module;

3) a full list of attractors for the full coupled system;

4) the steady state visitation probability of states and attractor basins in the coupled as well as uncoupled system of switches. In the case of synchronous noisy update the method described in 3.1.6.

5.6 The dynamical modularity of the cell cycle model – as compared to randomized versions

We calculated the three measures on the cell cycle model and got the following values: $AMM = 0.874$; $SMM = 0.905$ and $SQC = 0.446$. To validate the dynamical modularity of the empirical network we checked the values of the measures against those of randomized networks. We emphasize that dynamical modularity requires all three measures to be relatively high (or at least non-zero) to have the properties we observe on our empirical system. For example in a trivial case of a coupled system where we have no coupling links between the modules (like the left panel (A) of Figure 5.2) will have perfect AMM and SMM scores because the global attractors are just combinations of the module attractors ($AMM = 1$) and all module attractors are present in at least one global attractor ($SMM = 1$). However, in this case, the SCM and consequently the SQC will be 0 because the number of global attractors equals the product of the number of module attractors ($\prod_m q_m = q_c$). As stated earlier SSM and SQC together enforce a constraint: they require enough attractor-combinations to accommodate every module-attractor (Principle 2), but not more (Principle 3).

For the validation we performed three kinds of network randomization:

1. Complete link and rule randomization, except for the input node
2. Module id assignment randomization – randomizing which node belongs to which module (switch)
3. Randomized coupling links between cell cycle switches

In Figure 5.3 we show the measures computed on the many instances of different randomizations versus the cell cycle model.

AMM and SSM are rarely simultaneously high in random networks (blue dots). As we decrease the "entropy" of randomization by only scrambling the switch ID-s (red dots) but keeping the network structure the number of networks with relatively high AMM and SMM increases. We get even more such networks when we scramble the inter-links between the modules (the switch IDs being the same as for the cell cycle model). Randomized networks with high AMM as well as SSM are typically made of robust but loosely coupled modules, where nearly every module-attractor combination is a different global state. When AMM, SSM, and SQC are considered together (Figure 5.3 bottom), none of the random networks or randomized node assignments give rise to higher values on all three measures than the cell cycle model(large black point).

We often observe networks that score higher on two measures, but completely fail to satisfy the third (e.g., high SQC and AMM, but $SSM = 0$). This gives us confidence that our choice of switches within the Cell Cycle model is optimal. The only random networks capable of outranking the cell cycle are very rare instances within the link-randomization ensemble (larger green points).

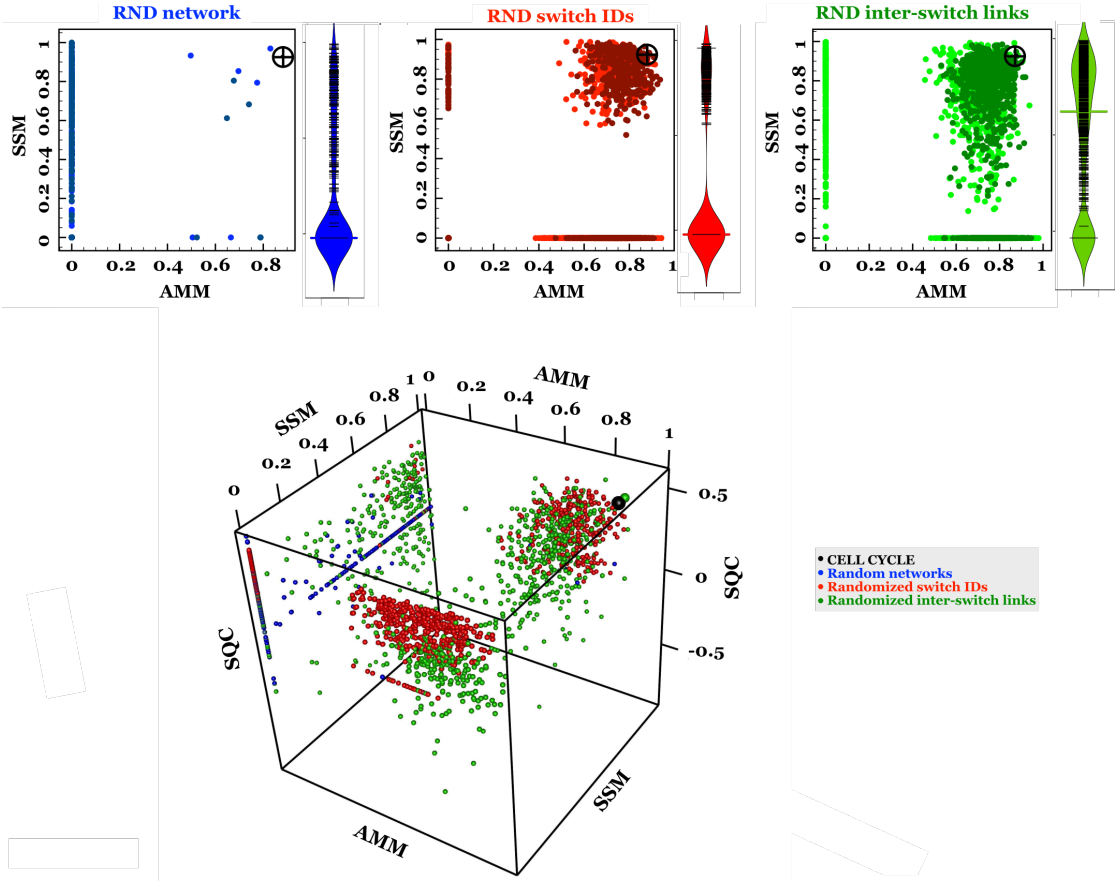

Figure 5.3. *The three dynamical modularity measures distinguish modular cell cycle models from their randomized counterparts. The dots of different colors represent different randomizations performed on the network model: black – cell cycle model; blue – random networks; red – randomized node-to-switch assignments; green – randomized links connecting the two cell cycle switches Top: Scatter plot of AMM and SSM in networks. The black circle with the cross: empirical cell cycle model. Bottom: 3D scatter plot of AMM, SSM, and SQC in randomized networks. The large black dot represents the empirical cell cycle model. The large green dot (next to the black one): 1 of 1000 random networks that outperform the cell cycle model on all three measures*

CHAPTER 6

A CIRCUIT AT THE CORE OF THE CELL CYCLE DRIVES THE CELL FROM CHECKPOINT TO CHECKPOINT

In this chapter, I am going to present the results of our collaboration following up on the cell cycle model introduced in Chapter 4. In this work, we mostly focus on a single module, the Phase Switch, and discuss a specific case when it becomes an autonomous oscillator - creating a cyclic attractor akin to a checkpoint free cell. This chapter is based on our paper titled *A feedback loop of conditionally stable circuits drives the cell cycle from checkpoint to checkpoint* co-authored with Jordan Rozum, Erzsébet Ravasz Regan and Réka Albert, published in Scientific Reports [62]. The initial main goal of our study was to understand why and how the characteristic feature of the cell cycle emerges – the global attractor of the coupled system toggles the attractors of its dynamical modules, a feature we called dynamical modularity. While doing this we discovered a feature inherent to the Phase Switch itself – it being able to robustly oscillate between the three checkpoints of the cell cycle. We call this model the *Phase Switch Oscillator* (PSO). We introduce a methodological innovation – a generalization of stable motifs, the *conditionally stable motif*, which is key in understanding both the robustness of biological oscillations as well as the mechanistic details of how dynamical modularity emerges. We use the conditionally stable motifs found in Phase Switch Oscillator to *coarse grain* the PSO into a simple 3 node higher-level model, that still keeps the main dynamic features of the PSO. The coarse-graining presented is an important step towards understanding how dynamical modularity emerges.

6.1 Three stable motifs and four conditionally stable motifs determine the three point attractors of the Phase Switch

To understand the structural causes of the toggle between the two modules of the cell cycle model, we first focused on characterizing the Phase Switch, i.e. the network among the 11 nodes already introduced in Section 4.2. For this analysis we follow the cell cycle model published in [60] and discussed in Section 4.3 in severing the inputs to the Phase Switch. Generally speaking, isolating a designated subset of a network's nodes means that only the edges that start and end at nodes of this subset are kept and the rest are deleted. For the dynamical system, the most important implication of this process is that certain influences incident on the nodes of the subset will be disregarded. In the specific case of a Boolean dynamical system in each of these nodes' regulatory functions only the terms that represent regulation from within the group are kept; the regulation that comes from outside of the group is disregarded. This isolation is a valid reflection of the original, full system if certain conditions about the disregarded regulators are satisfied. Otherwise, it is a useful approximation. (For a detailed discussion of the assumptions behind this isolation see point 1. of Section 5.5).

The interactions among the 11 nodes of the Phase Switch express either positive or negative regulatory effects mediated by protein-protein binding, complex formation, and post-translational modifications. The Phase Switch is strongly connected; all nodes within the module can be reached from all other nodes via at least one directed path. It contains both positive and negative feedback loops of various lengths. We used the expanded network formalism to express the regulatory functions of the Phase Switch (given in 4.4); Figure 6.1 depicts the resulting expanded network. We identified three stable motifs, P0 to P2, as shown in Figure 6.2. Additionally, there are four conditionally stable motifs: P3, P4, P5 and P6. Conditionally stable motifs P3 and P4 depend on the prior establishment of CyclinA=0 (which is part of the P0 motif). We represent this dependence on the prior locking in of the P0 motif as "P3|P0" and "P4|P0", respectively, in the motif label. Conditionally stable motif P5 is a stable motif only if P1 is already established (denoted P5|P1). Conditionally stable motif P6 is a stable motif only if P1 and P5 are already established (denoted P6|P5).

The stable motif succession diagram (see Section 3.2.4) of the Phase Switch (Figure 6.2) illustrates the relationship between stable motifs, conditionally stable motifs, and the three point attractors previously discussed in Section 4.2. Each of these attractors represents cells arrested before one of three checkpoints: the restriction point in G1, the DNA damage checkpoint in G2, and the spindle

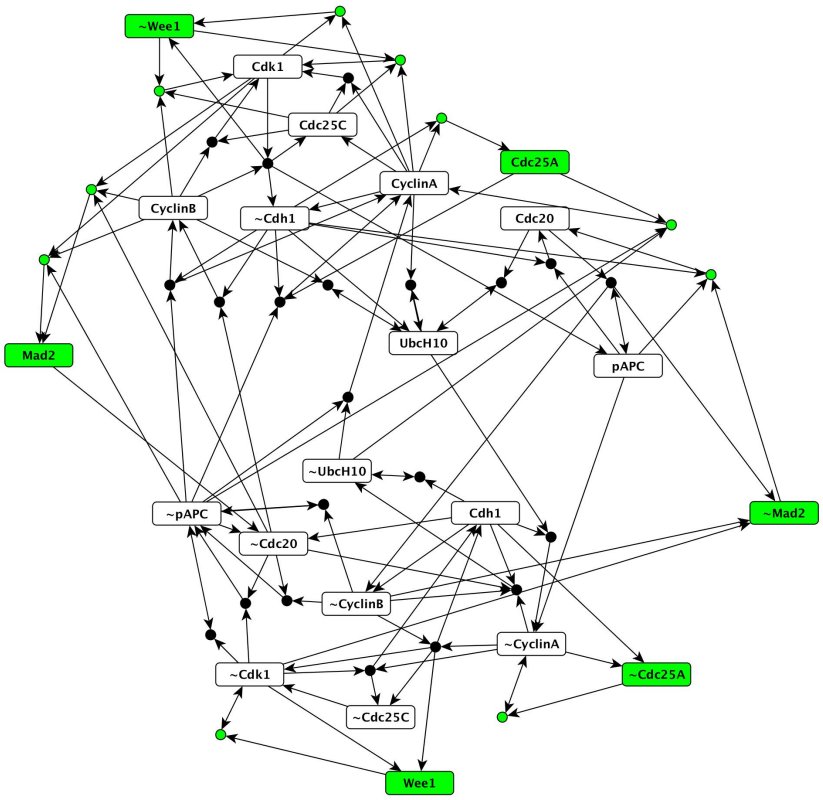

Figure 6.1. *The expanded network (see 3.2.1) of the Phase Switch model. The virtual nodes whose state later is fixed in the Phase Switch Oscillator are shown in green.*

assembly checkpoint (SAC). Each stable motif in the diagram represents a commitment to the dynamics of the switch. For instance, because in the succession diagram there is no path from P0 (i.e., the inactivation of Cdc25A and CyclinA) to the G2 state, wherein CyclinA is active, the G2 state is not attainable when P0 has been locked in. Similarly, the SAC state is not attainable when P1 is active. In the SAC state CyclinA is inactive, the CyclinB/ Cdk1 complex is active, and most importantly Mad2 is active, indicating the existence of unattached kinetochores on the cell's replicated chromosomes. The succession diagram indicates that only the SAC state is available when the P2 motif, which includes active Mad2, is locked in, consistent with the spindle checkpoint role of Mad2. Figure 6.2 thus identifies the attractors of the Phase Switch with combinations of

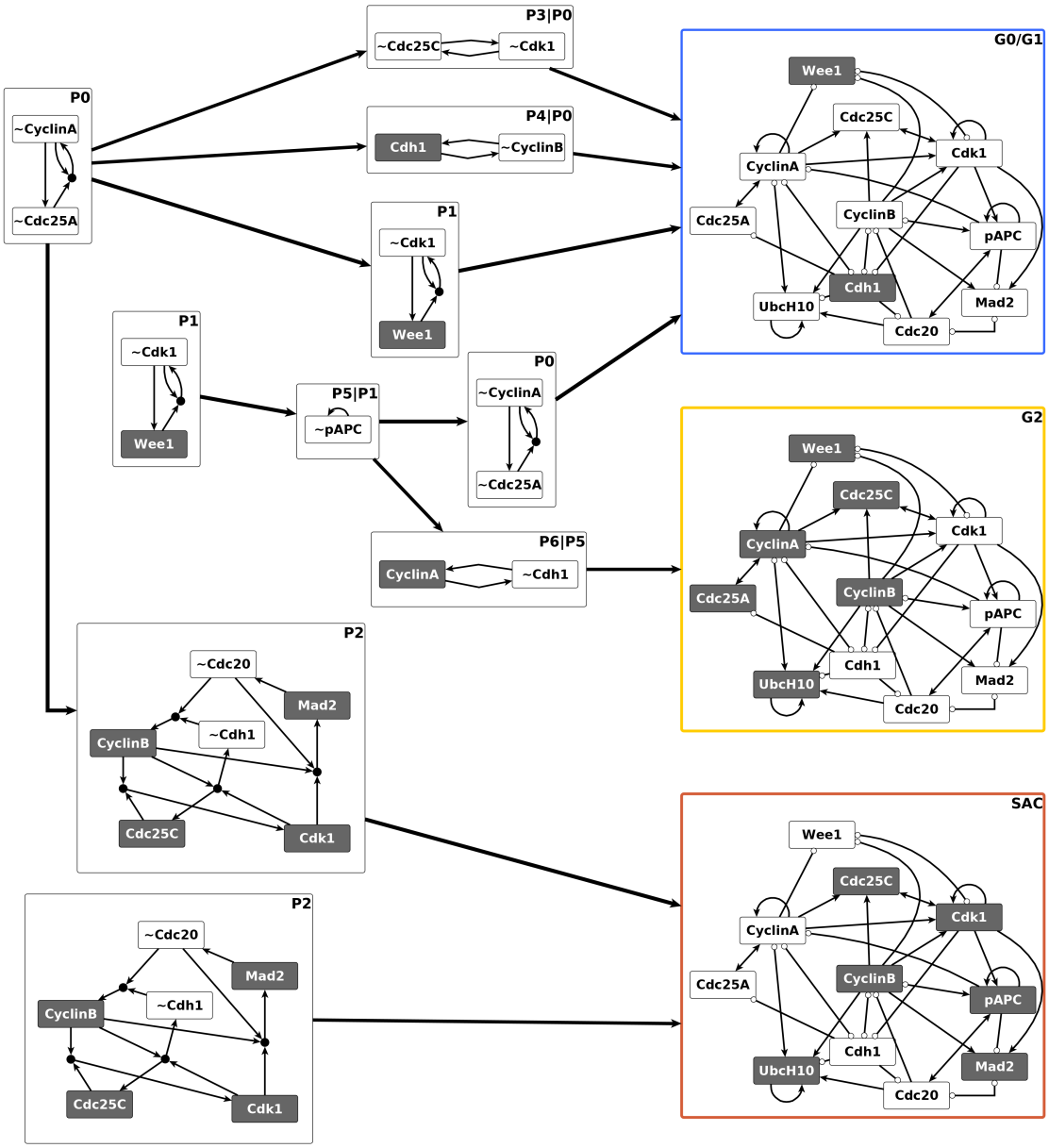

Figure 6.2. *Distinct sequences of stable and conditionally stable motifs commit the Phase Switch to its attractor states. The stable motifs are shown in the expanded network formalism where a virtual node labeled by the name of the corresponding node represents the state 1 of the node (dark grey background); a virtual node labeled by the node name preceded by ∼ represents the state 0 of the node (white background). Stable motifs P0, P1 and P2 are the stable motifs of the Phase Switch when considered in isolation. Each path in the diagram begins at one of these stable motifs, and (conditionally) stable motifs in the path are self-sustaining when those earlier in the path are locked in. Each path terminates in one of the three point attractors (G0/G1, G2, or SAC), visualized in the Phase Switch regulatory network using a white background for the off state of a node and dark grey for the on state. The outline color of the three attractors corresponds to the color-code used for differentiating the three attractors in Chapter 4*

stable motifs and conditionally stable motifs. The G0/G1 attractor of the Phase Switch is reached by multiple trajectories for which the P0 motif stabilizes together with P1, P3, or P4. Alternatively, stabilization of P0 could be paired with locking in the P2 motif to yield the SAC attractor of the Phase Switch. Finally, the combined locking in of the P1, P5 and P6 motifs yields the G2 attractor.

6.2 Stable motifs of the Phase Switch are conditionally stable motifs of the full cell cycle model

In the full cell cycle model the nodes E2F1 and CyclinE of the Restriction Switch and the three abstract nodes (Replication, Metaphase, and 4N-DNA) regulate four nodes of the Phase Switch, namely Cdc25A, CyclinA, Wee1 and Mad2 (see Figure 4.5). Because of these incident influences, the stable motifs of the Phase Switch are only conditionally stable in the context of the larger model. The stabilization of the P0 motif requires the OFF state of either E2F1 or CyclinE (see P0_CSM in Figure 6.3).

The stabilization of the P1 motif requires the ON state of the Replication node, while the stabilization of P2 requires the simultaneous OFF state of Metaphase and ON state of 4N DNA. All of these nodes are in their required states for only specific phases of the cell cycle; for example, E2F1 and CyclinE are OFF in the uncommitted state of the Restriction Switch. Because of this dependence on external regulators that are only transiently in the state necessary for stabilization, the P0, P1, and P2 motifs of the Phase Switch cannot stabilize permanently. In a dividing cell, the period during which one of these motifs maintains its stability corresponds to a cell cycle checkpoint: the P0 motif is stable before the restriction point (when E2F1 and CyclinE are inactive), the P1 motif is stable before the cell passes the G2 DNA damage checkpoint, and the P2 motif is stable before the cell passes the spindle assembly checkpoint [52]. The passage of each checkpoint changes the inputs to the Phase Switch such that the corresponding motif becomes unstable. To explore what alternative behaviors remain in the attractor repertoire of the Phase Switch, we consider an *extreme scenario for stabilization*. Namely, we assume that all three checkpoints are satisfied, which causes the stabilization of Cdc25A, Wee1 and Mad2 in the state opposite of their states in the stable motifs of the Phase Switch (see the left side of the bottom panel of Figure 6.3), and thus destabilizes all three stable motifs. The resulting system, shown on the right side of the bottom right panel of Figure 6.3, operates without any checkpoint control. This circuit shares some similarities with the network responsible for cell cycle progression in mammalian embryonic stem cells, in that it doesn't have a restriction point [72]. In embryonic stem

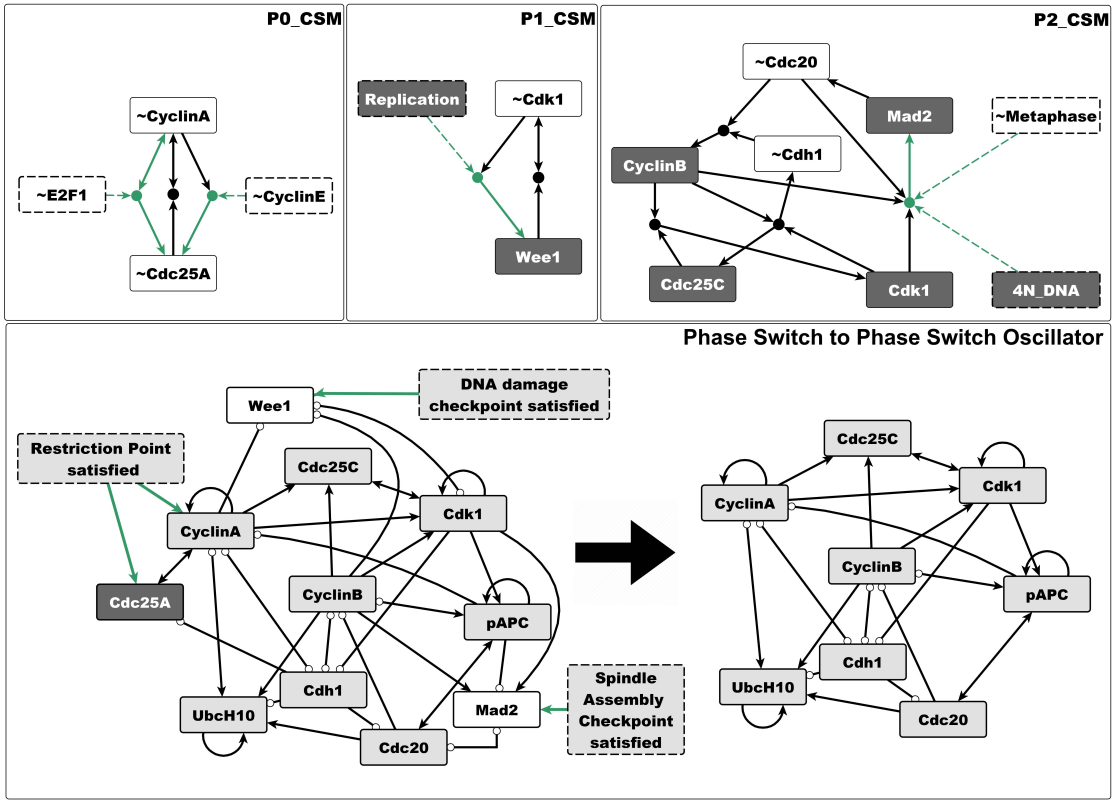

Figure 6.3. *The stable motifs of the Phase Switch become conditionally stable motifs in the larger context of the cell cycle model. Due to the influences from the rest of the cell cycle network on Cdc25A, CyclinA, Wee1, and Mad2 (shown with green lines), the P0 motif turns into two conditionally stable motifs which differ only in their condition (∼E2F1 or ∼CyclinE, respectively, see top left panel). The P1 motif can only stabilize if the abstract node Replication is ON. P2 can only stabilize if the abstract regulator Metaphase is OFF and 4N DNA is ON simultaneously (top right panel). The Phase Switch Oscillator (bottom right) is obtained from the Phase Switch (bottom left) by assuming that the restriction point, DNA damage checkpoint and spindle assembly checkpoint are satisfied, which implies that Wee1 = Mad2 = 0 and Cdc25A = 1. As in Figure 6.2, dark grey node background indicates the ON state of the node and white background refers to the OFF state.*

cells, E2F1, Cyclin E/Cdk2 and Cdc25A are continuously active in a cell cycle-independent manner [73], allowing these cells to cycle continuously [74]. Contrary to the network driving embryonic stem cell division, the small circuit in Figure 6.3 (right side of bottom panel) also lacks DNA damage and spindle assembly checkpoint. Thus, the checkpoint-free version of the Phase Switch captures the functioning of the cell cycle when (and only when) all checkpoints are cleared without difficulty or pause. After locking Cdc25A ON, and Wee1 and Mad2 OFF, the Phase Switch module is reduced to eight nodes and 28 edges. It is still strongly connected and contains positive and negative cycles of various lengths (right side of the bottom panel of Figure 6.3). Destabilizing the stable motifs of the Phase Switch might be expected to create a set of complex attractors, some of which may be dependent on the update scheme. Interestingly, we find a single limit cycle attractor of 9 states using synchronous update (Figure 6.4), and a single 141-state complex attractor under asynchronous update. All remaining states (out of the $2^8 = 256$ states of this 8-node system) converge to the limit cycle / complex attractor. This shows that this dynamical system's long-term behavior is a sustained oscillation. In recognition of this fact, we refer to this modified system as the Phase Switch Oscillator (PSO).

6.3 The Phase Switch Oscillator traces a robust cyclic trajectory through the three attractors of the Phase Switch

To evaluate to what extent the PSO's long-term dynamics depend on stochasticity, we sampled the most frequently visited states of the complex attractor corresponding to general asynchronous update, and overlaid the synchronous limit cycle on the resulting state transition graph (Figure 6.5).

We found that the PSO's synchronous and asynchronous attractor follow similar paths along the cell cycle. Both pass through a state in which all the nodes of the Phase Switch are inactive, except for Cdh1; this is reflective of a quiescent cell or the early G1 phase of a cycling cell. Both trajectories also visit a state wherein CyclinA, CyclinB, and Cdk1 are ON. Cells in this state have just cleared the G2 DNA damage checkpoint (hence Cdk1 is active), but have not yet moved on to the SAC. Thus we denote it "post-G2". In contrast, the state corresponding to a G2-arrested cell in which Cyclin A and B are expressed but Cdk1 is not yet ON (denoted G2) is only visited by one of three robust paths along the asynchronous complex attractor. The synchronous limit cycle updates three nodes in parallel during this step, and thus skips over the G2-arrested state. Following the post-G2 state, both attractors go through a state preceding the

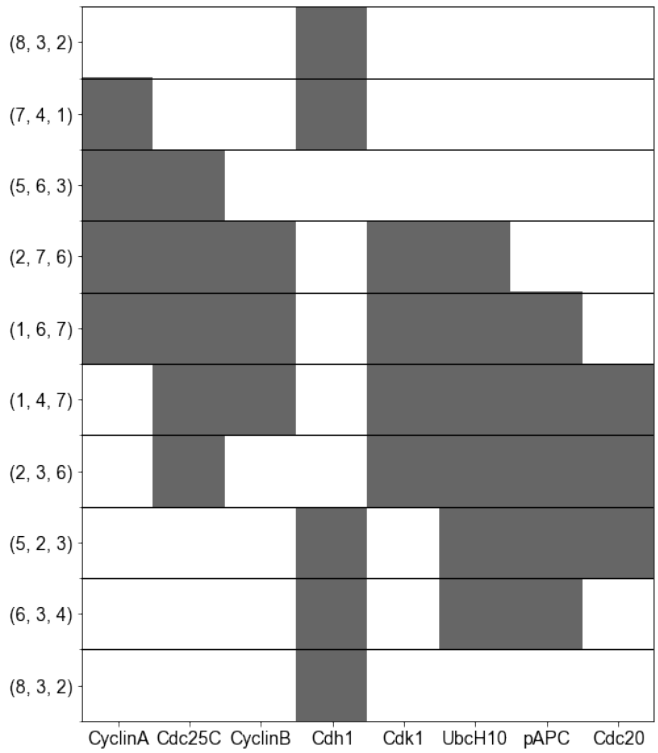

Figure 6.4. *The limit cycle of the Phase Switch Oscillator under synchronous update. Each column of squares indicates the states of the node written below the column. Each row corresponds to a state of the system. To use an identifier that is more economical than indicating the state of all 8 nodes, we describe the state by its overlap with the three attractors, in the order (G0/G1, G2, SAC). Each pair of successive rows (from the top down) indicates a single synchronous update, i.e. applying the regulatory functions on the first state gives the second state. A dark grey square indicates the ON (1) state of the node indicated below the column and white means OFF (0).*

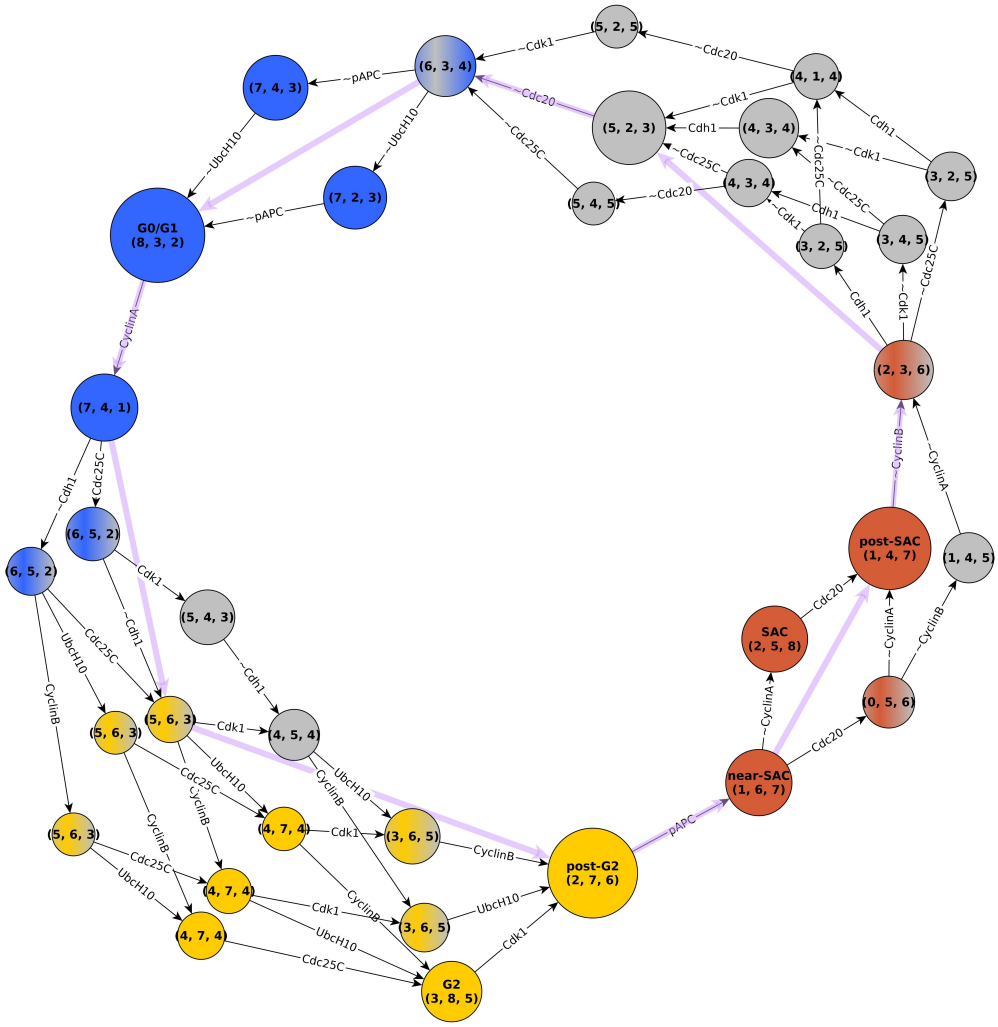

Figure 6.5. *State transition graph (STG) representation of the complex attractor of the Phase Switch Oscillator. Each circle represents a state of the Phase Switch Oscillator, which is made up of the states of all the 8 nodes. The node sizes represent the visitation probabilities of the corresponding states (see Section 3.1.5. States with visitation probability less than 0.5% are omitted. To provide a clear identifier without indicating the state of each node, each state of the system is labeled with its overlap with the three Phase Switch attractors, in the order G0/G1, G2, SAC (see Methods). If a system state overlaps one of the three attractors in 7 or 8 node states (more than 87% overlap), the node is colored with the color representing the relevant attractor, namely blue for G0/G1, yellow for G2 and brown for SAC. System states that have an overlap of less than 6 with an attractor are shown in grey. If the overlap is 6 the state is colored with a combination of grey with the color of the respective attractor. The color combinations mirror the transitions between the phases. Some important states are marked by a label representing the closest phenotype. Each edge label shows the node that changes state in the respective transition; if the node name is preceded by $\sim$ the node turns OFF, otherwise it turns ON. For simplicity, we omit the self-loops that correspond to the cases where a node state is re-evaluated but does not change. The state transitions corresponding to the synchronous update are shown in purple.*

spindle assembly checkpoint wherein CyclinA has not yet degraded (which we denote "near-SAC"), as well as a state where Cdc20 has already turned OFF (which we denote "post-SAC"). Here too, the state closest to that of a cell arrested at the SAC (thus matching the SAC attractor of the Phase Switch) is only visited by the complex attractor; Cyclin A degradation and Cdc20 activation co-occur in the synchronous model. Table 6.1 lists the state of all nodes in these labeled states.

	Cdc25C	CyclinA	Cdk1	CyclinB	Cdh1	pAPC	Cdc20	UbcH10	Mad2	Wee1	Cdc25A	
The attractors of the Phase Switch												
G0/G1	0	0	0	0	1	0	0	0	0	1	0	
G2	1	1	0	1	0	0	0	1	0	1	1	
SAC	1	0	1	1	0	1	0	1	1	0	0	
The states of the Phase Switch Oscillator closest to the attractors of the Phase Switch												Passing Prob
G0/G1	0	0	0	0	1	0	0	0	0	0	1	1
G2	1	1	0	1	0	0	0	1	0	0	1	0.33
SAC	1	0	1	1	0	1	0	1	0	0	1	0.55
The most likely closest states of the Phase Switch Oscillator												
G0/G1 (8,3,2)	0	0	0	0	1	0	0	0	0	0	1	1
Post-G2 (2,7,6)	1	1	1	1	0	0	0	1	0	0	1	0.89
near-SAC (1,6,7)	1	1	1	1	0	1	0	1	0	0	1	0.94

Table 6.1. *Phase Switch Oscillator states closest to Phase Switch attractors Top: The three fixed point attractors of the Phase Switch. Middle: the states of the Phase Switch Oscillator (wherein the states Wee1=Mad2=0 and Cdc25A=1, highlighted in gray, are fixed) that most closely approach the Phase Switch attractors under asynchronous update. The states closest to the G2 and SAC attractors are visited by part of the trajectories of the complex attractor (see Figure 6.5). Bottom: the states that almost every asynchronous trajectory of the complex attractor will cross and are as close as possible to one of the three Phase Switch attractors. These three states also lie along the synchronous limit cycle. The rightmost column, labelled passing probability, represents the likelihood of complex attractor trajectories passing through the state given in the row.*

The passing probability estimates in the rightmost column are based on the filtered complex attractor shown in Figure 6.5 for the middle table, and the backbone shown in Figure 6.6 for the bottom table. The actual probabilities are somewhat smaller due to small probability shortcuts, see Figure 6.6 and Supplementary Table 10.1. The G0/G1 state in the middle and bottom table is the same.

The close agreement between the asynchronous complex attractor and the synchronous limit cycle is surprising because consecutive states of the synchronous state transition graph differ in up to three node states (multiple nodes can change state during one synchronous update), while the edges of the asynchronous state transition graph always represent changes in a single node (indicated as edge labels in Figure 6.5). The loss of synchronicity between node state changes could have induced a dramatic departure from the synchronous

limit cycle, as was observed in a previous Boolean model of the mammalian cell cycle by Fauré et al. [51]; only after partially restoring synchronicity did the Fauré et al. model yield near-cyclic trajectories. Remarkably, in the case of the PSO the vast majority of the paths in the asynchronous attractor follow the synchronous limit cycle and robustly adhere to its temporal ordering of states. (For details: Supplementary Figure 10.1 compares the distribution of consecutive ON and OFF durations of each node with the case of a cycle in which each node switches state twice.)

Figure 6.6 compactly summarizes this agreement in a "backbone" representation of the complex attractor. To quantify how closely the asynchronous dynamics adheres to the synchronous cycle, we computed the aggregated probability of all paths of the asynchronous state transition graph (STG) that start and end at the states of the synchronous limit cycle without visiting other states of the limit cycle; these probabilities are indicated as edge labels in the network on the right panel in Figure 6.6.

Asynchronous update paths between limit cycle states that are not adjacent in the synchronous STG are deemed "shortcut transitions"; these transitions mix the node state changes involved in multiple steps of the synchronous update. A comprehensive list of the probability of all shortcut transitions is given in Supplementary Table 10.1. Despite the random update order of the asynchronous update, only six shortcut transitions have a probability higher than 0.05. In conclusion, despite the large variability of possible trajectories in a general asynchronous system, the emergent cycle of activations and deactivations in the PSO is remarkably deterministic.

6.4 The Phase Switch Oscillator contains a cycle of conditionally stable motifs that sequentially stabilize each other and cause their own destabilization

To understand what causes the robustness of the oscillation and the sequential approach of the Phase Switch attractors we analyze the expanded network (defined in Section 3.2.1) of the PSO, which encapsulates both the topological and logical features of the regulatory network.

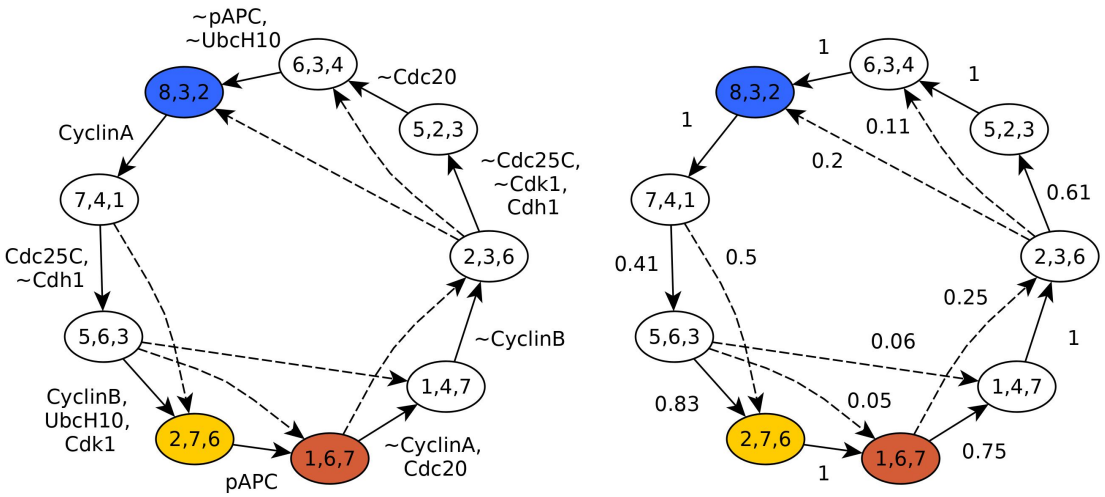

Figure 6.6. *The shared backbone of the synchronous limit cycle and asynchronous complex attractor. The nodes represent the nine states of the synchronous limit cycle (the nodes connected by purple edges in Figure 6.5; the node labels indicate the overlap of the corresponding state with the three Phase Switch attractors (in the order G0/G1, G2, SAC). The solid edges represent single state transitions obtained by the synchronous update. These state transitions also appear in the asynchronous state transition graph, either as edges or as paths. The dashed edges indicate cases where paths exist in the asynchronous state transition graph that skip a state visited by the synchronous state transition graph. The states marked in blue, yellow, and brown indicate the states closest to the G0/G1, G2, and SAC attractors, respectively. In the left panel the edge labels indicate the nodes that change state during the corresponding transition; nodes whose name is prefaced by ∼ turn OFF, the rest turn ON. For each synchronous state transition, the asynchronous state transition graph contains a path that corresponds to sequential state changes of the same nodes. In the right panel the labels on the state transition edges indicate the probability of the state transition when using asynchronous update. State transitions with a probability of less than 0.05 are omitted from this figure.*

6.4.1 Topological analysis of the expanded network of the Phase Switch Oscillator

As we describe in Section 6.2, we obtain the Phase Switch Oscillator from the Phase Switch by assuming that the conditions of the three cell cycle checkpoints (the restriction point, the DNA damage checkpoint and the spindle assembly checkpoint) are satisfied. Another, practical way of doing the same is to start from the isolated Phase Switch and fix the states Cdc25A = 1, Wee1 = Mad2 = 0. Each of these states contradicts one of the three stable motifs of the Phase Switch (see Figure 6.2). The virtual nodes corresponding to these fixed node states have out-edges only to composite nodes, thus no further node states stabilize as a direct consequence of their stabilization (see Figure 6.1). Moreover, these fixed node states do not create new stable motifs. In the Phase Switch model there is only one alternative combination of fixed node states that eliminates the original stable motifs and does not create new ones: Cdc25A=1, Cdk1=1, Mad2=0. This alternative combination has the same biological meaning as the one we considered.

The expanded network of the Phase Switch Oscillator contains 16 virtual nodes and 21 composite nodes as shown in Figure 6.7. Its 72 edges form 31 sufficient relationships between virtual nodes, each of which is either direct or mediated by a single composite node. Each of these sufficient relationships appears as a disjunctive ("or"-separated) clause in the regulatory function of the target node. For example, as shown in Table 4.4, the regulatory function of Cdc25C is f_{Cdc25C}= CyclinA or (CyclinB and Cdk1). Both terms separated by the "or" operator, i.e. "CyclinA" and "CyclinB and Cdk1" indicate a sufficient regulatory relationship, meaning that either the activity of CyclinA, or the simultaneous activity of CyclinB and Cdk1 can cause the activation of Cdc25C. Consequently, Cdc25C (a green-highlighted node in the top part of the expanded network in Figure 6.7) has two incoming edges, one from CyclinA and one from a composite node that in turn has two incoming edges, one from CyclinB and one from Cdk1. The average in-degree of the expanded network is less than two, markedly smaller than the average in-degree of the original Phase Switch Oscillator network, which is 3.5. This illustrates that regulators need to cooperate to induce state changes in target nodes [75, 76]. The whole expanded network is an *oscillating motif* (see Section 3.2.2): it is strongly connected, it is composite-closed, it contains the complementary of each virtual node, and it does not have any stable motifs.

As shown in Figure 6.8, the expanded network has more than 6000 cycles (closed paths with non-repeating virtual or composite nodes), the vast majority of which are inconsistent (i.e. they contain an internal contradiction either in the virtual or composite nodes of the cycle; see orange nodes and edges in Figure

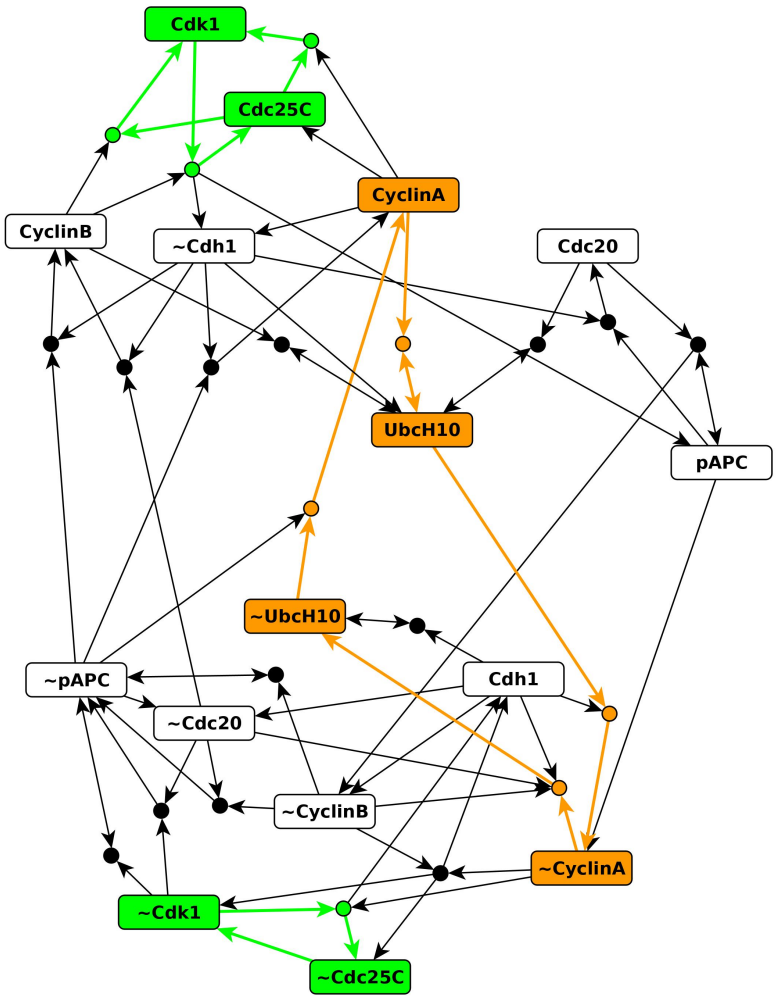

Figure 6.7. *The expanded network of the Phase Switch Oscillator embodies the logic relationships that drive its oscillating behavior. Colored nodes and edges highlight two characteristic subgraphs of the expanded network. The green nodes and edges indicate the subgraphs corresponding to the positive feedback loop between Cdk1 and Cdc25C (bidirectional edge in Figure 6.3 bottom panel). There are two overlapping cycles (i.e. closed paths with non-repeating virtual or composite nodes), both of length four. Each cycle involves Cdk1, Cdc25C, and two composite nodes (one shared by both cycles). These cycles indicate that the positive feedback can only sustain the on (1) state of Cdk1 and Cdc25C if CyclinB (for one of the cycles) or both CyclinA and CyclinB (for the other cycle) are also simultaneously on. There is a consistent cycle formed by ∼Cdk1, ∼Cdc25C and a composite node that receives input from ∼CyclinA; this means that Cdk1 and Cdc25 can simultaneously sustain their off (0) state if CyclinA is also off. Positive feedbacks form two disjoint (groups of) cycles. Each of these cycles is consistent. The disjoint cycles have opposite states and can have different conditions. The orange nodes and edges highlight the subgraph that corresponds to the negative feedback loop (bidirectional edge) between CyclinA and UbcH10 (Figure 6.3 bottom panel). In general, negative feedback loops result in a cycle in the expanded network involving both states of the involved nodes; we call this type of cycle an inconsistent cycle.*

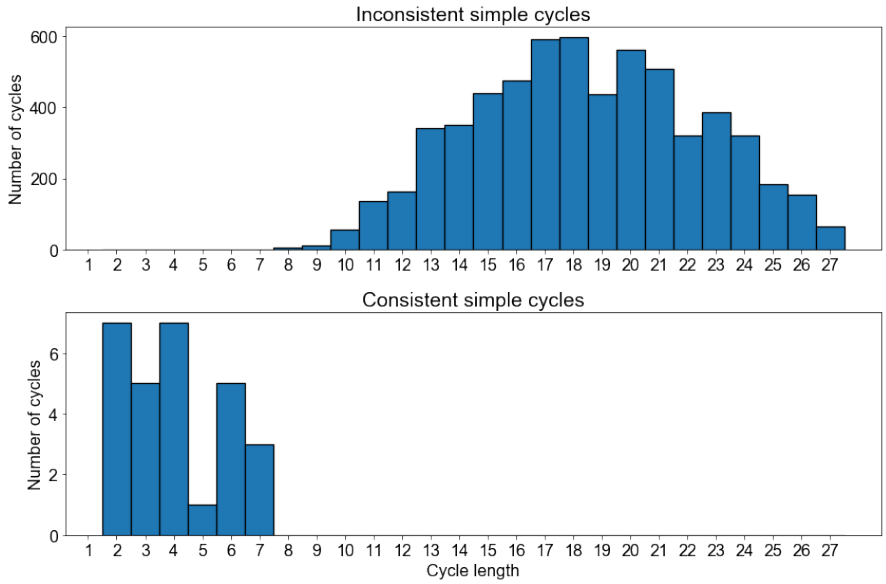

Figure 6.8. *Distribution of the length of consistent (bottom) and inconsistent (top) cycles on the expanded network. As illustrated by the green nodes and edges in Figure 6.7, consistent cycles correspond to positive feedback loops in the regulatory network. They are the building blocks of conditionally stable motifs. We define inconsistency as the involvement of two opposite states of the same node, either as virtual nodes or as determinants of a composite node. Inconsistent cycles are akin to traversing a negative feedback loop of the regulatory network twice (as illustrated by the orange nodes and edges in Figure 6.7)*

6.7). There are 28 consistent cycles (similar to the green cycle in Figure 6.7), all of which have fewer than 8 nodes. All the inconsistent cycles have 8 or more nodes. This difference in cycle sizes indicates that more conditions (in terms of the state of other nodes) need to be satisfied to ensure the oscillation of a node than a sustained state of a node in the Phase Switch Oscillator. In other words, nodes must rely on each other to achieve a sustained oscillation. Supplementary Figure 10.2 indicates examples of minimal subgraphs through which a virtual node (in combination with other virtual nodes) can induce its own negation.

6.4.2 Conditionally stable motifs that sequentially stabilize each other and cause their own destabilization

To summarize the details of this analysis are described in 6.4.1, we find that the whole expanded network is an oscillating motif: it is strongly connected, it is composite-closed, it contains the complementary of each virtual node, and it does not have any stable motifs. While all virtual nodes participate in this oscillating motif, their contributions to the connectivity of the oscillating motif are not equal: CyclinA, pAPC and Cdh1 are the strongest contributors and Cdc25C, ∼Cdc25C and ∼UbcH10 are the weakest. Parsing the logic sufficiency and necessity relationships embodied in the expanded network explains the trajectories of the state transition graph. The fact that the whole expanded network is a single oscillating motif explains why the PSO does not have point attractors, but by itself does not explain why there is a single complex attractor and why it is so close to a cycle. As a next step toward answering these questions, we identified all conditionally stable motifs (CSMs) in the PSO that have a single condition. These are depicted and labeled in Figure 6.9.

The smallest CSM is a node that can maintain its state with the help of another node. This situation appears in the expanded network as a virtual node that has an edge pointing to a composite node and receives an edge from the same composite node. The composite node's other regulator serves as the condition for the CSM. There are two such nodes, pAPC and UbcH10; both virtual nodes of each form CSMs (C6, C8, C12 and C13 in Figure 6.9). Other elementary CSMs of the Phase Switch Oscillator contain two or three virtual nodes that form one or more cycles. Several elementary CSMs overlap in yet larger CSMs, indicating that satisfying a single condition can often stabilize relatively large subnetworks. Four CSMs of the Phase Switch Oscillator coincide with the four CSMs of the Phase Switch: C0 is the same as P3, C1 coincides with P4, C6 is P5, and C9 coincides with P6, respectively (compare Figure 6.2 with Figure 6.9). The CSM C11 includes four of the five virtual nodes of the P2 stable motif (only Mad2, which is not present in the PSO, is absent); thus the C11

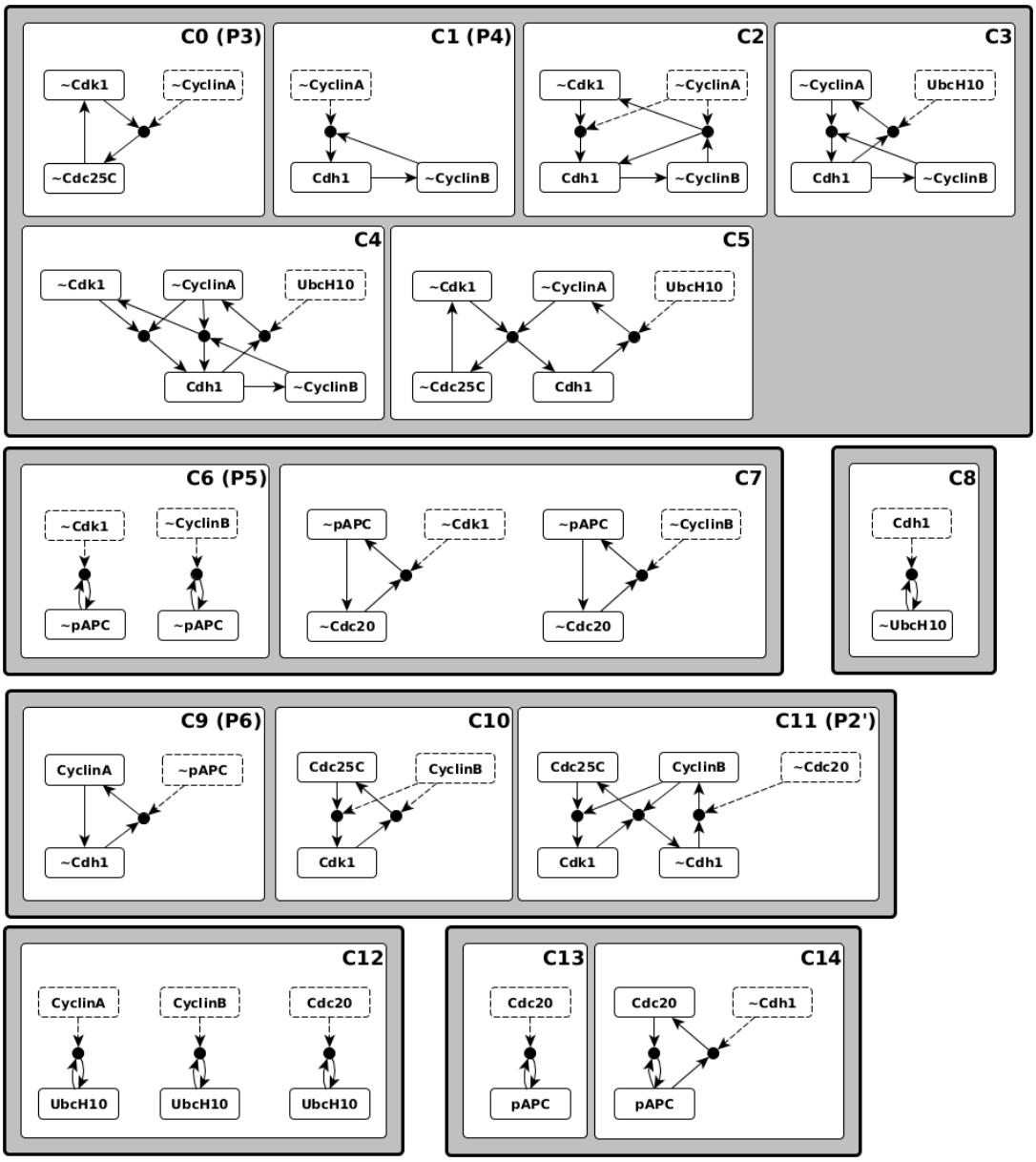

Figure 6.9. *Conditionally stable motifs of the Phase Switch Oscillator (PSO). Conditionally stable motifs are represented here as subgraphs of the expanded network of the PSO. Virtual nodes with a dashed outline represent the conditions. The labels in the top right corner of the white boxes indicate the name of the conditionally stable motif as well as the corresponding Phase Switch motif. Multiple motifs in the same white box (e.g. C7) consist of the same virtual nodes but with different conditions. The grey boxes around groups of white boxes illustrate that CSMs with shared states naturally fall into groups.*

(P2') notation. This preservation of conditionally stable motifs indicates that the PSO's dynamic trajectory can at least transiently visit the attractors of the Phase Switch. Additionally, the PSO has CSMs that are not present in the Phase Switch; notably, C14, which contains pAPC=1 together with the Cdc20=1 state absent from all three attractors of the Phase Switch. The activation of this conditionally stable motif represents the activation of the pAPC/Cdc20 complex, which starts chromosome separation [77] (also discussed in Section 4.2).

Inspection of the single-condition CSMs in Figure 6.9 suggests merging multiple overlapping CSMs into larger CSMs. One large group unites conditionally stable motifs C0-C5 and is composed of the virtual nodes ∼CyclinA, ∼CyclinB, ∼Cdk1, ∼Cdc25C, and Cdh1. Strikingly, these virtual nodes' complementary nodes, i.e., CyclinA, CyclinB, Cdk1, Cdc25C, and ∼Cdh1, also form an overlapping group of conditionally stable motifs, namely C9-C11. For a detailed view of the interactions of the overlapping CSMs see Figure 6.10.

We denote the CSM composed of this latter group of virtual nodes "Cyc", as it corresponds to the activation of the key cyclins. Similarly, we name the CSM formed by the merger of C0-C5 "∼Cyc", as it represents the inactivation of the key cyclins and is complementary to the Cyc CSM. The overlapping CSMs C6 and C7 can also be merged to create a larger CSM that contains the virtual nodes ∼Cdc20 and ∼pAPC. This merger has a complementary counterpart in the union of the C13 and C14 CSMs. We call the C13-C14 merged CSM "Cyclosome" in reference to the Cdc20-bound APC/C complex known as the cyclosome. Its complement, the C6-C7 merger, is called "∼Cyclosome". Finally, the various forms of C12 can be merged to form a larger CSM containing only UbcH10 as a state, while the CSM C8 acts as the complementary CSM. As these contain only UbcH10 and ∼UbcH10 as states, we refer to these CSMs by the names "UbcH10" (C12) and "∼UbcH10" (C8). We note that these six merged CSMs are the six largest CSMs in the expanded network.

The merged CSMs and their regulators are depicted in Figure 6.11 as expanded networks. Each of the six boxes in Figure 6.11 graphically indicates the regulatory functions for each node of the corresponding CSM. Thus, each box indicates the states of the regulators for which all the nodes of the CSM will achieve their corresponding state. Regulators whose states serve as conditions of the CSM are shown in dashed outline, while regulators that are outside the CSM (able to influence it but not necessary for stabilization) are shown in the dash-dotted outline. An important feature shared by several CSMs of the Phase Switch Oscillator is that they cause the deactivation of their own conditions. In other words, the sustained activity of the virtual nodes in these CSMs eventually leads to the activation of virtual nodes that contradict the states of the CSM conditions.

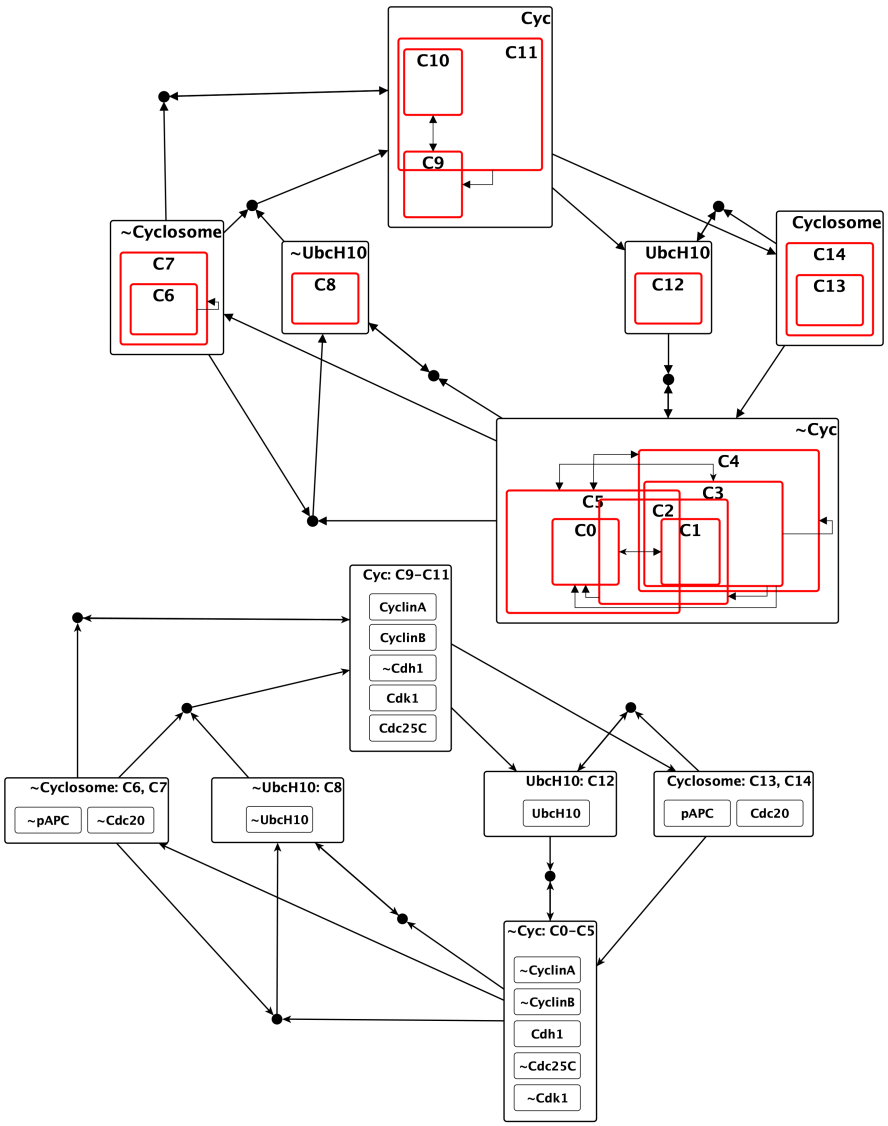

Figure 6.10. *Two complementary views of the relationships among conditionally stable motifs of the Phase Switch Oscillator. The information content of this figure is the same as that of Figure 6.11; by showing two additional views we aim to better communicate the information. In the top panel each black rectangle represents a group of conditionally stable motifs (CSMs), each of which is shown as a red rectangle. The overlaps between red rectangles illustrate that the CSMs share virtual nodes. The CSMs also activate each other, indicated as arrows between red rectangles. In the bottom panel the same groups of CSMs are characterized by the virtual nodes that participate in each. It is thus apparent that the complementary nodes of a group also form a group. Edges among groups of CSMs are defined based on the logic implication between them. For example, the virtual nodes of Cyc are sufficient to activate the virtual nodes of Cyclosome, as can be seen from the last two rows of Figure 6.11. The virtual nodes of ∼Cyclosome together with ∼UbcH10 are sufficient to activate Cyc, as shown in the second and third rows of Figure 6.11. Collapsing each black rectangle into a single meta-node makes the two panels identical, and also identical to the middle panel of Figure 6.12.*

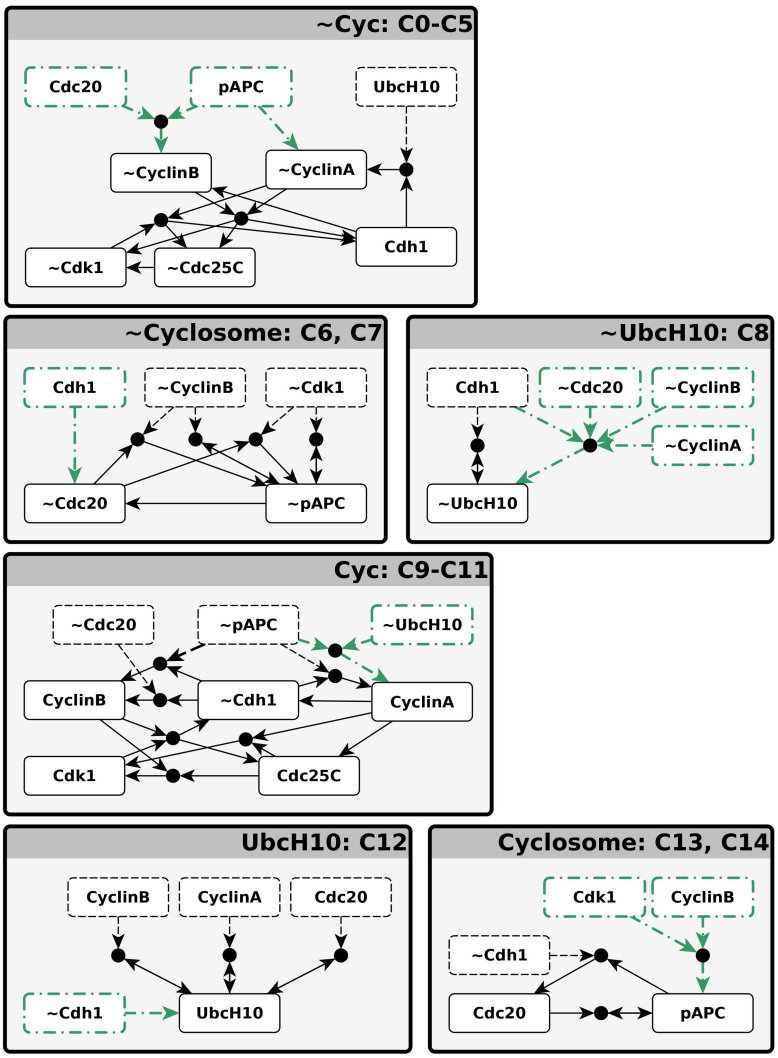

Figure 6.11. *The logical relationships between conditionally stable motifs (CSMs) of the Phase Switch Oscillator. The fifteen single-condition CSMs fall into six groups of overlapping CSMs, indicated by the boxes labeled Cyc, ∼Cyc, Cyclosome, ∼Cyclosome, UbcH10, and ∼UbcH10. The union of the CSMs in each group is depicted as a subgraph of the expanded network within each of the boxes. The box labels list the CSMs that are merged in each case; the six CSM groups correspond to those of Figure 6.9. Within each box, black dashed lines indicate the conditions of the merged CSM and the green dash-dotted lines indicate regulation external to CSMs (not required for its stabilization). Importantly, the sustained activity of each row of boxes leads to activation of the next row (with the last row looping back to the first).*

We determine the logical implications of the stabilization of the states of a conditionally stable motif (CSM) using the concept of the logic domain of influence (LDOI). The LDOI of a given "seed" set of virtual nodes is the set of node states that are causally stabilized by the seed set when it is held fixed [78]. We used the LDOI identification algorithm developed by Yang et al., available at https://github.com/yanggangthu/BooleanDOI. In this algorithm the LDOI is defined and built via an iterative process on the expanded network, beginning with the empty set. On each iteration, every child node of every virtual node in the seed set is considered (breadth-first) and added to the LDOI set if the child node does not contradict any nodes in the seed set and either 1) the child node is a virtual node or 2) the child node is a composite node and all its parent nodes are already in the set. This process is continued, considering child nodes of the nodes already included in the LDOI until no new nodes can be added. The LDOI of a stable motif includes the motif itself and no contradictions. We found that the LDOI of five CSMs includes the complementary of the virtual node that serves as the condition of the CSM. This means that the CSM sooner or later leads to a contradiction with its own condition, thus to its own deactivation. These five CSMs are indicated in Supplementary Table 10.2. Also, Supplementary Figure 10.2 illustrates the LDOI of CSM 3 on the expanded network.

The merged CSMs have the same self-destabilizing properties. For example, by examining Figure 6.11, one can determine that sustained activity of the ∼Cyc CSM (C0-C5) eventually leads to activation of the ∼Cyclosome CSM (C6-C7) because the five virtual nodes within ∼Cyc contain the two conditions (nodes with dashed outlines) and the external regulator (in dash-dotted outline) necessary to activate the two virtual nodes of ∼Cylosome. The five virtual nodes within ∼Cyc are also sufficient to activate ∼UbcH10 (C8). The CSMs ∼Cylosome and ∼UbcH10 contradict all the conditions and external regulators of ∼Cyc. Indeed, the sustained activity of ∼Cyclosome and ∼UbcH10 eventually leads to the activation of Cyc, which contradicts ∼Cyc in every virtual node. Similar relationships exist between each row of Figure 6.11 and the row below it (or between the bottom row and the top row).

6.5 A higher-level network of three nodes qualitatively replicates the oscillation

It is possible to make the relationships between the six CSMs of Figures 6.10 and 6.11 precise by designating a new Boolean variable for each complementary pair of the merged CSMs. Each of the six CSMs can thus be viewed as a virtual

node, corresponding to one of two states of a corresponding meta-node. We label these three meta-nodes Cyc, Cyclosome, and UbcH10. The higher-order logic of the CSM meta-nodes can be distilled into the regulatory functions:

$f_{\text{Cyc}} =$ (not Cyclosome and Cyc) or (not Cyclosome and not UbcH10)

$f_{\text{Cyclosome}} =$ Cyc

$f_{\text{UbcH10}} =$ Cyc or Cyclosome and UbcH10

These regulatory functions express the following logical relationships: Cyclosome and UbcH10 inactivate Cyc; the only possibility for Cyc activation is the simultaneous inactivity of both Cyclosome and UbcH10. Existing Cyc activity can be maintained if Cyclosome is inactive. Cyc is sufficient for the activation of Cyclosome and UbcH10. UbcH10 activity can also be sustained if Cyclosome is active. Figure 6.12 illustrates the regulatory and expanded networks of meta-nodes as well as the corresponding STG.

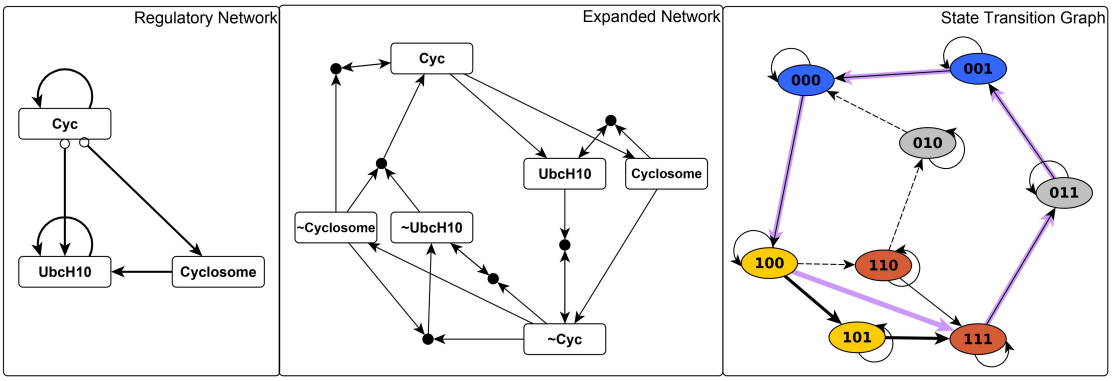

Figure 6.12. *The logical relationships that determine the transitions of the PSO can be effectively illustrated by defining aggregated meta-nodes for overlapping conditionally stable motifs. The Cyc meta-node contains CyclinA, CyclinB, Cdc25C, Cdk1, and ∼Cdh1. The Cyclosome meta-node includes the virtual nodes pAPC and Cdc20. The complementary node (negation) of a meta-node includes the complementary nodes of the meta-node's constituent virtual nodes. The first two panels indicate the regulatory and expanded network of meta-nodes. The panel on the right shows the state transition graph of the meta-node network. In this panel, the labels of each state are in the order Cyc, Cyclosome, UbcH10. Node background color indicates the states closest to the attractors of the Phase Switch: blue for G0/G1, yellow for G2, brown for SAC. The synchronous cycle is shown by purple edges. The asynchronous complex attractor is made up of two cycles of unequal size, but each of which approaches the three attractors in the same order. The difference between the two cycles is whether UbcH10 activates and then deactivates (longer cycle) or stays inactive (short cycle with dashed edges). This latter process has a very low probability.*

The resulting regulatory network relating the three meta-nodes preserves

certain structural properties of the regulatory network of the PSO. Most importantly, all negative feedback loops between nodes in the PSO are represented as negative feedback loops between meta-nodes, while each positive feedback loop in the PSO is internal to exactly one meta-node (or is represented explicitly as a positive self-loop). The higher-order regulatory logic of the CSM meta-nodes explains the PSO's cycling between states close to the G0/G1, G2, SAC attractors, as shown in the right panel of Figure 6.12. The G0/G1 state corresponds to the inactivity of all three meta-nodes. This is not an attractor; inactivity of pAPC and Cdc20 implies that Cyc will activate. When this is achieved, the system is closest to the G2 attractor of the original Phase Switch. Next, the activity of Cyc drives the activation of UbcH10 and Cyclosome in a stochastic order. The probability of UbcH10 turning on before Cdc20 and pAPC, and thus activating the UbcH10 meta-node before the Cyclosome meta-node, is at least 0.98 (see Supplementary Table 10.1). The rare case in which Cyclosome activates before UbcH10 leads to a path of state transitions (shown with dashed lines) from a G2-like state to the G0/G1 state without ever activating UbcH10, consistent with the observation that fixing UbcH10 off preserves the complex attractor. In the more likely scenario, UbcH10 activates first, and then the activation of the Cyclosome node (pAPC and Cdc20) marks the spindle assembly checkpoint. This state is also short-lived, as Cyc is deactivated by Cyclosome, which in turn causes the inactivation of both Cyclosome and UbcH10. Thus, the system returns to the G0/G1 state.

6.6 Examining the motif structure and dynamics of networks with a locked node reveals the differences between the nodes' influence

All eight nodes of the Phase Switch Oscillator participate in the oscillation and spend a similar amount of time in their two states (see Supplementary Figure 10.1). All 16 virtual nodes participate in at least one CSM, but their contribution to the connectivity of the expanded network is not equal (discussed in Section 6.4.1). Next, we asked whether all nodes contribute equally to the oscillation. To evaluate each node state's contribution to the complex attractor, we systematically set each node in its active or inactive state and identify the motif structure and attractor repertoire of the thus-modified dynamical system. The modified systems' dynamic behaviors fall into three categories: 1) in three cases the PSO oscillation is preserved as the sole attractor, 2) in 11 cases the modified system has a single point attractor, and 3) in two cases the modified system has multiple point attractors (described in detail Supplementary Table 10.3). The expanded

networks for representatives of each of the three categories are shown in Figure 6.13, alongside the original system's expanded network.

The most interesting example is Cyclin B, whose locking ON creates two highly dissimilar fixed point attractors (see right panels of Figure 6.13). The bistability in the presence of forced CyclinB expression is due to the fact that sustained CyclinB is the (direct or indirect) condition for two mutually exclusive CSMs (C10 and C12). In contrast, when CyclinB is held inactive the CSMs C7 and C9 can stabilize, resulting in a single point attractor most similar to the G2 attractor. Thus, control of CyclinB can yield any of the three attractors of the Phase Switch, consistent with biological knowledge [79, 46, 52, 47]. Moreover, enforced step-wise changes between fixed states of CyclinB can induce attractor transitions that mimic cell cycle progression. The constraint CyclinB = 0 drives the Phase Switch Oscillator to a unique G2-like state in all update schemes. This state is in the basin of attraction of the SAC-like attractor of the CyclinB = 1 constrained PSO (in particular, the C10 conditionally stable motif is active). Thus, if CyclinB is absent until a steady state is reached, and is then reintroduced, the model system undergoes a transition from a G2-like state to a SAC-like state. This model behavior matches experimental observations, as the introduction of Cyclin B to frog oocytes with replicated DNA but no cyclin expression was shown to drive these cells into mitosis [79, 46, 47]. Furthermore, if we remove CyclinB after the SAC-like state is reached, then the system passes through a G0/G1-like state [80, 81, 82], which was not visited by the trajectory from the G2-like state to the SAC-like state. A similar hysteresis in response to the increase vs. a decrease of CyclinB was experimentally observed in Xenopus embryonic cells [79]. In conclusion, we predict that there exists a sequence of repeated changes in CyclinB that can drive the system to visit the attractors of the Phase Switch in the same order as the cell cycle.

I briefly discuss a potential application of the timed Cyclin B driven control of the cell cycle in the case of Alzheimer's disease in the outlook Section 9.2.

6.7 Discussion of the results

In this chapter, I presented the results of the paper [62], a follow-up analysis of a Boolean model of the mammalian cell cycle published in [60] and discussed in Chapter 4. This model agrees with continuous (ODE-based) models in recognizing the importance of bistable switches (based either on mutual activation or mutual inhibition) in this regulatory logic. As beautifully illustrated in a recent review article by Novák et al. [83], these switches are concatenated and nested. Matched pairs of mutually inhibitory bistable switches underlie the cell cycle checkpoints. Once the pair of switches is toggled, the transition through

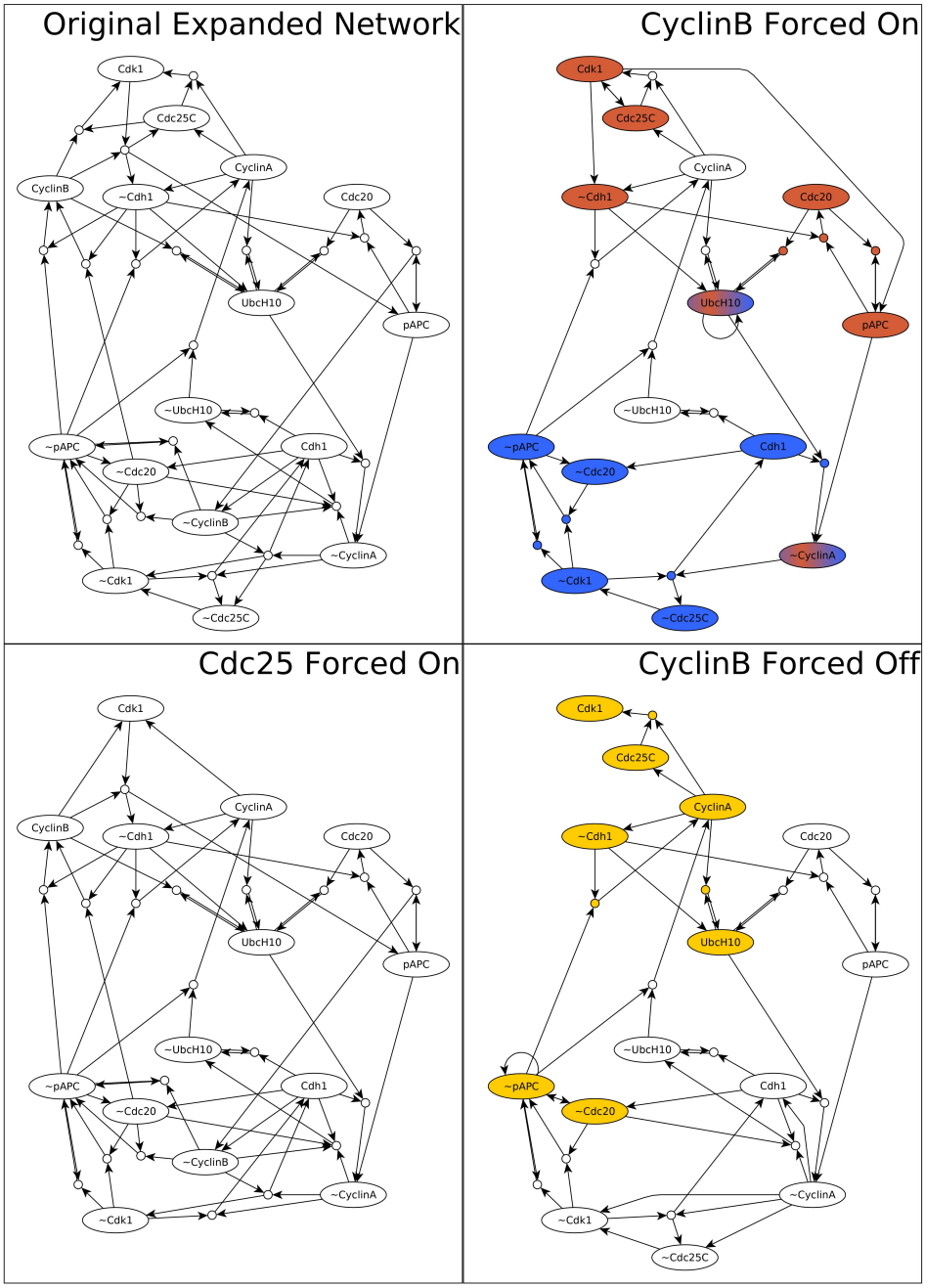

Figure 6.13. *The expanded network that results from no intervention (top left panel) or three characteristic interventions (other panels as indicated by panel titles). Virtual nodes whose label is the node name preceded by ∼ indicate the off state of the relevant node. The three interventions exemplify each of the three attractor categories outlined in the main text: retained oscillation (bottom left, UbcH10 off), single point attractor (bottom right, CyclinB off), and multiple point attractors (top right, CyclinB on). The group of virtual nodes that make up each point attractor are highlighted in color. The blue state has the greatest overlap with the G0/G1 attractor of the Phase Switch, the yellow state most closely overlaps with the G2 attractor, and the brown state is most similar to the SAC attractor.*

the checkpoint is irreversible. The logic-based methods we present here offer a related and complementary way to understand the attractor repertoire that arises from coupled and nested bistable switches. The concept of stable motif expresses a stable switch state. Thus, the activation of a stable motif marks a point of no return in a system's trajectory. Here we introduced conditionally stable motifs, which can maintain a fixed state of their constituent nodes as long as the state of one or more nodes external to the motif is maintained. Intuitively, conditionally stable motifs are reversible switches that can maintain their state when their conditions are fulfilled but are reversed when their conditions are violated. Our analysis focused on understanding the connection between reversible switches and the cyclic activation and deactivation of cyclins during the cell cycle. To do this, we considered a cell that lacks the restriction, DNA damage and spindle assembly checkpoints. Our results indicate that the negative feedback loop formed by a group of strongly coupled switches (encompassing CyclinA, CyclinB, Cdk1, Cdh1, Cdc25C), on the one hand, and the complex of pAPC and Cdc20, on the other hand, is a main contributor to this cyclic behavior.

Conditionally stable motifs are useful generalizations of stable motifs. Stable motifs are well-defined within the context of a model. Yet, as all models are ultimately incomplete, it is possible that a more complete model would have additional regulators that transform the stable motif into a conditionally stable motif. Through our analysis of the Phase Switch and the Phase Switch Oscillator, we have uncovered three key features of conditionally stable motifs (CSMs). First, they can play an important role in the decision-making of multi-stable systems. For example, in the Phase Switch module the stable motif P1 is compatible with both G0/G1 and G2 attractors. The subsequent stabilization of the conditionally stable motif P5 and P0, alternatively, P5 and P6, steers the system into one or the other attractor respectively (see Figure 6.2). Second, in systems with complex attractors, CSMs reduce noise introduced by stochastic update order by temporarily eliminating degrees of freedom. Indeed, CSMs with the fewest conditions capture the temporary stability of short-range positive feedback loops, which temporarily fix the states of the nodes in the feedback loop. Third, oscillation requires that no CSM has stabilized conditions, and therefore the pattern of CSM condition activation and deactivation can illuminate the nature of the oscillation.

Both the Phase Switch and Phase Switch Oscillator contain induced strongly connected subgraphs that lack negative feedback loops (in other words, they are sign-consistent). A significant body of work applied to both continuous and discrete dynamical systems indicates that sign-consistent systems (also called monotone systems) have highly predictable and ordered dynamics [84]. Bio-

logical networks tend to be close to sign-consistent [84], thus identifying their largest sign-consistent subgraphs, and studying the connections of these subgraphs is a fruitful way forward. In the specific case of the Phase Switch Oscillator, the largest sign-consistent subgraph is the group of switches made up by CyclinA, CyclinB, Cdk1, Cdh1, and Cdc25C, a group whose two opposing states make up the two largest conditionally stable motifs, Cyc and ∼Cyc. The second-largest sign-consistent subgraph is formed of pAPC and Cdc20 and determines the Cyclosome and ∼Cyclosome CSMs. Merging the sign-consistent, strongly connected subgraphs into single meta-nodes yields the coarse-grained system of Figure 6.12, which reveals the negative feedback loops of the Phase Switch Oscillator. Studying the general relationship between the largest sign-consistent subgraphs and largest CSMs is an interesting topic for future work.

Our analysis yields novel biological insights and predictions. For example, our analysis of the Phase Switch Oscillator with a locked-in state of CyclinB confirms the important role of CyclinB in driving the cell cycle of embryonic cells and mitosis in somatic cells. We predict that there exists a sequence of repeated changes in CyclinB that can be used to drive the system to visit the attractors of the Phase Switch in the same order as the cell cycle. More broadly, our findings support the conclusion that a combination of bistability and negative feedback underlies many biochemical oscillators [85, 79]. Our newly introduced concept of conditionally stable motifs may also help address biological learning and adaptation in a network framework [86].

The expanded network framework is part of a broader effort to characterize and represent a network as the causal relationships between variables of a dynamical system. Related concepts include signed interaction hypergraphs [87] and dynamics canalization maps [75]. For example, the logic domain of influence of a node state [78] is a subgraph of the expanded network that is conceptually similar to the three-valued (0, 1, unknown) logical steady state that results from fixing a node state [87] and to the dynamical modules of dynamics canalization maps, which represent the states inexorably stabilized by an input configuration [75]. The concepts of expanded network and stable motif have been generalized and implemented in multi-level discrete systems and continuous-variable systems described by ordinary differential equations [88, 89]. When considered generally, the expanded network encodes causal links between regions of state-space. Each of its virtual nodes represents a region of state-space (e.g., the region in which a particular variable takes a specified value or range of values) and the composite nodes represent the intersection of the virtual node regions. Once an expanded network is constructed for a given dynamical system, be it discrete or continuous, the concept of a conditionally stable motif is immediately applicable. Thus, it is possible that by using the methods of

Rozum & Albert 2018 [89], many of the concepts we have introduced here can be generalized to multi-level discrete dynamical systems and ODE models.

Our analysis indicates that the influences on the Phase Switch originating from the other modules become functional in a manner that allows the Phase Switch to approach one of its attractors (as the cell reaches the relevant checkpoint), but then they destabilize this attractor as the checkpoint is cleared. In other words, the network around the Phase Switch helps provide the conditions that govern its stable motifs. Nevertheless, we found that the robust channeling of its dynamics along a limit cycle is intrinsic to this network. Thus, the Phase Switch balances the need to stably maintain the cell at each checkpoint with the need for a robust limit cycle when checkpoints are cleared without issue. The methodology described in this chapter can be used to understand the complex oscillation that emerges from the coupling of the Phase Switch and the Restriction Switch in the presence of growth factors. As explained in Deritei et al. 2016 [60] and Chapter 4 and illustrated in Figure 4.6, this attractor recapitulates the cell cycle in the presence of the checkpoints we removed in this study while toggling the combinations of the module attractors. Analyzing the conditionally stable motifs of the coupled model could shed light on an even more comprehensive coarse-grained logical network that drives the cell cycle, and offer further insight on dynamical modularity. I briefly address our preliminary results on the coarse-graining of the full cell cycle model in Section 9.2.

The analysis of the cell cycle model, under general asynchronous update with the stable motif analysis of the Restriction Switch, is presented in the next chapter.

CHAPTER 7

ANALYSIS OF THE CELL CYCLE MODEL UNDER GENERAL ASYNCHRONOUS UPDATE

In this chapter I am going to present the results of extending the analysis of the Phase Switch Oscillator (PSO) presented and discussed in Chapter 6 to the full cell cycle model published in [60] and introduced in Chapter 4. As a reminder, the cell cycle model includes the Phase Switch module, the Restriction Switch module, as well as 4 abstract nodes. We simulate the cell cycle model under general asynchronous update to study its behavior subject to variable timing. We then present a more general method to generate the "backbone" of the complex attractor encompassing a probabilistic view of the relevant trajectories the model can take. We also analyze the stable motif structure of the Restriction Switch module, and how the stable motifs change as a result of the coupling with the Phase Switch. With this, we explain the role and behavior of the Restriction Switch in the complex dynamics of the cell cycle.

7.1 The cell cycle model maintains its relevant behavior under general asynchronous update

We are using the same 21 node cell cycle model that we already discussed in detail in Chapter 4, however, since we are assuming constant growth factor stimulation the GF input node is permanently set to 1. This leads to the node Myc also being turned permanently on. As these nodes are fixed we can slightly simplify our model to 19 node system by substituting the values of GF and Myc. We

sampled the complex attractor of the model (for the sampling method see 3.1.5) emerging from general asynchronous update. The resulting sample of the state transition graph is shown in Figure 7.1. The node colors represent the closeness of each state to the attractors of the Phase Switch and Restriction Switch. We identify four distinct parts of the graph: three loops representing three different cyclic paths and a central "spine" where the loops join and diverge from. The largest loop robustly follows the cell cycle trajectory of the synchronous update, highlighted with the wider purple edges (as seen also in Figure 4.6). This loop, the same way as the synchronous limit cycle, toggles the attractors of its constituent modules, as the colors of the nodes representing the states indicate. This behavior adheres to the rules of dynamical modularity discussed in detail in Chapters 4 and 5. We would like to highlight that in some cases the asynchronous update reveals pathways where the dynamical modularity is even more pronounced than it is when using synchronous update. For example, the Before RP attractor state of the Restriction Switch is approached more (yellow-green nodes on the bottom left of Figure 7.1) by the complex attractor than by the synchronous limit cycle (marked by the nodes connected by the purple edges).

The nodes on the complex attractor are labeled if they have some outstanding biological significance and/or are highly probable states. One such prominent state just before the turning on of Cdc25A is labeled G1+PRP. This state has almost perfect overlap with the G0/G1 attractor of the Phase Switch, and perfect overlap with the past restriction point (Past RP) attractor of the Restriction Switch. Contrary to the "textbook" description of restriction point passage (irreversible commitment to division) between phases G0/G1 and G2, one can see that the states corresponding to the G1 phase (nodes with blue primary color) have the Restriction Switch nodes already in the Past RP phase (represented by pink secondary color). The only time the Restriction Switch is in the Before RP phase along the main loop is where the Phase Switch is in the G2 phase (yellow primary color and green secondary color). As the attractor follows the main loop and progresses into the G2 phase, there are several states where the attractor perfectly matches the node states of the G2 attractor we see in an isolated Phase Switch. The most prominent such state in our sample is labeled G2 + BRP. This phenomenon is actually in accordance with biological observations, where cells exposed to constant growth factor stimulation can pre-commit to the next cell cycle even before the cytokinesis of the mother cell [63]. The pre-commitment is visible on the complex attractor on the main loop around in the SAC phase where the nodes are colored with a combination of brown and pink, meaning that the Restriction Switch is already past the restriction point. There is also a "tangent" trajectory that we can observe along the G2 section of the main

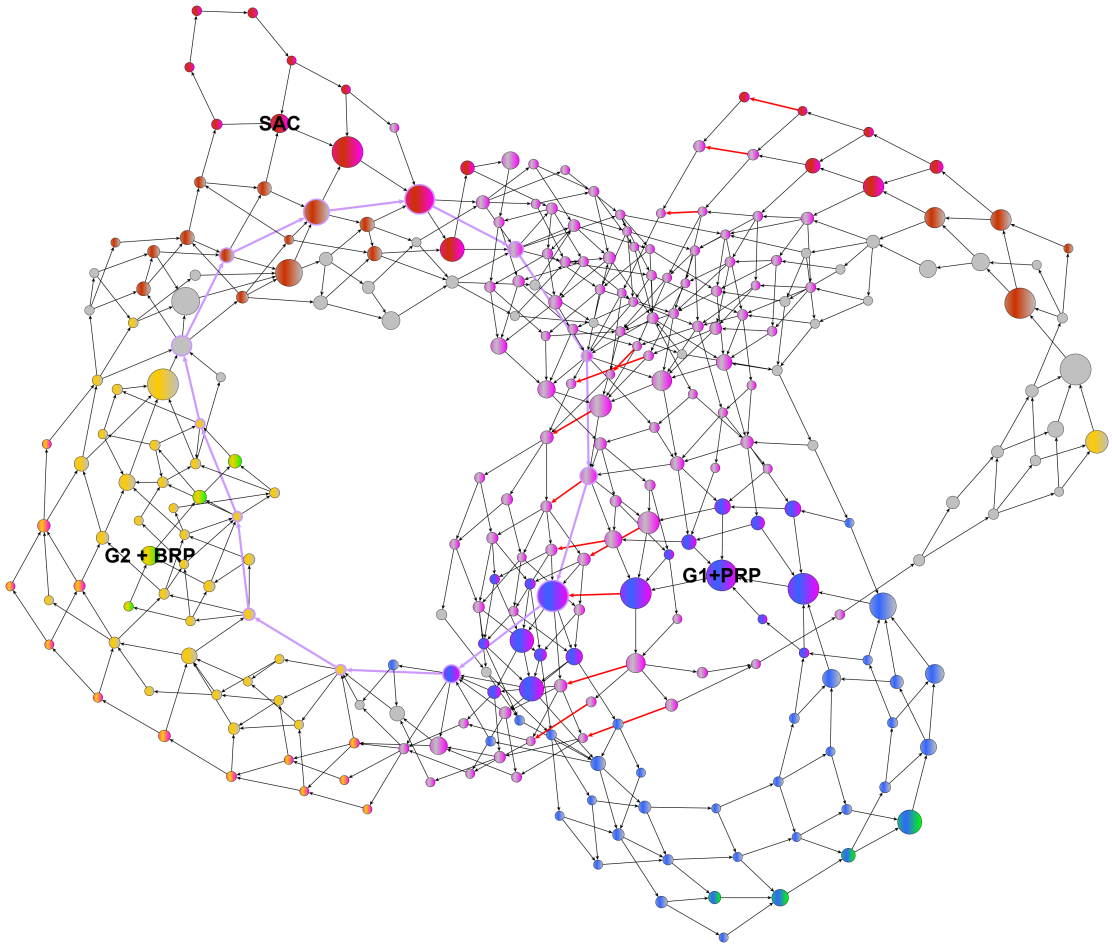

Figure 7.1. *State transition graph (STG) representation of the complex attractor of the Cell Cycle. Each circle represents a state of the Cell Cycle, which is made up of the states of all the 19 nodes. The node sizes represent the visitation probabilities of the corresponding states. States with visitation probability less than 0.5% are omitted. Each node is composed of two colors. If a system state overlaps with an attractor of the Phase Switch or Restriction Switch by at least 80%, the node is colored with the color representing the relevant attractor, namely blue for G0/G1, yellow for G2 and brown for SAC in the case of the Phase Switch (color on the left) and light green for the Before RP, pink for the Past RP in the case of the RS (color on the right). System states that have less than 80% overlap with an attractor state are shown in grey. For simplicity, we omit the self-loops that correspond to the cases where a node state is re-evaluated but does not change. The state transitions corresponding to the synchronous update are shown in purple. Transitions where the abstract node Replication turns on are highlighted with red. The three nodes with labels represent nodes of biological significance: G1+PRP indicates the first growth phase following cell cycle commitment (past the restriction point), G2+BRP indicates the second growth phase where the restriction switch reset to its uncommitted state, SAC marks the spindle assembly checkpoint.*

loop, where the Restriction Switch is actually never reset, it only goes through a more neutral state (shown in grey) between the G2 and SAC phases.

The small blue-green loop is partially an artifact of our model's simplified treatment of DNA replication. In cells, starting the process of DNA replication is irreversible. Cells that start the S phase cannot reset to G1 even if they lose CyclinE or Cdc25A activity. Instead, these cells pause in S-phase until they can resume DNA replication. The irreversible nature of commitment to replication could have been incorporated in the model by making the Replication node self-sustaining. We did not do this because this assumption can easily result in a separate stable S-phase attractor that is more stable than an S-phase arrest might be. Thus, asynchronous update allows a model trajectory in which Replication turns ON (red edges), which turns CyclinD1 OFF, which pushes the Restriction Switch back to its uncommitted state (marked in green secondary color), which then turns Replication OFF without achieving the outcome of replication, the ON state of the 4N_DNA node. This trajectory constitutes the first part of the blue-green loop: the Phase Switch is in the G1 phase (blue primary color) and the Restriction Switch goes from committed to uncommitted (pink to grey to green secondary color). As CyclinD inhibition is subsequently lost, and growth stimulation goes on, the Restriction Switch commits once more (grey and then pink) thus the loop converges into the "committed G1" spine.

The "middle" yellow/grey/red loop is a consequence of a somewhat different non-biological feature of the model, which has been since corrected in the updated model published in Sizek et al. [90] discussed in Chapter 8. Following the state transitions along this loop reveals that they represent a full cycle of the Phase Switch alone, without ever engaging DNA replication or metaphase (see Section 6.2). Our model allows this to occur due to the fact that it only factors in the existence of replicated sister chromatids (4N_DNA) in the logic gates of the SAC checkpoint node Mad2, and the abstract process node Metaphase itself. In live cells, however, key regulators of the mitotic CyclinB/Cdk1 complex, such as Cdc25C and Cdc25B (see [90]) are controlled by localization to structures along replicated sister chromatids [91, 92, 93]. For example, Cdc25C is initially activated by a small pool of Cyclin B / Cdk1 (below the ON-threshold of Cdk1 in our model) which starts out at the replicated centrosomes. Moreover, the pool of mitotic Cdc25C co-localized with active Chk1/Cyclin B is found on condensed chromosomes, again requiring the presence of 4N_DNA [94]. By ignoring this requirement, our model allows the cell cycle control machinery to enter a mitotic state without 4N_DNA and allows the Phase Switch to go through G2 $\rightarrow$ SAC $\rightarrow$ G1 without the processes triggered and monitored by it in live cells.

7.2 The backbone of the complex attractor

The same way as we did in Section 6.2 we construct the backbone of the complex attractor. This allows us to answer two questions. First, how robustly does the general asynchronous attractor follow the synchronous one, and as such how faithful it is to the biological features of the cell cycle? Second, what non-trivial transitions are created by the noisy update and their probabilities together with the constituting node changes? The robustness analysis including only the states of the synchronous cycle is shown in Figure 7.2. Looking at this figure we can conclude that the main asynchronous loop is a fairly robust oscillation with the transitions that follow the synchronous cycle have probabilities above 0.5. The transition probabilities are somewhat smaller between the states labelled (4,4,8);(1,5), (7,5,3);(0,6), (7,5,5);(0,6). These states are also part of the "spine" of the complex attractor, where the extra, non-biological, loops begin.

In contrast to the case of the PSO, where we had one consistent cycle, in this case, we have some new, unexpected features – in the form of the extra loops – that we would also like to preserve in the backbone. To do this, it is not sufficient to only use the states of the synchronous attractor as proxy nodes, because that only captures the main loop. To include relevant nodes from every distinct loop we adapt a local version of betweenness centrality that gives high betweenness values for nodes in sections of the graph that are part of a consistent trajectory, such as the loops. We also wanted to capture states where the complex attractor reaches maximal overlap with a module attractor. In cases where there were multiple states with the same overlap value, we chose the most visited state. The union of the top 15 nodes of highest local betweenness, the 13 states of the synchronous limit cycle, and the 5 most probable maximally overlapping states (one for each module-attractor) make up the set of proxy nodes that we use to generate the backbone shown in Figure 7.3.

In Figure 7.3 one can see that the compressed attractor with the selected proxy nodes maintains the key structural features of the complex attractor shown in Figure 7.1. As the 13 states of the synchronous cycle are included, the most prominent structural feature of the figure is the main loop. The nodes of the synchronous cycle, as well as the transitions between them, are highlighted with purple. Along the main loop, we observe a few side-trajectories that are biologically interesting and are consequences of the asynchronous update. The first such trajectory is the restriction point reset during the G2 phase, reached at the node (6,10,6);(5,1); this is the only point along the cycle where the Restriction Switch is in the Before RP state. There is also the yellow-grey node labeled (5,11,5);(2,4), a state that perfectly overlaps the G2 attractor of the Phase Switch and is also more probable than any close-to-G2 state of the synchronous cycle.

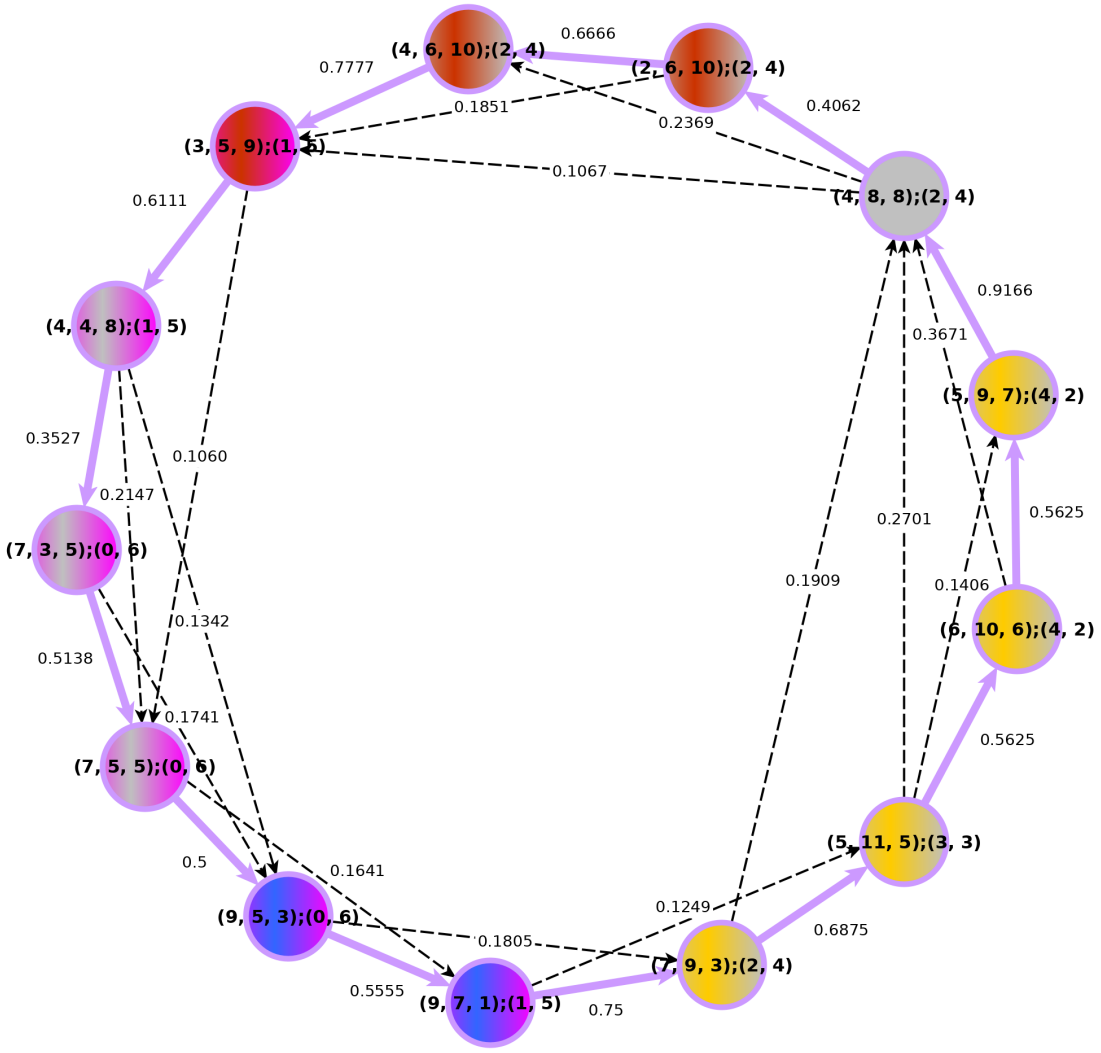

Figure 7.2. *The shared backbone of the synchronous limit cycle and asynchronous complex attractor. The nodes represent the thirteen states of the synchronous limit cycle (the nodes connected by purple edges in Figure 7.1); the node labels indicate the overlap of the corresponding state with the three Phase Switch and Restriction Switch attractors (in the order G0/G1, G2, SAC and Before RP and Past RP). The purple edges represent single state transitions obtained by the synchronous update. These state transitions also appear in the asynchronous state transition graph, either as edges or as paths. The dashed edges indicate cases where paths exist in the asynchronous state transition graph that skip a state visited by the synchronous state transition graph. The nodes are colored to represent module attractor proximity, according to the same coloring scheme as explained in Figure 7.1. Edge labels of the state transition edges indicate the probability of the state transition when using asynchronous update. State transitions with a probability of less than 0.1 are omitted from this figure.*

This state (5,11,5);(2,4) also behaves as a shortcut along the states associated with G2. The grey node labeled (4,8,8);(2,4) is a state of strong convergence and it also represents the transition between the G2 and SAC phases. The red-pink node labeled (3,5,11);(1,5) is a state where the system reaches perfect overlap with the SAC attractor of the Phase Switch, and it is also a state where the Restriction Switch pre-commitment occurs.

The blue-pink node labelled (10,4,4);(0,6) is relevant for several reasons. First, it is one of the most visited states along the "spine". The reason for this is that both extra loops converge onto this state with relatively high probability. The "middle" loop also starts from this state and it can loop back into it. The state (10,4,4);(0,6) also reaches a better overlap with the G0/G1 attractor of the Phase Switch than any state along the synchronous cycle.

Each of the extra loops is captured by three nodes of the backbone. The smaller blue-green loop consists of the states and transitions (11,5,3);(5,1) $\rightarrow$ (10,4,4);(5,1) $\rightarrow$ (10,4,4);(4,2). The most likely transition to start the loop is from the state represented by the blue-grey node (10,6,2);(2,4), which has incoming edges from three states of the synchronous cycle. From this state there is an approximately 50% chance of transitioning into the state (11,5,3);(5,1). (11,5,3);(5,1) is interesting because it has a perfect overlap with the G0/G1 attractor of the Phase Switch and it is as close as possible to the Before RP state of the Restriction Switch, i.e. it is the best representation of a cell before "textbook" restriction point passage in G1 we get in this version of the model. All three backbone nodes of the loop have a nonzero chance of transitioning into (10,4,4);(0,6), where the Restriction Switch is Past RP once again; the loop eventually ends up in (10,4,4);(0,6) 100% of the time. By this, we can conclude that this loop is one of the most robust sections of the complex attractor. This loop can also be interpreted as a sort of oscillation of the Restriction Switch as it starts from the Past RP phase, goes through the Before RP phase (with the exception of Myc) and then goes back to Past RP, while the nodes of the Phase Switch are relatively stable in the G1 phase.

The middle loop where the Phase Switch oscillates without a completed replication is captured by the nodes (7,7,3);(2,4) $\rightarrow$ (8,6,4);(2,4) $\rightarrow$ (3,7,9);(2,4). It has a circa 10% chance of initiating from (10,4,4);(0,6). It's less prominent on the backbone, but it's visible on the complex attractor that this loop toggles through the G2 and SAC phases of the Phase Switch. However, the nodes with the highest local betweenness that were selected as proxies are more transitional and thus are colored grey. The loop robustly converges into the red-grey state labeled (3,7,9);(2,4) but afterward there is a lot of freedom in where the trajectories return to the spine of the complex attractor. The two transitions that have a probability larger than 10% are to the proxy states (10,4,4);(0,6) (closing the

loop) and (7,5,5);(0,6) (part of the synchronous cycle). Every other transition from (3,7,9);(2,4) has a likelihood of less than 10% and thus is not shown on the figure.

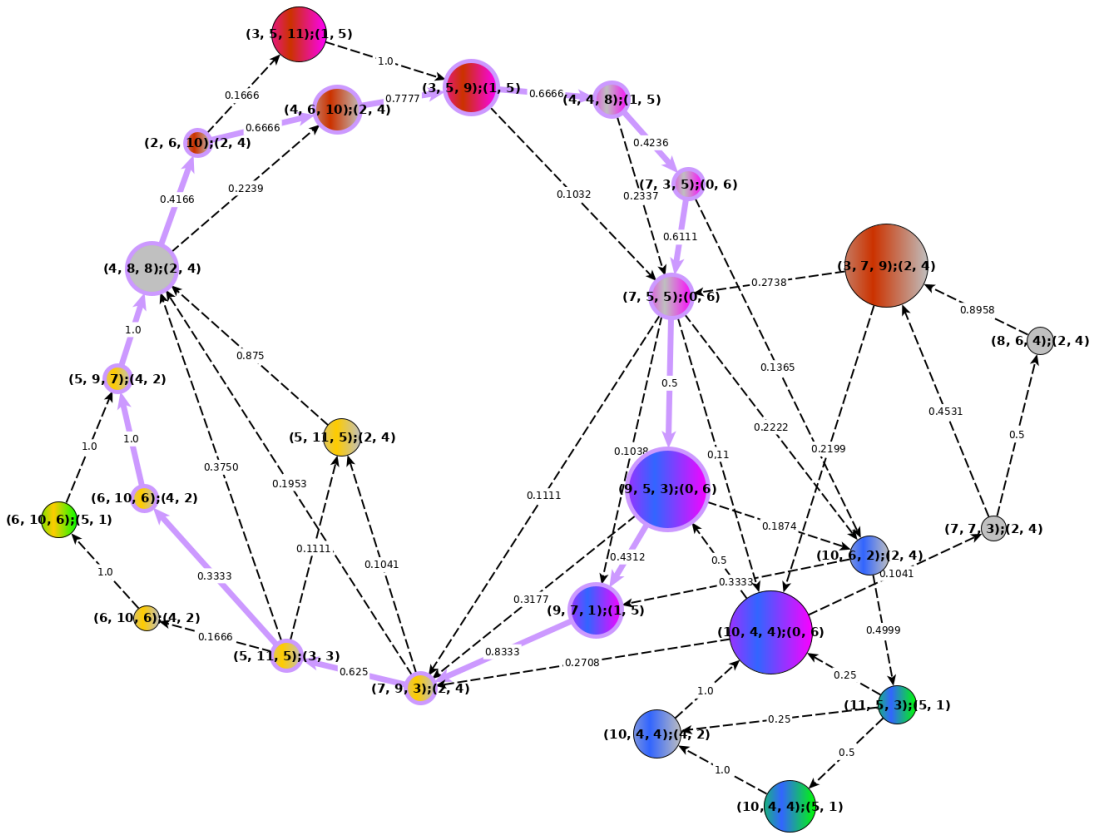

Figure 7.3. *The backbone of the synchronous limit cycle and asynchronous complex attractor. The nodes represent the thirteen states of the synchronous limit cycle (the nodes connected by purple edges in Figure 7.1) and other selected "proxy nodes"; the node labels indicate the overlap of the corresponding state with the three Phase Switch and Restriction Switch attractors (in the order G0/G1, G2, SAC and Before RP and Past RP). The purple edges represent single state transitions obtained by the synchronous update. These state transitions also appear in the asynchronous state transition graph, either as edges or as paths. The dashed edges indicate cases where paths exist in the asynchronous state transition graph that skip a state visited by the synchronous state transition graph. The nodes are colored to represent module attractor proximity, according to the same coloring scheme as explained in Figure 7.1. Edge labels of the state transition edges indicate the probability of the state transition when using asynchronous update. State transitions with a probability of less than 0.1 are omitted from this figure.*

7.3 Stable motif analysis of the Restriction Switch module

Following the logic of Chapter 6 we conduct the stable motif analysis of the Restriction Switch, the same way as we did for the Phase Switch in Section 6.1. The stable motif succession diagram of the Restriction Switch shown in Figure 7.4, reveals four stable motifs and no conditionally stable motifs, which means that if any of the stable motifs locks in, it will directly lead into its corresponding attractor. The stable motifs R0 and R1 both lead the Restriction Switch into the Before RP attractor while the stable motifs R2 and R3 lead the Restriction Switch into the Past RP attractor.

7.4 Stable motifs of the Restriction Switch are modified in the full cell cycle model

In Figure 7.5 we indicate the additional regulators of the Restriction Switch in the cell cycle model. The detailed description of the regulatory interactions discussed in this section, supported by references from the experimental literature can be found in [60] Supplementary Tables S1 and S3. The Boolean rules and the coupling interactions discussed here are also listed in Tables 4.2 and 4.6.

When considering solely the Restriction Switch module Myc is activated by E2F1, however, in the full cell cycle model active growth factor stimulation is sufficient to activate Myc regardless of the status of E2F1. The rule Myc changes from **Myc* = E2F1** in the isolated Restriction Switch to **Myc* = GF or E2F1**. Because of this, in the case of constant GF stimulation Myc is permanently turned on. It is worth noting that in most of our analysis when we study the cell cycle (instead of the G0 quiescent attractor) we work with **GF=Myc=1**.

The activation of Cyclin E is done by an active E2F1 but only in the absence of RB and p27Kip1, both of which bind Cyclin E. The rule of Cyclin E in the Restriction Switch is: **CyclinE* = E2F1 and not RB and not p27Kip1**. In the context of the larger model the activation also requires the presence of Cdh1 or that the cell is not in metaphase. The Cdh1 contingency is not direct but compresses a chain of regulation events involving molecules that are not explicitly included in our model. The fact that Cyclin E cannot activate during metaphase either is encoded by the inhibition from the Metaphase abstract node, which also encompasses multiple regulation events. The rule of Cyclin E in the coupled model is thus: **CyclinE* = (Cdh1 or not Metaphase) and (E2F1 and not RB and not p27Kip1)**

The activation of the E2F1 transcription factor is contingent on the absence

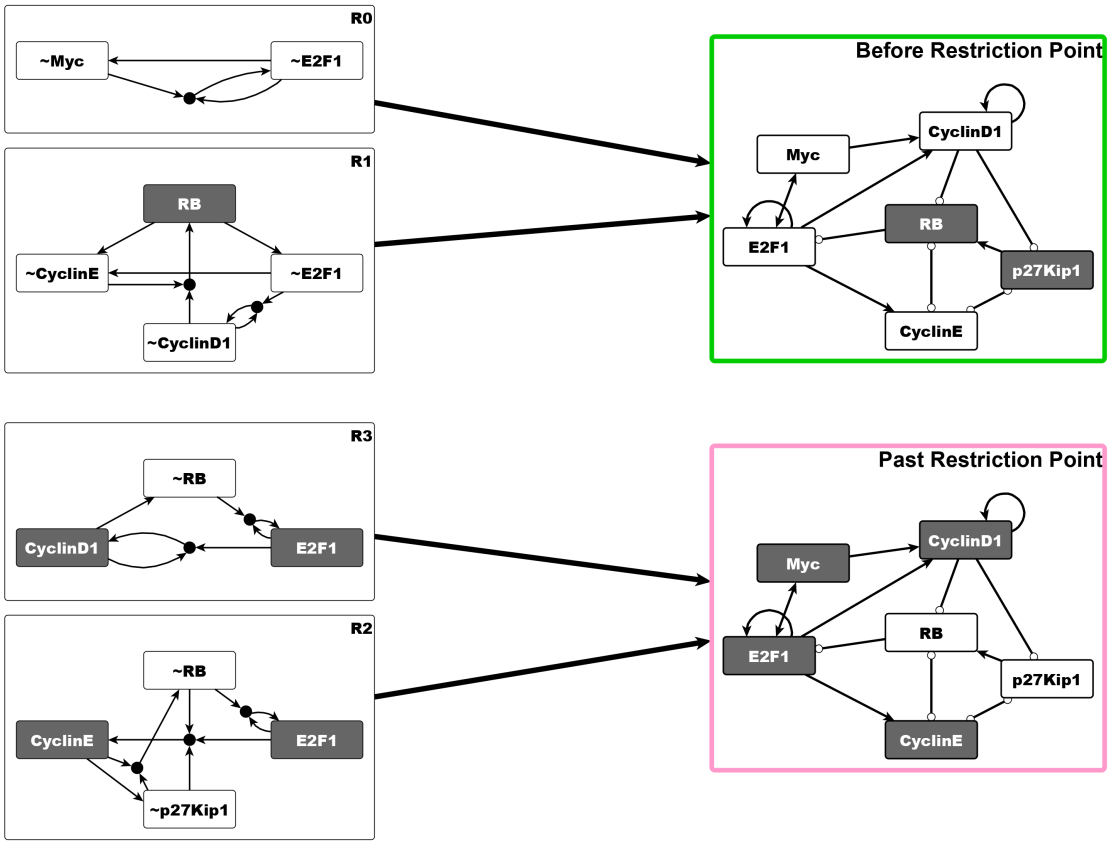

Figure 7.4. *Distinct sequences of stable motifs that commit the Restriction Switch to its attractor states. The stable motifs are shown in the expanded network formalism where a virtual node labeled by the name of the corresponding node represents the state 1 of the node (dark grey background); a virtual node labeled by the node name preceded by* $\sim$ *represents the state 0 of the node (white background). Stable motifs R0, R1, R2 and R3 are the stable motifs of the Restriction Switch when considered in isolation. Each path terminates in one of the two point attractors (Before Restriction Point, Past Restriction Point), visualized in the Restriction Switch regulatory network using a white background for the off state of a node and dark grey for the on state. The outline color of the two attractors corresponds to the color-code used for differentiating the two attractors in Section 4.1.*

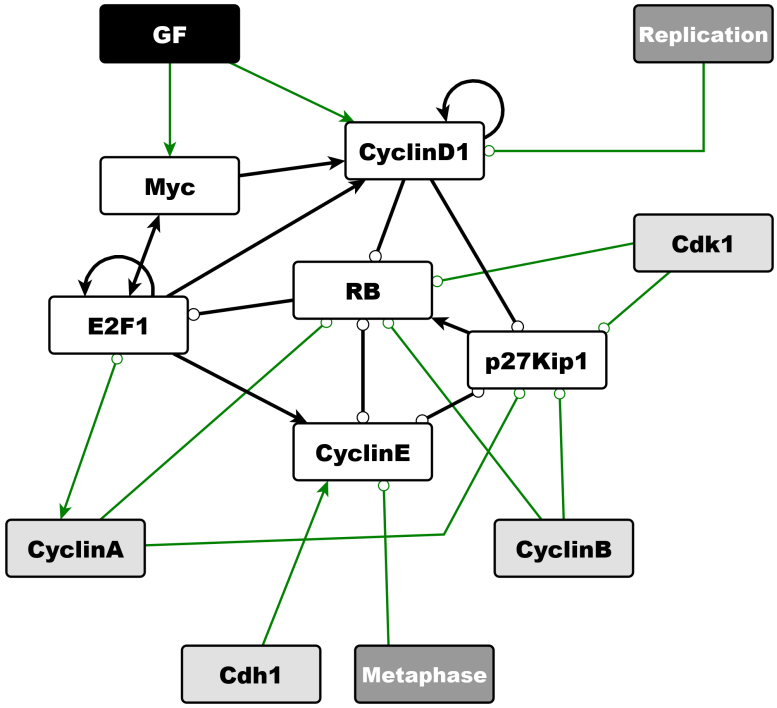

Figure 7.5. *The Restriction Switch module and its inputs from the rest of the cell cycle model (highlighted with green edges). All the nodes of the Restrictions Switch are affected by external regulators. Edges with terminal arrows indicate positive regulation, edges that end in open circles indicate negative regulation, and edges that have endings on both sides (i.e., bidirectional edges) indicate the superposition of two edges with opposite directions. The white nodes represent the nodes of the Restriction Switch, the light grey nodes are nodes of the Phase Switch, the dark grey nodes are abstract nodes. The black node represents the Growth Factor input.*

of active RB and it can be turned on by an active Myc or it can sustain its own activity in the absence of RB. This leads to the rule: **E2F1* = (not RB) and (E2F1 or Myc)**. In the larger model, the activity of E2F1 is also contingent on the absence of Cyclin A, as Cyclin A directly binds E2F1. Thus both RB and Cyclin A can deactivate E2F1, which modifies the rule of E2F1 to: **E2F1* = not (CyclinA or RB) and (E2F1 or Myc)**

p27Kip1 is bound by Cyclin D and its associated Cdk complexes, while Cyclin E can mark p27Kip1 for degradation. Within the Restriction Switch module p27Kip1 can only activate in the absence of both: **p27Kip1* = not (CyclinD1 or CyclinE)**. However, in the context of the full model, the degradation induced by Cyclin E only happens when Cyclin A is also active. In addition, the Cyclin B-Cdk1 complex phosphorylates p27Kip1 in a way that promotes its export from the nucleus. The extended rule of p27Kip1 is: **p27Kip1* = (not (CyclinB and Cdk1)) and (not (CyclinD1 or (CyclinA and CyclinE)))**

The RB complex is bound and phosphorylated by Cyclin D and its Cdk complex. It can also be deactivated by CyclinE but p27Kip1 can counteract the effect of Cyclin E, leading to the rule: **RB* = (not CyclinD1) and ((not CyclinE) or p27Kip1)** Similarly to p27Kip1, the inhibitory effect of Cyclin E on RB is contingent on an active Cyclin A. RB also can be deactivated by an active Cyclin B-Cdk1 complex, and thus the rule becomes: **RB* = not (CyclinB and Cdk1) and (not CyclinD1) and (p27Kip1 or not (CyclinA or CyclinE))**

CyclinD1 is activated by the simultaneous presence of Myc and E2F1 and an already active CyclinD1 can sustain its own activation in the presence of either Myc or E2F1: **CyclinD1*= (Myc and E2F1) or (CyclinD1 and (Myc or E2F1))** Instead of stringing additional regulations to the rule of CyclinD1, in the full cell cycle model the rule of CyclinD1 is modified to: **CyclinD1* = (not Replication) and ((GF and (Myc or E2F1)) or (Myc and E2F1))** Ongoing replication inhibits CyclinD1 (thus the not Replication), furthermore, the presence of GF overrides the self-loop of CyclinD1. In the case of constant growth factor stimulation, i.e. GF=Myc=1, CyclinD1 is only regulated by Replication. In other words, if we substitute the ON values of GF and Myc into the model the rule of CyclinD1 is reduced to: **CyclinD1* = not Replication**

These modifications change the stable motifs of the Restriction Switch. Unlike the Phase Switch, the stable motifs of the isolated Restriction Switch do not simply become conditionally stable motifs of the full cell cycle. Figure 7.6 summarizes how the stable motifs of the Restriction Switch change in the cell cycle model.

When Myc is fixed to 1 the stable motif R0 (not shown) is reduced to a single virtual node (∼E2F1) that is not self-sustaining. The modification of the rule of CyclinD1 remove the self-loop of ∼CyclinD1 conditioned on ∼E2F1 and re-

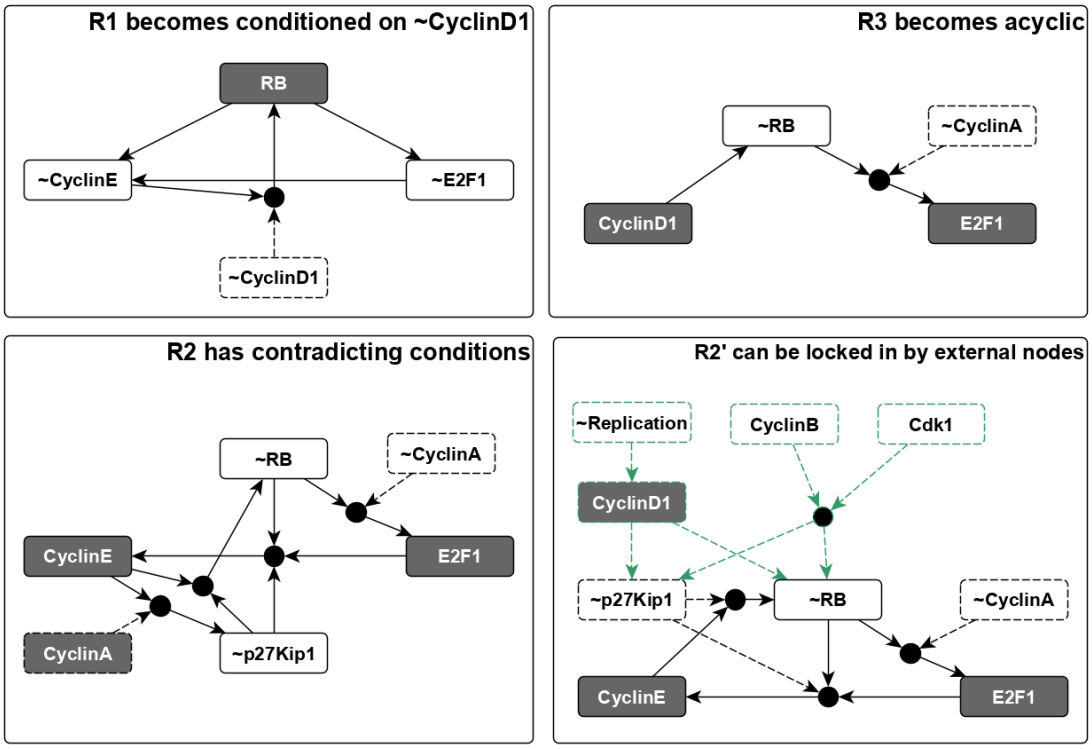

Figure 7.6. *The stable motifs of the Restriction Switch (see Figure 7.4) change in the cell cycle model due to the modifications to the rule of CyclinD1 and the substitution of GF=Myc=1. The motifs are shown in the expanded network formalism where a virtual node labeled by the name of the corresponding node represents the state 1 of the node (dark grey background); a virtual node labeled by the node name preceded by ∼ represents the state 0 of the node (white background). Conditions external to the motifs as well as the directional arrow representing their effect are marked with a dashed outline. On the bottom right panel, the green dashed arrows represent interactions that are not part of the CSM but are sufficient to elicit a virtual node or condition of the motif and thus greatly contribute to the motif's stabilization.*

duce R1 to a smaller cycle. This smaller cycle becomes a CSM conditioned on ∼CyclinD1. R2 has two conditions that are the two states of CyclinA, thus they are contradicting. In order for a conditionally stable motif to be able to stabilize, all of its conditions need to be fulfilled simultaneously. This can never be the case for R2 in the cell cycle, thus it is not a CSM. Yet, a subset of the R2 motif is a CSM that is conditioned on ∼Cyclin A and ∼p27Kip1 (see bottom right panel of Figure 7.6. R3 becomes acyclic, CyclinD1 → ∼RB → E2F1, with the activation of E2F1 also contingent on ∼CyclinA. Thus R3 is not a CSM in the cell cycle model.

7.5 The coupling between the Phase Switch and the Restriction Switch is asymmetric

The lack of clearly emerging CSMs from the stable motifs of the Restriction Switch raises the question: what sustains the attractors of the Restriction Switch in the complex attractor of the cell cycle model? We can see on the complex attractor (Figure 7.1) as well on the backbone (Figures 7.2 and 7.3) that from the SAC section (brown primary color) of the cycle along the spine all the way until the start of the G2 section the Restriction Switch is reliably stabilized in its Past RP attractor (pink secondary color). The biological interpretation of this is what we called pre-commitment to the next cell cycle in the presence of growth factors (see Section 7.1). The constituent states of the Past RP attractor can stabilize conditionally due to the surviving subset of the R2 motif, the R2′ CSM. On the bottom right panel of Figure 7.6 we show the R2′ motif with some of its immediate upstream regulators and regulatory interactions highlighted with green dashed outline. This shows that the lack of ongoing replication (indicated by the ∼Replication virtual node) is sufficient to turn on CyclinD1, which is sufficient to turn off both p27Kip1 and RB. As Replication is on for only a relatively short period of time in the cell cycle, this is a likely chain of events. If the other condition, ∼CyclinA is also fulfilled, R2′ can stabilize, making E2F1 and CyclinE turn on. In Figure 7.7 we show the complex attractor of the cell cycle with nodes colored in cases where the Restriction Switch has at least 5 out of 6 nodes matching either of the two Restriction Switch attractors. The deactivation (orange edges) and eventual reactivation of CyclinA (red edges) mark the beginning and the end of the reliably stable Past RP (pink) section of the complex attractor. It is important to note that E2F1 would not be able to turn on without Myc also being permanently on. Constant GF stimulation is also an implied condition in this case.

The role of the Restriction Switch is to allow or halt the Phase Switch to pass

from G1 to G2. We have seen that the Phase Switch locks into the G0/G1 attractor if the P0 stable motif (∼Cdc25A, ∼CyclinA) stabilizes (see Figure 6.2). P0 is a conditionally stable motif of the cell cycle model, contingent on the off state of either E2F1 or Cyclin E (see Figure 6.3). Our analysis of the PSO has shown that the on state of Cdc25A, and satisfying E2F1's regulation of Cyclin A, is sufficient to let the oscillation proceed towards G2. The simultaneous activation of E2F1 and Cyclin E is sufficient and necessary to activate Cdc25A, thus letting the cycle proceed. In theory, Cyclin A combined with either E2F1 or Cyclin E could also activate Cdc25A, but this never happens in practice, because the activation of Cyclin A requires an already active Cdc25A. This means that Cdc25A is merely reinforced by Cyclin A, and both E2F1 and Cyclin E are needed for its activation. An active E2F1 is also needed for the subsequent activation of Cyclin A. Other than these interactions the Restriction Switch has no direct influence on the Phase Switch. As the biological intuition suggests, the Restriction Switch creates a checkpoint that can halt the autonomous cycling of the Phase Switch at the boundary of G1 and G2.

The degree of coupling between the two switches is not symmetric. As we have discussed earlier, the Phase Switch regulates most nodes of the Restriction Switch and affects its behavior as the cell cycle progresses. The CyclinB - Cdk1 complex (which we consider active when both CyclinB and Cdk1 are on) is active in the mitotic (M) phase of the cell cycle (see Section 2.1.1 and Figure 4.6), and inhibits RB and p27Kip1 of the Restriction Switch. Thus CyclinB together with Cdk1 can also trigger or reinforce the pre-commitment in the presence of growth factors (as can CyclinD1) via contributing to the stabilization of the R2' CSM (see Figure 7.6 bottom right panel). Based on autonomous oscillation we observed in the PSO model (Chapter 6) and the interaction patterns between the Phase Switch and the Restriction Switch we discussed above, a more general cell cycle picture emerges. The PSO behaves as a "motor" at the core of the cell cycle, which can robustly cycle through the cell cycle phases. Decision-making modules, such as the Restriction Switch, can halt the oscillation, or let it proceed. The decision-making modules are regulated by external signals but also receive feedback from the core module. It is worth investigating how other modules not explicitly included in this model, or included in the form of abstract nodes, interact with the PSO. Our model presented in Chapter 8 has three new modules that offer a straightforward next step in investigating this question in the future.

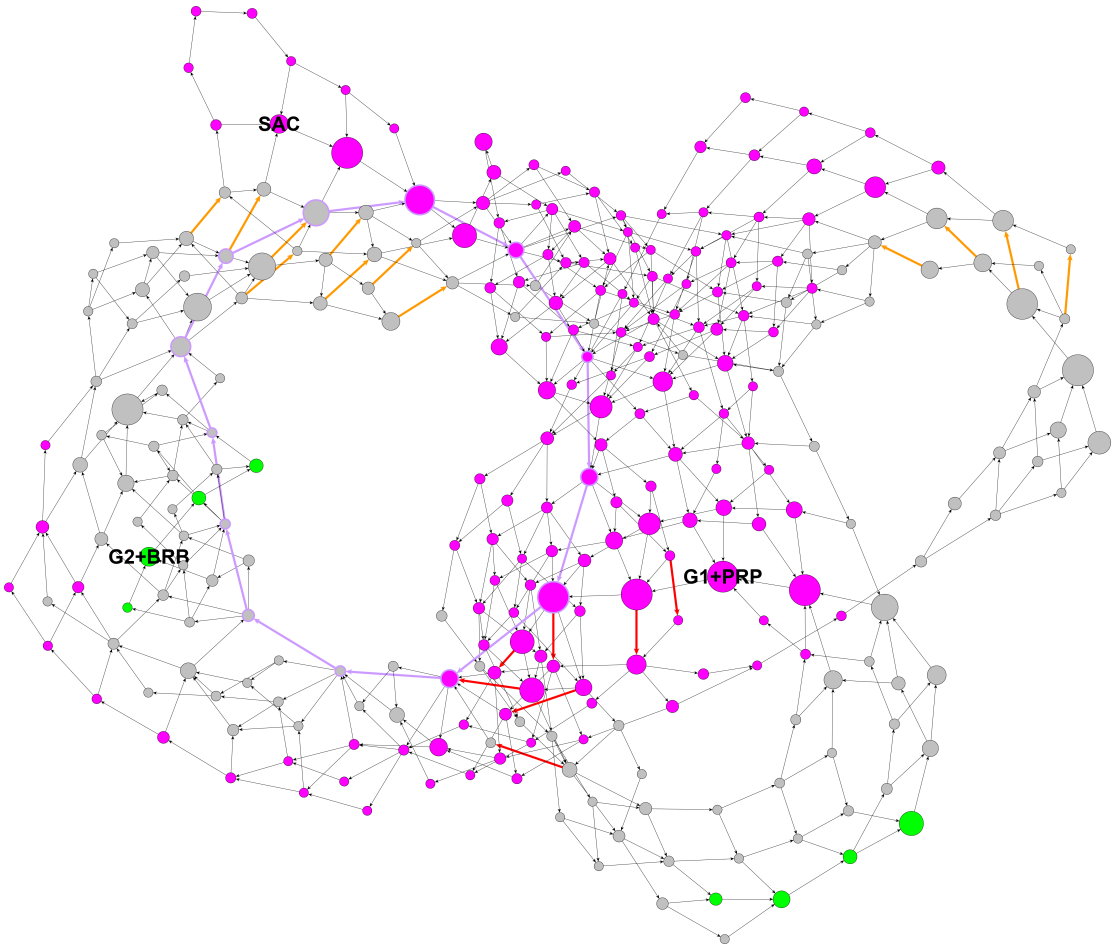

Figure 7.7. *The state of CyclinA determines the period during which the Restriction Switch is near the Past Restriction state. As in Figure 7.1, each circle represents a state of the cell cycle, which is made up of the states of all the 19 nodes. The node sizes represent the visitation probabilities of the corresponding states. If a system state overlaps with an attractor of the Restriction Switch by at least 80%, the node is colored with the color representing the relevant attractor, namely light green for the Before RP, pink for the Past RP. System states that have less than 80% overlap with a Restriction Switch attractor state are shown in grey. The state transitions corresponding to the synchronous update are shown in purple. Transitions where the node CyclinA turns on are highlighted with red and transitions where CyclinA turns off are highlighted with orange. The three nodes with labels represent nodes of biological significance: G1+PRP indicates the first growth phase following cell cycle commitment (past the restriction point), G2+BRP indicates the second growth phase where the restriction switch reset to its uncommitted state, SAC marks the spindle assembly checkpoint.*

CHAPTER 8

A FIVE MODULE MODEL OF THE CELL CYCLE

In this chapter, I am going to present a new Boolean model – a significant expansion of the cell cycle model introduced in Chapter 4, by three other modules in addition to the Phase and Restriction Switches. These new modules are also, as the original two, dynamical modules, with relevant functional roles when viewed in isolation, while also contributing to the larger emergent behavior of the global system. The construction of this model was largely driven by the many observations and experimental data on the aberrant cell cycle progression observed in cancerous cells. The focus, in this case, is the interaction between the core drivers of the cell cycle and the *PI3K/AKT signaling pathway*. The model explains the details of aberrant cell cycle behavior in the case of hyperactive PI3K along with a number of other nontrivial predictions that have experimental validation in the literature.

This chapter is based on the paper titled *Boolean model of growth signaling, cell cycle and apoptosis predicts the molecular mechanism of aberrant cell cycle progression driven by hyperactive PI3K* [90], published in PLOS Computational Biology, co-authored by Herbert Sizek, Andrew Hamel, Sarah Campbell, Erzsébet Ravasz Regan and myself, with acknowledged contribution and guidance from Réka Albert. My own contribution was in making the comparison of different update schemes – particularly, as the model was built with synchronous update being the main way of validation, making the analysis with different forms of asynchronous update and verifying which of the predictions still hold with stochastic timing added to the model. I also implemented some of the "in-silico" experimental simulations and developed the code that constitutes the accompanying notebook for the paper.

8.1 Biological background of the PI3K/AKT signaling pathway's role in the cell cycle and the oscillation of the p110 catalytic sub-unit

The PI3K/AKT signaling pathway plays a role in most cellular functions. As such it is linked to cancer progression, including cell growth, proliferation, cell survival, tissue invasion, and angiogenesis. It is generally recognized that hyperactive PI3K/AKT are oncogenic due to their boost to cell survival, cell cycle entry, and growth-promoting metabolism. The dynamics of PI3K and AKT1 during cell cycle progression are highly nonlinear. In addition to the negative feedback that reduces PI3K activity, the protein expression of its subunits has been shown to oscillate in dividing cells. Here I present a proposed Boolean model of growth factor signaling that can reproduce PI3K oscillations and link them to cell cycle progression and apoptosis.

As discussed in earlier chapters, mammalian cells require extracellular growth signals to divide and specific survival signals to avoid programmed cell death (apoptosis) [95]. The pathways leading to proliferation, quiescent survival, or apoptosis are not fully independent; rather, they have a large degree of cross-talk. For example, most pathways activated by mitogenic growth signals such as PI3K $\rightarrow$ AKT1 and MAPK signaling also promote survival [96, 97]. Moreover, several regulatory proteins required for normal cell cycle progression, such as E2F1, Myc, and cyclin-dependent kinases (Cdks) can promote apoptosis as well [98, 99]. As several of our most intractable diseases – cancer, cardiovascular problems, and cellular aging-related complications – all involve dysregulation of these processes [100, 101]. The widely studied PI3K $\rightarrow$ AKT1 pathway is a major relay for growth and survival signals [102], as phosphorylated AKT1 has more than a hundred known direct targets [103, 104]. There is mounting evidence, however, that PI3K $\rightarrow$ AKT1 activity during cell cycle progression is more complex [103, 104]. Overactive AKT1 in cancer cells has been associated with driving cells into senescence (an aging cell state characterized by permanent cell cycle arrest) [105, 106]. More intriguing are studies showing that active FoxO3 and/or FoxO1 (also part of the growth signaling pathway) not only block cell cycle entry but are paradoxically required for its subsequent completion [107].

There are several known feedback mechanisms that can explain the pulse-like spike and subsequent attenuation of AKT1 following growth factor stimulation (detailed in the introduction of [90]), but most of these only explain changes in the activity of PI3K and/or AKT1. There is further evidence, however, that the p110 catalytic subunit of the PI3K enzyme complex is itself rapidly degraded

following PI3K/AKT1 activation. Its rapid disappearance immediately terminates the AKT1 activity peak triggered by growth stimulation, and it is followed by its slow re-accumulation over the next few hours. As a result, PI3K protein levels, PI3K activity, and AKT1 activity *all oscillate during the cell cycle*, an oscillation that is critical for healthy cell cycle progression. Current computational models of the regulation of mammalian cell life and death do not account for dynamic p110 expression [108]. High PI3K activity is itself the trigger for its own degradation.

The proposed model is bringing together several separately published, disconnected pieces of evidence regarding p110 protein and mRNA regulation [109, 110, 111]. The resulting growth signaling layer is then connected to an updated version of the cell cycle model (Chapter 4), as well as the molecular network responsible for survival vs. apoptosis.

8.2 Assembling a five-module Boolean model

Using a modular approach proposed in [60] discussed in Chapter 4, the proposed model collects the key signaling pathways driving cell cycle commitment in a new *Growth Signaling* module responsible for the dynamics of PI3K, AKT1, MAPK and mTORC. This module replaces the simple Growth Factor (GF) input node of the previous model, although it has its own input nodes. At the core of the new model are the two switches discussed thoroughly in this work: the Restriction Switch (section 4.1) guarding the initial commitment to DNA synthesis, the Phase Switch driving cell cycle progression from G2 to M and back to G1 (Section 4.2, Chapter 6), expanded to account for the mitotic role of the Plk1 gene [112]. A new regulatory switch is added to model *replication origin licensing*, that simply put makes sure that the same DNA is not replicated twice in the same cell. Finally, several published models of the survival vs. apoptosis decision are synthesized into the *Apoptotic Switch*. These modules are tied together into an 87-node network by direct regulatory crosstalk, as well as a few nodes that represent cellular processes we do not track in molecular detail (e.g., DNA Replication, mitotic spindle assembly or cytokinesis).

8.2.1 The Growth Signaling module – modeling the dynamic regulation of the p110 expression during growth factor signaling

The Growth Signaling module incorporates the molecular drivers of p110 dynamics found in the literature, specifically mechanisms that can drive rapid

p110 degradation and gradual re-synthesis. [109, 110]. This module models two major mechanisms, with the biological and mechanistic details discussed in Sizek et al. [90]. First, PI3K activation initiates a negative feedback loop leading to its own degradation, independently of its effect on AKT1. The network representation of this negative feedback is shown by the red links in Figure 8.1. In the model and in Figure 8.1 p110 is represented by p110_H, which is an abstract node whose OFF state indicates normal p110 activity and whose ON state indicates a higher-than-normal level of p110 activity.

The second mechanism the model considers is p110 re-synthesis. Studies of the p110 promoter indicate it is positively regulated by FoxO3 [111]. The hypothesized mechanism is that reactivation of FoxO3 in the G2 phase of the cell cycle after the initial AKT1 activation subsides, is the driving force behind p110 re-synthesis (Figure 8.1 A, orange links).

The degradation and resynthesis of p110 on 8.1 can be observed by following the different colored arrows. The node p110_H has two inputs (not counting the self-loop), an inhibition from NeddL4, which represents the NeddL4-catalyzed degradation of p110 and activation from FoxO3, which represents the FoxO3-catalyzed (re)synthesis of p110. The degradation is initiated when NeddL4 turns on. The re-synthesis can happen if NeddL4 is off and FoxO3 is on. The activation of NeddL4 is part of the negative feedback loop highlighted in red. This loop indicates that p110 indirectly activates the driver of its degradation. The orange loop indicates that p110 indirectly inactivates FoxO3. The inhibition of FoxO3 is no longer sustained after the p110 level goes down, enabling re-synthesis of p110. In summary, both the inhibition and activation links are embedded in negative feedback loops that together are causing the module to oscillate.

To integrate these negative feedback loops with the canonical PI3K / AKT signaling cascade activated by growth receptors separate Boolean nodes were introduced to track basal vs. peak PI3K and AKT activity (Figure 8.1; Boolean rules: [90] S1 Table A). The model can thus distinguish between survival signaling in a low growth factor environment (where basal PI3K and AKT are ON) and peak PI3K/AKT activation following the arrival of a strong mitogenic stimulus. Complemented by a linear MAPK cascade and mTORC1/2 signaling, this non-linear PI3K/AKT axis dominates the behavior of the resulting Boolean Growth Signaling module.

Modeling the two feedback loops controlling p110 expression in isolation shows that they generate a sustained, robust oscillation (Figure 8.2), even though the model does not account for the fact that p110 degradation is significantly faster than its re-synthesis. This oscillation is the only attractor state of the small module regardless of the update scheme. As Figure 8.2 indicates, the

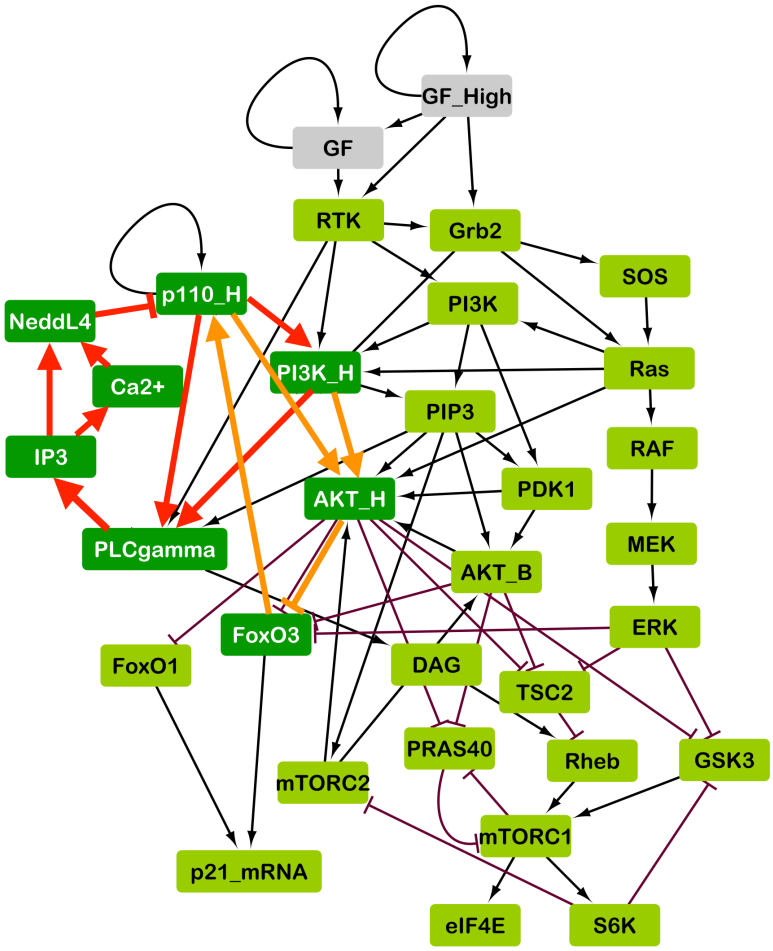

Figure 8.1. *Growth Signaling Module of the Boolean model, including the degradation/re-synthesis circuit in control of p110 expression (left, dark green), basal PI3K/AKT signaling (middle), downstream effectors of AKT1 (mTORC1 signaling, GSK3 & FoxO1, bottom), and the MAPK cascade (right). Edges types: →: activation; ⊣: inhibition; thick red links: p110 degradation; thick orange loop: p110 re-synthesis.*

synchronous attractor cycle clearly maps onto the cyclic succession of complex attractor states of the general asynchronous model. In addition to never leaving the complex attractor shown in Figure 8.2, asynchronous time series repeatedly walk through cycles of states that resemble the synchronous limit cycle. Within the context of the larger Growth Signaling module, this oscillation only occurs under ongoing high growth factor stimulation.

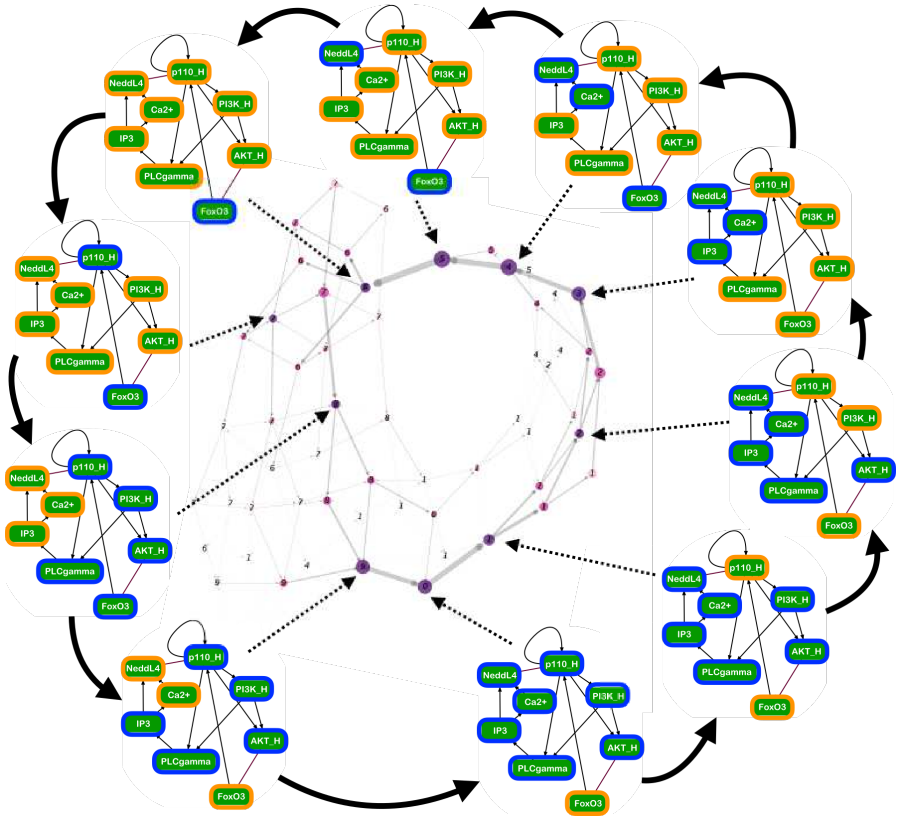

Figure 8.2. *Periphery: sequence of network states along the synchronous limit cycle of the core PI3K circuit. Orange/blue borders: ON (expressed and/or active) / OFF (not expressed and/or inactive) node. Middle: state transition graph of the general asynchronous model (one random node updated per timestep; sampled for 10,000 steps), yielding a complex limit cycle that covers the synchronous cycle. Node size: visitation frequency; label: most similar synchronous cycle state; node color: overlap to the most similar synchronous cycle state (one minus normalized Hamming distance)*

8.2.2 The core cell cycle elements and the Origin Licensing Switch

First,the switch-like restriction point control guarding cell cycle entry is added by reusing the Restriction Switch (Figure 8.3 A, blue subgraph & box; detailed in Section 4.1).
Second, the Phase Switch (detailed in Section 4.2) has been added and expanded to account for the regulation and key functions of Polo kinase 1 (Plk1) (Figure 8.3, purple subgraph & box) [112]. Plk1 is activated in early G2 by the FoxM1 transcription factor [113], but evidence of decreased Plk1 expression in the absence of FoxO3 [107] and/or FoxO1 [114] during G2 also connects Plk1 availability to the dynamics of PI3K $\rightarrow$ AKT1 $\dashv$ FoxO signaling. The updated Phase Switch still retains three steady states, matching the activity pattern of this network in G0/G1, at the G2 checkpoint, and at the Spindle Assembly Checkpoint (SAC). In this version of the Phase Switch, Mad2 acts as an external node to the module.

Origin Licensing Switch

The third addition is a small switch that tracks the assembly, licensing and firing of replication origins, shown in Figure 8.3 A, brown subgraph & box; (more details in [90] Methods & Model, Boolean Network Modules Representing Distinct Cellular Regulatory Functions Growth Factor Signaling). The Boolean rules of the Origin Licensing Switch are shown in Table 8.1. This two-state switch reproduces the stability of assembled Pre-Origin of Replication Complexes; its two steady states correspond to unlicensed and licensed origins.

node	regulatory function
Pre_RC*	= ORC and Cdt1 and Cdc6
Cdt1*	= Pre_RC and ORC and Cdc6
ORC*	= Pre_RC and Cdt1 and Cdc6
Cdc6*	= Pre_RC and ORC and Cdt1 and Cdc6

Table 8.1. *Regulatory functions (Boolean rules) of the Origin Licensing Switch*

Abstract and supporting nodes

Fourth, progression and completion of cell cycle processes not modeled in molecular detail had been accounted for via the Replication and 4N DNA nodes (as in Chapter 4), an unattached kinetochore node (U_Kinetochore) to denote incomplete mitotic spindle assembly, and an attached kinetochore

node (A_Kinetochore) to mark the completion of the mitotic spindle (Figure 8.3 B, orange nodes). Finally, key regulators of the coupling between regulatory switches and cell cycle processes such as S-phase checkpoint signaling (Chk1), the unattached kinetochore sensor Mad2 (previously part of the Phase Switch module), and a marker of contractile ring assembly and cytokinesis (Ect2) linked these modules (Methods & Model, [90] Boolean Network Modules Representing Distinct Cellular Regulatory Functions Growth Factor Signaling; Boolean rules: S1 Table E).

8.2.3 The Apoptotic Switch

To account for the apoptotic effects of growth factor withdrawal and death due to mitotic failure, published models of apoptotic commitment were synthesized to create a detailed Boolean regulatory switch (Figure 8.3 B, dark red subgraph & box; Boolean rules in Table 8.2) [115, 116, 60, 117, 118, 119, 120, 121]. This switch has two stable states corresponding to survival and apoptosis, and it is flipped when extrinsic signals from death receptors or intrinsic signals due to mitotic failure trigger Mitochondrial Outer Membrane Permeabilization (MOMP), which leads to the activation of the executioner Caspase 3 activity [115]. While the positive feedback loops that stabilize apoptosis are common to most models, the signals that trigger mitotic catastrophe have not yet been modeled. To do this Caspase 2 activation had been incorporated for the case of prolonged or perturbed metaphase [122, 123]. Literature indicates that a normal mitotic progression is a balancing act on the part of Cyclin B/Cdk1 and Plk1. On one hand, both kinases phosphorylate and inhibit the anti-apoptotic BCL2/BCL-XL proteins, priming cells for apoptosis [124, 125, 126]. On the other hand, Cyclin B/Cdk1 also inhibits Caspase 2, keeping cells alive as long as mitosis is not stalled [127]. In addition to the loss of Cdk1 activity, metaphase cells also undergo Caspase 2 mediated apoptosis in the absence of Plk1 [128]. The model captures this balance of pro- and anti-apoptotic signals such that loss of Cdk1 or Plk1 activity before cells clear the spindle assembly checkpoint can push them to mitotic catastrophe.

8.3 The network of linked regulatory models reproduces environment-dependent proliferation, quiescence, and/or apoptosis

Linked together, the modules generate a dense 87-node Boolean model with 375 links shown in Figure 8.3 B.

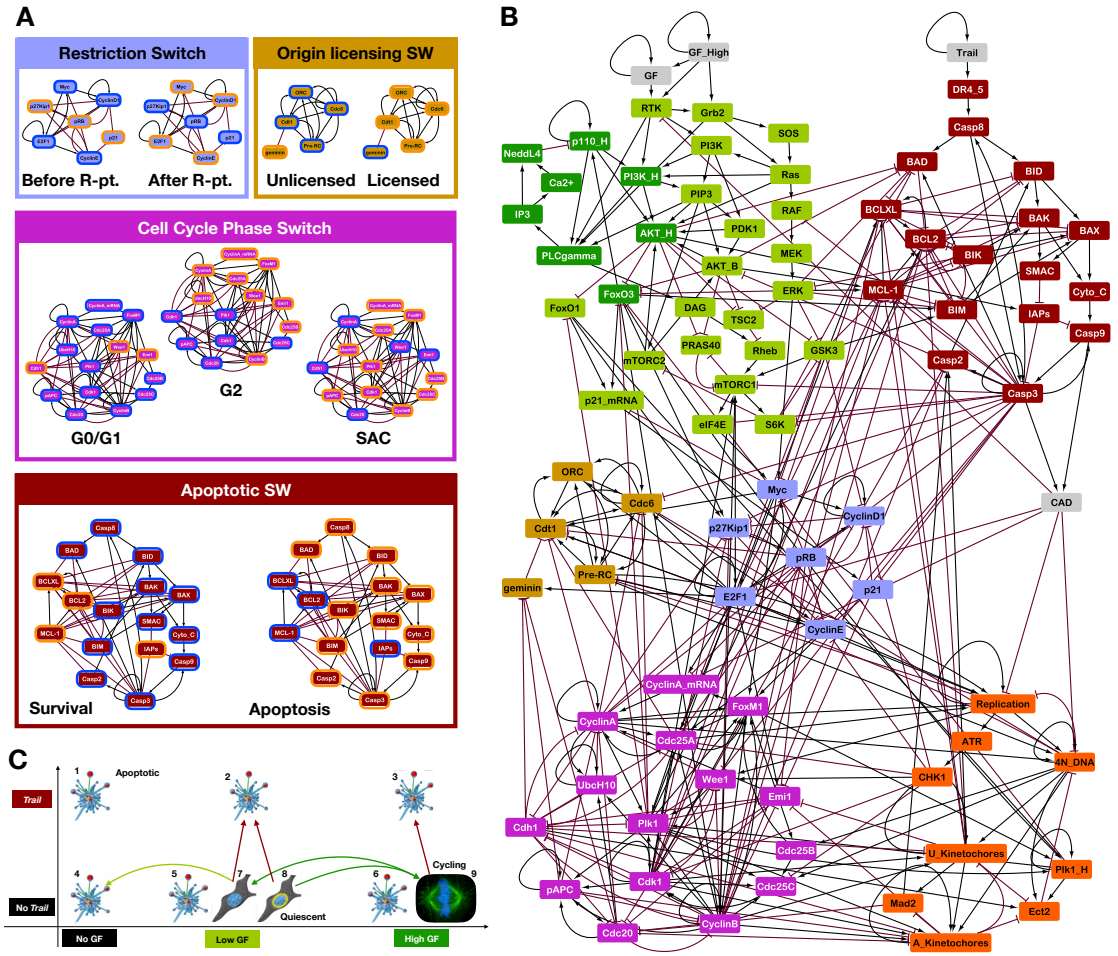

Figure 8.3. *Modular Boolean model reproduces quiescent, apoptotic, and cell cycle phenotypes expected in various extracellular environments. (A) Stable attractor states of isolated regulatory switches. Blue / light brown / purple / dark red boxes: stable states of the Restriction / Origin of Replication Licensing / Phase / Apoptotic Switch. Orange / blue node border: ON / OFF state. (B) Network representation of the Boolean model partitioned into regulatory switches and processes. Gray: inputs representing environmental factors; green: Growth Signaling; dark red: Apoptotic Switch; light brown: Origin of Replication Licensing Switch; blue: Restriction Switch; purple: Phase Switch; orange: cell cycle processes and molecules that bridge between the multi-stable modules. Black →: activation; red ⊣: inhibition. (C) Cell phenotypes predicted for every combination of no/low/high growth-factors (x-axis) and Trail exposure (y-axis). Network-wide ON/OFF state of each attractor, along with the molecular signatures that define each phenotype are detailed in S2 Table. Blue fragmented cells: apoptotic states (#1-6); gray elongated cells: quiescent/non-dividing states (#7-8); cells with mitotic spindle: cell undergoing repeated cycles (#9). Yellow circle around nucleus: 4N DNA content; double-/single-headed arrows between cells: reversible/ irreversible phenotypic transitions in response to changing environments; green arrow: change in growth factor levels; red: change in Trail exposure.*

node	regulatory function
Casp9*	= Casp3 or (not IAPs and Cyto_C)
IAPs*	= not SMAC
Casp2*	= Casp3
BID*	= Casp8 or (not MCL_1 and Casp2 and not BCLXL and not BCL2)
Casp3*	= (Casp9 and Casp8) or (Casp9 and Casp3) or (Casp8 and Casp3) or (not IAPs and Casp9) or (not IAPs and Casp8) or (not IAPs and Casp3)
MCL_1*	= not Casp3 and not Casp2
BAK*	= (not MCL_1 and BIM and not BCLXL) or (BID and not BCL2) or (BID and not BCLXL) or (not MCL_1 and BID) or (not MCL_1 and BIK and not BCLXL) or (BIM and BID) or (BIK and BID)
SMAC*	= BAX or BAK
Casp8*	= Casp3
BIK*	= not MCL_1 and not BCLXL and not BCL2
BCLXL*	= (not Casp3 and not BAD) or (not Casp3 and BCL2)
Cyto_C*	= BAX or BAK
BIM*	= not MCL_1 and not BCLXL and not BCL2
BAD*	= Casp8 or Casp3
BCL2*	= (MCL_1 and not Casp3 and not BIM and not BIK and not BAD) or (not Casp3 and not BIM and not BIK and BCLXL and not BAD)
BAX*	= (BIM and not BCLXL) or (BIK and not BCLXL and not BCL2) or (BID and not BCLXL and not BCL2) or (BIM and BID) or (BIM and BIK) or (BIM and not BCL2) or (not MCL_1 and BIM)

Table 8.2. *Regulatory functions (Boolean rules) of the Apoptotic Switch model*

The model reproduces the cell-cycle dependent role of PI3K, AKT1 and FoxO proteins [107, 129]. As expected, it generates straightforward behaviors such as lack of cell cycle commitment in the absence of high p110 expression [129], or G1 shortening in the presence of hyperactive PI3K / AKT1. The novelty and value of the model, however, stems from its ability to reproduce more intricate, non-intuitive phenotypic outcomes. *First*, the model reproduces the path to apoptosis in the event of a mitotic catastrophe [122]. *Second*, the model generates four distinct cell fates in response to Plk1 inhibition, depending on the timing of Plk1 loss [112]:

1. G2 arrest [130],
2. mitotic catastrophe [112, 131, 132, 133],
3. premature anaphase and chromosome mis-segregation leading to aneu-

ploidy (the presence of an abnormal number of chromosomes in a cell) [134],

4. failure to complete cytokinesis following telophase [135, 136, 137], which can lead to genome duplication [134]

Third,the model can replicate failure of cytokinesis and accumulation of binucleate telophase cells driven by hyperactive PI3K / Ak1 or FoxO inhibition [107].

The synchronous dynamics of the full model is heavily constrained by the switch-like behavior of its modules, as evidenced by the small number of tightly coordinated behaviors (phenotypes) it generates. Indeed, when the state space of the network is sampled extensively using noisy synchronous update, every attractor corresponds to a distinct cellular phenotype. These attractors are characterized in detail in [90] S2 Table, along with key molecular signatures that allow the matching of each attractor to a specific phenotype. Figure 8.3 C summarizes the attractors according to the extracellular environment (combination of input values) each phenotype occurs in; namely, the absence / low abundance / high abundance of growth factors (x-axis in Figure 8.3 C) combined with the presence / absence of the apoptotic signal Trail (y-axis). The matching of experimentally documented cell behaviors (in multiple cell types) with the attractors of the model is detailed in Table 1 of Sizek et al. [90]. As biologically expected, irreversible apoptosis is stable in every environment. Moreover, the ongoing presence of saturating Trail (i.e., Trail input is ON 100% of the time) destabilizes every other cell state, leaving apoptosis as the only stable option [138, 139, 140, 141]. Similarly, the complete absence of growth / survival signals also leads to apoptosis [142, 143, 144]. In contrast, low levels of growth signaling support quiescent cell states, and the model identifies two distinct forms. First is a healthy cell state with 2N DNA content (Fig 8.3 C, the elongated cell with the blue nucleus on). Second, the model also produces a G0-like state representing cells that have failed to complete mitosis or cytokinesis in the past, now stuck with a 4N DNA content (Fig 8.3 C, the elongated cell with a yellow circle around the nucleus). Finally, exposure to high growth factor levels results in a cyclic attractor representing continuously cycling cells (Fig 8.3 C, mitotic cell).

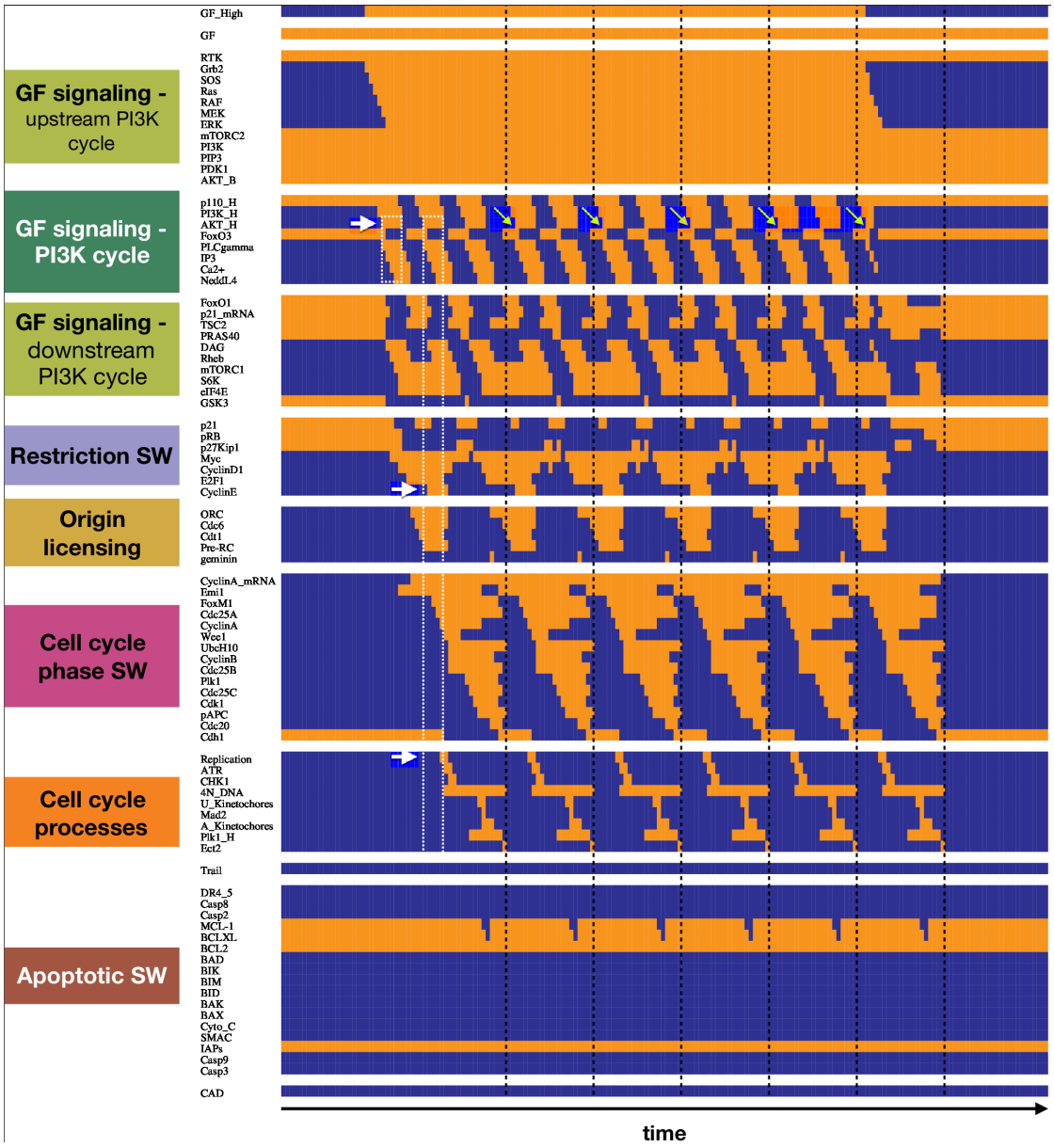

Figure 8.4. *Module-level switches toggle each other to generate the cell cycle, locking PI3K oscillations to the rhythm of division. Dynamics of regulatory molecule expression/activity during cell cycle entry from G0, showcasing the phase-locking of PI3K oscillations to the cell cycle. X-axis: time-steps; y-axis: nodes of the model organized in modules; orange/blue: ON/OFF; white boxes & arrows: first two peaks of AKT1 activation with respect to DNA replication; black dashed lines: cytokinesis; lime arrows: first AKT1-high pulse in each division cycle.*

8.4 The model's trajectory is robust to fluctuations in signal propagation and reproduces the cell cycle with synchronous and asynchronous update

To test whether the orderly progression through the cell cycle is robust to random fluctuations in signal arrival time as they propagate through the network, we tested the model's behavior under random order asynchronous update (see Section 3.1.2). As steady states of a Boolean model remain the same regardless of the update scheme, we focused on the cell cycle. As Figure 8.5 shows, a random update order does not abolish the model's capacity to execute a correct cell cycle sequence, but it does introduce several non-biological behaviors as well. First, the signals that couple successful DNA replication to the establishment of a G2 state are lost under a subset of update orders, leading to a G2 $\rightarrow$ G1 transition followed by a new cell cycle. Second, the signals that drive cytokinesis can also be disrupted by certain update orders. Third, the balance of pro- and anti-apoptotic signals during metaphase can tip in favor of apoptosis as if the cell experienced mitotic catastrophe. Interestingly, all three cell cycle errors are common in cell populations experiencing knockdown or overexpression of a variety of cell cycle regulators [108, 112, 145], leading us to conclude that the asynchronous model with random update order mimics the occasional short-term loss of regulators.

In order to create a restricted random order that forbids asynchronous state transitions resulting from these non-physiological breaks in signal transduction, we identified the nodes and processes that deviated from their expected activity every time a particular error occurred. We then created an asynchronous version of the model with *biased random update*. To do this, we placed a small subset of nodes at the start or at the end of the update order, depending on their activation status (11 nodes; list and rationale in Sizek et al. [90] S3 Table). Using this biased update our model repeatedly and *correctly executes the cell cycle*, in spite of the asynchronous update. Our update bias did not completely eliminate non-biological behaviors, but the incidence of these errors drastically decreased. As these errors do occasionally occur in naturally occurring cells, we choose not to restrict our update order to the point where we eliminate them. In order to quantify the rate at which the two update schemes produce normal cell cycle events vs. different errors, we ran a series of simulations at varying levels of growth factor and Trail stimulation. We did this by setting GFH or Trail ON with probability p in each time-step, OFF otherwise.[90] Figure 5B indicates that the asynchronous model with biased update shows a similar response to growth factors and Trail as the synchronous model.

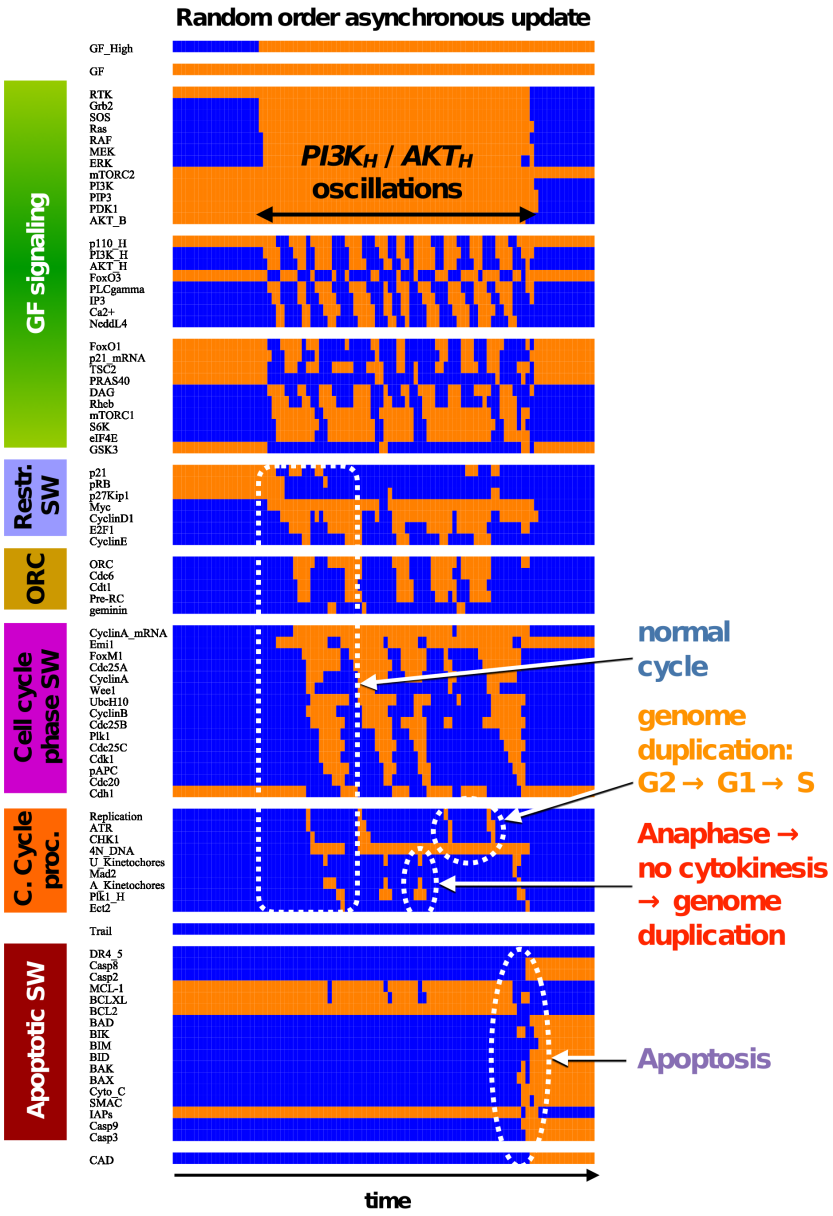

Figure 8.5. *Dynamics of regulatory molecule activity during cell cycle entry from G0 using random order asynchronous update (example time-course chosen to illustrate errors). X-axis: time-steps; y-axis: nodes organized in modules; orange/blue: ON/OFF. Black arrows: robust PI3K oscillations; white box: normal cell cycle; white circles: common cell cycle progression errors (labeled).*

The apoptotic fixed-point is reachable from the cell cycle under both random order and biased random order asynchronous update, indicating that the cell cycle is not, strictly speaking, a complex attractor. Nevertheless, starting an asynchronous time series from any state along the synchronous cell cycle attractor results in long time-courses featuring repeated (if occasionally incorrect) cycles, indicating that the system's state space has a meta-stable region that traps its dynamics in a way that resembles complex attractors. In order to test whether this meta-stable collection of states is also a cycle, we sampled the state transition graph of the asynchronous model with both update schemes (random order and biased random order) by starting 10 independent time courses of 1000 steps from each state along the synchronous cell cycle. In order to sample the meta-stable basin rather than the path to the apoptotic attractor, we prematurely interrupted each run if it reached a fixed point. We then merged all observed states and transitions and visualized the largest strongly connected component, shown in Figure 8.6. To test whether these state transition graphs are consistent robust execution of the cell cycle, we classified each state as representing G1, S, G2, metaphase, anaphase, telophase, and cytokinesis depending on the ON/OFF state of key processes ([90] S6 Fig). Instead of a cycle, however, the resulting network revealed distinct regions of state-space representing G1, S and G2, then a few highly restricted and often-visited paths through anaphase and to lesser extent cytokinesis. Thus, asynchronous update indicates that there may be widespread molecular heterogeneity in G1, S and G2, but most of the network we model locks into a few unique states during anaphase.

It is worth noting that the model features two internal oscillators, the core cell cycle and the PI3K degradation / re-synthesis cycle. As Figure 8.5 and [90] Figure 5 indicate, these two cycles are not completely phase-locked under asynchronous update. As the cell cycle proceeds, the small PI3K oscillator and the downstream mTORC1 pathway can be found in nearly any state. The sole exception is anaphase, where the two cycles appear to synchronize. To show that the heterogeneity is chiefly due to the growth pathway, we projected the state transition graph of each asynchronous model onto a subspace where each model state represents a unique ON/OFF state within the core cell cycle modules, regardless of the state of all other nodes (Restriction Switch, Origin Licensing Switch, Phase Switch and abstract nodes). This process collapsed the complex state transition graph of the biased model onto a clear cyclic flow of transitions, representing normal cell cycle progression (Figure 8.6, bottom right). In contrast, the random asynchronous model's dynamics has a loop corresponding to the cell cycle, but it is dominated by prominent "backward" transitions representing endoreduplication from G2 (Figure 8.6, top right).

An extensive list of the biological predictions of the different emergent be-

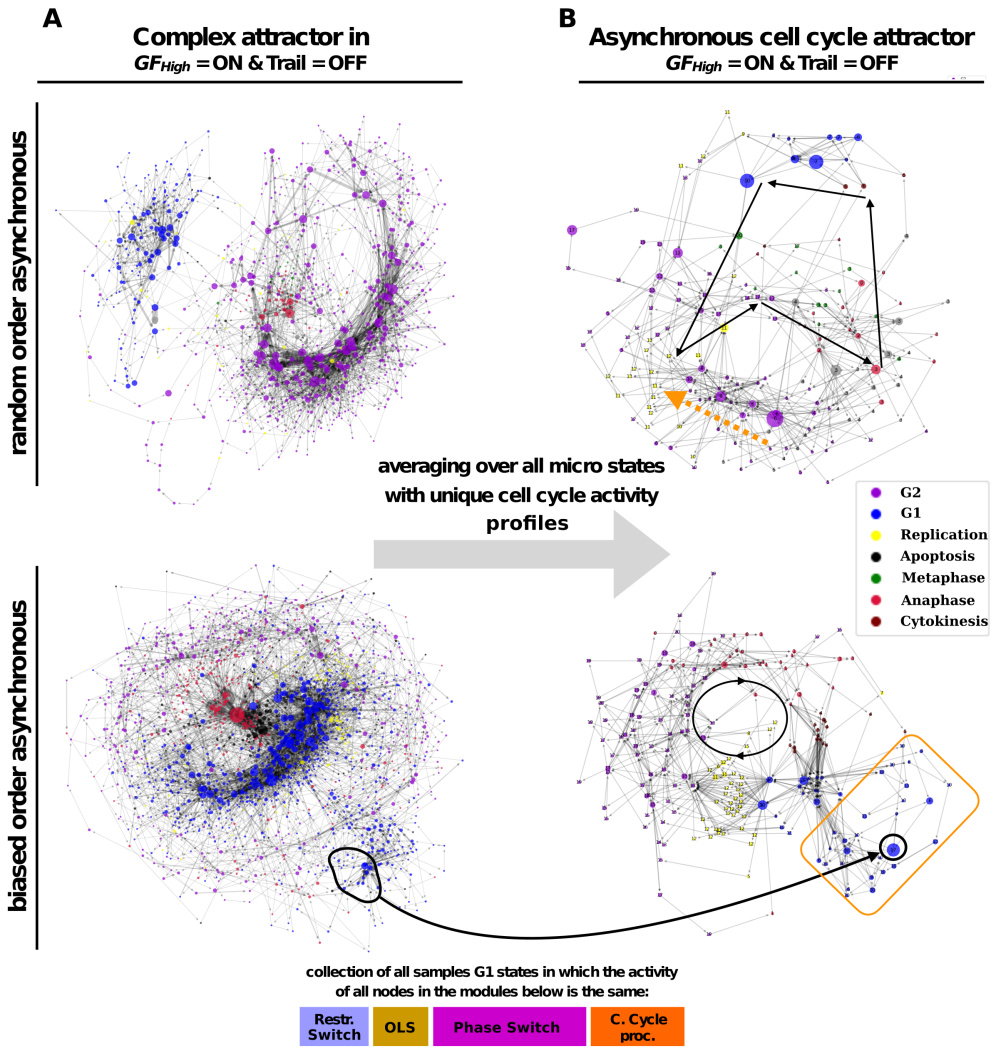

Figure 8.6. *(A) State transition graph of the random order (top) vs. biased random order (bottom) asynchronous models, sampled for 10 independent runs of 1000 time-steps starting from each of the 21 synchronous cell cycle attractor states (cut short if the model reached apoptosis). The largest strongly connected component of each resulting state transition graph representing the cell cycle pseudo-attractor. (B) Projection of each state transition graph onto the sub-space defined by the expression of core cell cycle modules (bottom). Nodes: a collection of all states that have identical core cell cycle node activity but differ in the activity of nodes in other modules such as Growth Signaling, illustrated by linked black circles from (A) to (B); Node color: cell cycle phase best approximated by each sampled state; node size: state visitation count; node label: most similar synchronous cell cycle state; black loop (top) & black cycle (bottom): areas of the projected state transition graph with a cyclic pattern of transitions that match the cell cycle; orange arrow (top): direct G2 → S transition (endo-reduplication); orange box (bottom): G0-like pause in the G1 phase of the cell cycle, forming a distinct module apart from the G1 states of cells that pre-commit in their previous cycle.*

haviors of the model are summarized in [90] Table 2 and described them in detail in [90] S1 Text A-D.

CHAPTER 9

SUMMARY AND OUTLOOK

9.1 Summary of the thesis

In Chapters 1 and 2 I have presented a case for the need for systemic, network-based approaches to better understand the underlying natural principles of the biology of cells. These systemic modeling approaches, more specifically Boolean dynamic models, have consistently proven useful in a diverse range of biological problems. During our research, we have predominantly focused on the topic of the cell cycle – the main driving process of the proliferation of cells.

In Chapter 3 I have defined and introduced the key concepts and methodological tools that we used to obtain the results presented in this work.

In Chapter 4 I have introduced the Boolean model of the cell cycle published in 2016 [60] as the interaction of two Boolean switches or modules. The two modules, the Restriction Switch and the Phase Switch, both have biologically relevant steady states but when they are coupled together a global cyclic attractor (limit cycle) emerges. The global limit cycle toggles the attractors of its constituent modules in a sequence of events consistent with the biological knowledge of the cell cycle. Thus the two modules keep their functionality in the coupled system while contributing to global phenotypes that are nontrivial combinations of the module-phenotypes. We call this property dynamical modularity and hypothesize that this could be a general feature of biological systems, which need to be both robust and adaptive to different environments.

In Chapter 5 I have defined the three principles of dynamical modularity that have to be simultaneously true for a system to exhibit the behavior we observed in the case of the cell cycle. We also introduced three measures that quantify the three principles and make them possible to measure on any Boolean model where we know dynamical modules. We show that the dynamical mod-

ularity is a non-trivial property of the cell cycle model as randomized versions of it almost always fail at least one of the principles.

In Chapter 6 I have discussed our discovery and analysis of an even more elementary network at the core of the cell cycle, which is driving the cell between the checkpoints, published in 2019 [62]. The Phase Switch Oscillator is a subgraph of the previously published Phase Switch model and it exhibits an extremely robust oscillation between the phases of the cell cycle, which are the attractors of the original Phase Switch model. We explained this behavior with a new concept, the conditionally stable motif, which is a generalization of the concept of stable motif introduced by Zañudo and Albert [61]. Conditionally stable motifs cause often large parts of the network to stabilize as long as just a few nodes outside the motif maintain a specific state, thus creating "funnels" in state space that lead to robust trajectories. Leveraging the interaction of conditionally stable motifs we presented a way to reduce the 8 node model into a 3 node version that still keeps the relevant features of the larger model. This reduction presents an alternative view on dynamical modularity.

In Chapter 7 I have presented our analysis of the full cell cycle model (both modules coupled) with general asynchronous update using some of the methods applied in Chapter 6. We showed that the full model's complex attractor is also a considerably robust oscillation, however, it exhibits some non-biological behaviors in the presence of stochastic timing, such as completing the cycle without a replicated DNA. We also explained how the stable motif structure of the Restriction Switch module is affected by the coupling interactions, and we discuss its overall role in the cell cycle progression.

In Chapter 8 I have discussed a more recent model, published in 2019 [90] that builds on the cell cycle model discussed in Chapter 4 by adding three additional modules. First, a growth factor module with an internal oscillator of its own, involving the PI3K and p110 molecules (which are often found to be hyperactive in cancerous cells), second, the Apoptotic Switch that can drive the model into steady states corresponding to apoptosis (programmed cell death) and the Origin Licensing Switch that makes sure the DNA is only replicated once within the same cell. The coupled model of 87 nodes has a limit cycle and several steady state attractors and it makes several non-trivial biological predictions confirmed by the literature. My analysis has shown that the main cycle also maintains many of its features under timing variability (general asynchronous update).

9.2 Possible directions for future research and discussion

An important follow-up research direction is to generalize the coarse-graining methods presented in 6.5. Such a method has important practical implications in reducing the state-space of larger models while keeping the essential emergent behaviors. Moreover, it can also reveal theoretical insights into how dynamical modularity emerges in natural decision-making systems. One of our main conclusions in Chapter 6 was that conditionally stable motifs (CSMs) capture the feedback mechanisms that make the trajectories of the dynamical system robust to stochastic timing while also driving them towards specific attractors. We've seen in the case of the Phase Switch Oscillator (PSO) that the interaction between the groups of CSMs explained both the robust oscillation and the sequential approach of the Phase Switch attractors by the complex attractor. For the Phase Switch Oscillator, the so-called "cycle graph" – a graph representation of all overlapping CSMs (see Supplementary Figure 10.3) had 6 disjoint components that perfectly corresponded to the 6 possible states of the three groups that formed the meta-nodes of the coarse-grained model (Cyc, Cyclosome, UbcH10). The three meta-nodes of the PSO behave as dynamical modules: all three are bistable when considered in isolation and when linked, the coupled model fulfills the principles of dynamical modularity (Chapter 5): the global attractor is a non-trivial combination of the meta-node states, and no meta-node state is lost in the global attractor. The only problem is with fulfilling the Switch Quality Measure, which requires multiple global attractors, but in this case, we only have one. Further investigation into dynamical modularity is needed to reveal (i) how CSMs contribute to or form dynamical modules and (ii) the rules of coupling such modules so that a dynamically modular global attractor emerges.

The identification of the dynamical modules of the cell cycle model work (Phase Switch, Restriction Switch, Apoptotic Switch, etc.) was the result of biological intuition based on my collaborator Dr. Ravasz-Regan's years of work with experimental data and literature. However, our work with the PSO has given us a first case where we could identify dynamical modules purely from the model, using the expanded network formalism and the concept of conditionally stable motifs instead of specific biological knowledge.

We have already taken steps towards applying the coarse-graining methodology on the full cell cycle model. Unfortunately, cycle-graph of the model does not yield internally consistent disjoint components the same way the PSO does, so any general coarse-graining method we adapt has to have some extra conditions. We propose to relax the criterion of meta-node (dynamical module)

membership and only track nodes that interact with nodes of other meta-nodes. We also have an algorithm for finding of emergent higher-level logical rules between the meta-nodes using truth table manipulation. I believe these are important steps towards a better understanding of the overall dynamical hierarchy of biological systems.

Regarding the three measures of dynamical modularity discussed in Chapter 5 we are aware that some are very complicated and difficult to comprehend. Their complexity developed mainly due to the difficulty of comparing cyclic attractors made up of many states to each other and to single state attractors. The measures are also filled with conditions and constraints encoding biological intuitions. For example, biological intuition suggests that in the case where both a module attractor and the global attractor are cyclic, dynamical modularity is only fulfilled if the states of the cyclic module attractor are visited in the same order in the global attractor as in the module. The current implementation of the AMM Measure includes a large penalty if the order of visitation is scrambled. It may be fruitful to consider simplified versions of these measures that relax some of the many constraints.

Another logical follow-up to this work is further extending our analysis on the 5 module Sizek et al. model [90] discussed in Chapter 8, involving the stable motif analysis of the new modules such as the Apoptotic Switch and Origin Licensing Switch. Such an analysis can have important implications in controlling the cell cycle in non-intuitive ways. While our analysis of the Phase Switch, described in Chapter 6, indicated stable motifs of a module can become conditionally stable motifs of the full system, our analysis of the Restriction Switch suggests other possibilities: the module stable motifs may destabilize by having contradictory conditions, or may reduce in size. Our preliminary analysis suggests that the stability of the attractors of the Origin Licencing and the Apoptotic Switch is very asymmetrical. The stable motifs of the *Survival* attractor are all very large, comparable to the size of the module, suggesting that maintained stability requires a lot of conditions to be fulfilled simultaneously. Conversely, the cascade leading to *Apoptosis* can be triggered by a single node (Casp3) and can lock in by the activation of just another node (Casp8 or Casp9). Similarly, in the case of the Origin Licencing Switch the *Licensed* state is only self-sustaining if all of the nodes are on, while the *Unlicensed* state has several smaller motifs that can individually lock in the attractor. It is encouraging that the stable motif formalism once again captures biological intuitions into the more formal network terms and give us means to make predictions for interaction and control. It would be interesting to investigate how the asymmetric stability is handled by the other modules coupled to these switches, and how it manifests in the global attractor. Our Switch Stability Measure (defined in Chapter 5) of dynam-

ical modularity is a way to quantify how well the relative probability of the module-attractors is maintained in the global attractor. Based on that, the next step would be understanding the mechanistic principles of the coupling that maintain (or balance) the asymmetry in different environments.

The internal PI3K oscillator exhibits an oscillation robust to timing variability. The expanded network of this oscillator, shown in Figure 9.1, is simpler than that of the PSO (compare with Figure 6.7). It does not have conditionally stable motifs except for a self-loop on p110H. This seems to be an efficient way of generating simple natural oscillations with some delay, however, it would be worthwhile to see how robust it is to external perturbations as compared to an oscillator reinforced by a lot of positive feedback loops such as the PSO.

If our coarse-graining methods advance to a stage where we can apply them to the Sizek et al. model, we could create a higher-level model of the cell cycle that has all the relevant features but has a much smaller state-space.

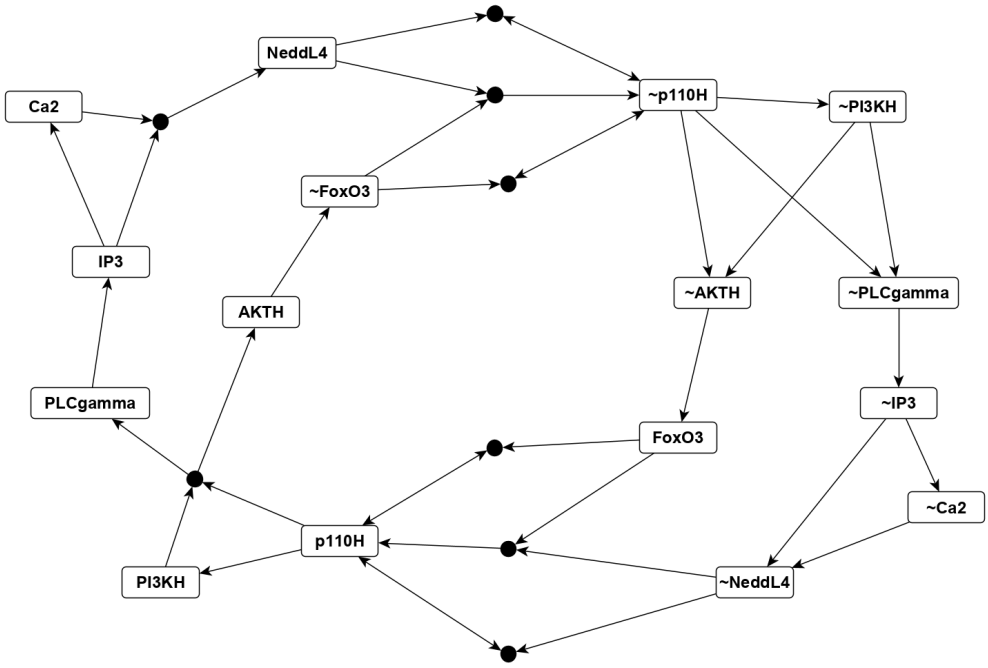

Figure 9.1. *The expanded network of the PI3K oscillator. The expanded network reveals the logical relationships that make the oscillation possible: a negative feedback loop closing two parallel chains of linear activation (and deactivation). The only conditionally stable motifs are the two states of p110H (visible as bidirectional edges between a composite node and the virtual nodes).*

A potential application for our cell cycle model is a better understanding of Alzheimer's disease. Multiple experimental studies are suggesting that before

and during the onset of Alzheimer's disease the naturally quiescent (G_0) neural cells re-enter the cell cycle [146, 147, 148]. This re-entry then results in apoptosis, which then leads to the gradual degradation of the brain. As many of these emergent processes are already included in our models, adapting the models to neurons would be relatively straightforward. Then applying the methodology discussed in this work could help us understand (probably non-trivial) mechanistic details of why the re-entry into the cell cycle happens and why it leads to apoptosis. This understanding will lead to predictions of how to reverse the process. For instance, Cyclin B is a key molecule that the experimenters detect in a significantly larger concentration in the brains of Alzheimer's patients [148]. We have shown in Section 6.6 that timed over-expression (forced on state) or knock-out (forced off state) of Cyclin B can theoretically drive the cell cycle into any of its main phases. An intervention involving the knock-out of Cyclin B together with another cell cycle regulator could potentially reset the cell cycle into G_0. Conversely, over-expressing Cyclin B and simultaneously preventing the apoptosis cascade would drive cells to finish the cell cycle then settle. All this requires a profound understanding of how the dynamical modules of the system interact: Prevention of an apoptotic cascade necessitates an understanding of the interaction of the core cell cycle modules with the apoptosis module. Triggering or halting cell cycle entry requires an understanding of the interaction of the growth signaling and core cell cycle modules. The Sizek et al. model includes many of the key modules and coupling interactions and it is a good stepping stone for further research. As pharmaceutical giants such as Pfizer are ending funding for Alzheimer's research due to lack of any breakthrough [149], our systemic approach could potentially provide a viable alternative research direction.

When working with Boolean models one has to be conscious about the implicit simplifications and assumptions. The binary abstraction of gene activity is often not justified, as there can be more than two different levels of effective molecular concentration and thus simple Boolean logic is not sufficient to plausibly encode the biochemical interactions. In these cases, multi-level models and ODE models offer viable alternatives. Another issue is the timing of events, as there is no straightforward way to encode the duration of biological processes into a Boolean model. Because of this we usually test the two extremes: everything happening in perfect synchrony (synchronous update scheme) or any event can happen at random times (general asynchronous update scheme). The biological truth is usually somewhere between the two extremes, and the features that are maintained in both extreme cases are usually reliable biological predictions. I have shown multiple examples of such comparisons of timing; however, one always has to consider the actual biological system and adjust the

particularities of a model in a case by case basis.

9.3 Conclusion

There is overwhelming support of the need for a more holistic, systems-level understanding of biology. A systems-level analysis is not just a method to comprehensively synthesize a large amount of experimental data available, but also a path to explore the *design principles* [150] of life and evolution. Our goal is to apply the same modeling approach that made physics successful: based on the integration of small-scale, local interactions we explain the emergent macroscopic behavior of a system. In this work, I argued that the same principles are operating at multiple scales of the hierarchy of interactions in living organisms. We used the Boolean dynamic systems framework, which offers a useful abstraction of complex biochemistry into networks of logical decision-makers. What we have found is that the interacting simple decision-makers on one scale (such as genes) cooperate in creating dynamical modules that make decisions on a higher scale. The dynamic behaviors at an even higher scale represent combinations of the states of the decision making modules. The Boolean models of the cell cycle I presented (Chapters 4 and 8) confirm this view. First, the dynamic behaviors that emerge from the local interactions of the nodes accurately match the known biology, second, the dynamic behavior is a combination of the decisions of lower-level decision-making modules. Moreover, the decision-making modules are themselves emergent from the interactions of simple binary nodes (which encode lower level biochemical decisions). Our effort to formulate the principles of dynamical modularity and quantify their presence is a step towards a better understanding of the general principles that give rise to the simultaneous robustness and adaptive nature of living organisms.

I also presented our discovery of an internal oscillator that cycles between the checkpoints of the cell cycle and can be halted by the modules responsible for the checkpoints (Chapter 6). We introduced a general concept, the conditionally stable motif (a part of a network that stabilizes to specific states as long as conditions external to it are fulfilled), which can explain how robust trajectories and oscillations emerge in nature. We demonstrated that conditionally stable motifs are also useful in explaining the robust decision-making process of dynamical modules and as such they help to understand the emergence of dynamical modularity (see Sections 6.1 and 6.5). This framework is general enough to be further utilized to explore and simplify other biological systems (see 9.2).

In terms of biological and medical applicability, the models presented in this work can be useful tools in the hands of any research team doing experiments

that interact with the core regulators of the cell cycle. In the case of molecules targeted for knock-out and/or overexpression, using these models to simulate the downstream effects of the interventions (in the larger context of the cell) is straightforward and can save a lot of time and resources. Moreover, when only the desired end state of a cell is known (e.g. apoptosis or quiescence), our models combined with methods from control theory can suggest non-trivial interventions that drive the system into the desired state. All of the applications above have already been used for Boolean models of other biological systems and have been experimentally validated (as discussed in Section 1.4).

Cancer is ultimately an aberration of the cell cycle, where the checkpoints no longer function properly and cells start to grow and divide without control. The multiple forms of cancer indicate that this complex system can go awry in many different ways. Targeted cancer therapies (e.g. by small molecules) would be more effective by considering the tangled web of nonlinear interactions in the larger network. Our preliminary investigation of the literature on Alzheimer's disease indicates that a model of the cell cycle adapted to neurons could help understand the disease and predict interventions to cure it (see 9.2).

Finally, I would like to emphasize the scientific and philosophical value in finding the general organizing principles of the dynamical decision-making hierarchy of interactions inside living organisms. Our research has shown cases where we can identify general principles, such as the principles of dynamical modularity, but further generalizing and perfecting them will take considerable effort. I do believe it can be a worthy one.

CHAPTER 10

APPENDIX

10.1 Implementations

10.1.1 IPython notebook reproducing the main results of Chapter 6

For synchronous and asynchronous simulation of the dynamic models of the Phase Switch and Phase Switch Oscillator we used the BooleanNet python library available at: https://github.com/ialbert/booleannet.

The identification of the stable motifs was done using the Java library available at: https://github.com/jgtz/StableMotifs. The building of the expanded network based on the regulatory functions was done using the BooleanDOI python library available at: https://github.com/yanggangthu/BooleanDOI.

A descriptive supplementary Jupyter Notebook that reproduces our main computational results of Chapter 6 is available at: https://github.com/deriteidavid/conditionally_stable_circuits. The notebook includes the following implementations:

1. Creating a BooleanNet instance of the PSO model.
2. Identifying the synchronous attractor by simulation.
3. Sampling the complex attractor with general asynchronous update scheme, where the resulting state transition graph can be arbitrarily filtered and exported into a graphml object. This includes the comparison of the states with the Phase Switch attractors.
4. Determining the full state transition graph of the PSO and using the PageRank algorithm to validate the filtered sample.

5. Determining the coarse-grained 'backbone' of the complex attractor.

6. Generating the expanded network of the PSO.

7. Finding the conditionally stable motifs of the PSO.

10.1.2 IPython notebook reproducing the main results of Chapter 8

To simulate the dynamics of the Boolean model and work through key methods, see: https://github.com/deriteidavid/cell_cycle_apoptosis_Sizek_etal_PloSCompBio_2019.

The code in this notebook uses the BooleanNet python library available at https://github.com/ialbert/booleannet.

The notebook includes the following implementations:

1. Simulating for the PI3K oscillator (synchronous and general asynchronous update).

2. Sampling and visualizing the general asynchronous state transition graph of the PI3K oscillator.

3. Simulating the full model with random order asynchronous and biased asynchronous update.

4. Sampling the full state space of the individual network modules.

5. Mapping the cell cycle pseudo-attractor of the full model

6. Simulating the full model with probabilistically changing inputs.

10.2 Supplemetary Material

10.2.1 Supplementary Table 10.1: Probability of state transitions among pairs of states of the synchronous limit cycle in the complex attractor found by general asynchronous update

The first two columns indicate the start and end state. The paths do not go through any other nodes of the synchronous limit cycle. The paths of the complex attractor (indicated in the fourth column) are grouped by the nodes that change state along the path. The turning on of a node is indicated by the node

name and the turning off is indicated by preceding the node name by $\sim$. If there are paths that involve fewer or more node state changes than the synchronous limit cycle, the third column separately indicates the probability of the path that involves the same node state changes as the synchronous limit cycle (prefaced by "Synch") and the probability of shorter (prefaced by "S") or longer paths (prefaced by "L") that have the same end state. The probability of longer paths is generally much smaller than the probability of shorter paths. The probability of the shorter path between states labelled (5,6,3) and (8,3,2) represents the probability of a system trajectory from the G2 state to the G0/G1 state through an SAC-like state that has UbcH10=0 (see dashed edges in the right panel of Figure 6.12).

Starting state	End state	Transition probability	States that change on the path (ignoring permutations)
(8, 3, 2) G0/G1	(7, 4, 1)	1	CyclinA
(1, 4, 7) post-SAC	(2, 3, 6)	1	$\sim$CyclinB
(5, 2, 3)	(6, 3, 4)	1	$\sim$Cdc20
(6, 3, 4)	(8, 3, 2) G0/G1	1	$\sim$pAPC, $\sim$UbcH10
(2, 7, 6) post-G2	(1, 6, 7) near-SAC	1	pAPC
(5, 6, 3)	(2, 7, 6) post-G2	0.8333	Synch: Cdk1, CyclinB, UbcH10
		0.0003	L: CyclinB, Cdk1, pAPC, $\sim$CyclinA, Cdc20, $\sim$CyclinB, Cdh1, $\sim$Cdc20, $\sim$pAPC, CyclinA, $\sim$Cdh1, UbcH10, CyclinB
			L: CyclinB, Cdk1, pAPC, $\sim$CyclinA, Cdc20, $\sim$CyclinB, Cdh1, $\sim$Cdc20, $\sim$Cdk1, $\sim$pAPC, CyclinA, Cdk1, $\sim$Cdh1, UbcH10, CyclinB
			L: Cdk1, CyclinB, pAPC, $\sim$CyclinA, Cdc20, $\sim$CyclinB, Cdh1, $\sim$Cdc20, $\sim$pAPC, $\sim$Cdc25C, CyclinA, $\sim$Cdh1, UbcH10, CyclinB, Cdc25C
(1, 6, 7) near-SAC	(1, 4, 7) post-SAC	0.75	$\sim$CyclinA, Cdc20
(2, 3, 6)	(5, 2, 3)	0.6111	Synch: $\sim$Cdc25C, Cdh1, $\sim$Cdk1
		0.0002	L: $\sim$Cdc25C, Cdh1, $\sim$Cdc20, $\sim$pAPC, $\sim$UbcH10, CyclinA, $\sim$Cdh1, UbcH10, CyclinB, pAPC, $\sim$CyclinA, Cdc20, $\sim$Cdk1, $\sim$CyclinB, Cdh1
(7, 4, 1)	(2, 7, 6) post-G2	0.5000	Synch: $\sim$Cdh1, CyclinB, UbcH10, Cdc25C, Cdk1
		10^5	L: $\sim$Cdh1, CyclinB, Cdc25C, Cdk1, pAPC, $\sim$CyclinA, Cdc20, $\sim$CyclinB, Cdh1, $\sim$Cdc20, $\sim$pAPC, CyclinA, $\sim$Cdh1, UbcH10, CyclinB
(7, 4, 1)	(5, 6, 3)	0.4166	Synch: $\sim$Cdh1, Cdc25C
		0.0001	L: $\sim$Cdh1, CyclinB, Cdc25C, Cdk1, pAPC, $\sim$CyclinA, Cdc20, $\sim$CyclinB, Cdh1, $\sim$Cdc20, $\sim$Cdk1, $\sim$pAPC, CyclinA, $\sim$Cdh1

			L: Cdc25C, Cdk1, ∼Cdh1, CyclinB, pAPC, ∼CyclinA, Cdc20, ∼CyclinB, Cdh1, ∼Cdc20, ∼pAPC, ∼Cdc25C, CyclinA, ∼Cdh1, ∼Cdk1, Cdc25C
			L: ∼Cdh1, CyclinB, Cdc25C, Cdk1, pAPC, ∼CyclinA, Cdc20, ∼CyclinB, ∼Cdk1, UbcH10, Cdh1, ∼Cdc20, ∼UbcH10, ∼pAPC, CyclinA, ∼Cdh1
(1, 6, 7) near-SAC	(2, 3, 6)	0.25	Cdc20, ∼CyclinB, ∼CyclinA
(2, 3, 6)	(8, 3, 2) G0/G1	0.2006	Synch: ∼Cdc25C, Cdh1, ∼Cdc20, ∼pAPC, ∼UbcH10, ∼Cdk1
		0.0002	L: ∼Cdc25C, Cdh1, ∼Cdc20, ∼pAPC, ∼UbcH10, CyclinA, ∼Cdh1, CyclinB, pAPC, ∼CyclinA, ∼Cdk1, Cdh1, ∼pAPC, ∼CyclinB
			L: ∼Cdc25C, Cdh1, ∼Cdc20, ∼pAPC, ∼UbcH10, CyclinA, ∼Cdh1, CyclinB, pAPC, ∼CyclinA, Cdc20, ∼Cdk1, ∼CyclinB, Cdh1, ∼Cdc20, ∼pAPC
			L: ∼Cdc25C, Cdh1, ∼Cdc20, ∼pAPC, ∼UbcH10, CyclinA, ∼Cdh1, CyclinB, pAPC, ∼Cdk1, Cdc25C, ∼CyclinA, ∼pAPC, Cdh1, ∼CyclinB, ∼Cdc25C
			L: ∼Cdc25C, Cdh1, ∼Cdc20, ∼pAPC, ∼UbcH10, CyclinA, ∼Cdh1, UbcH10, CyclinB, pAPC, ∼CyclinA, ∼Cdk1, ∼pAPC, Cdh1, ∼CyclinB, ∼UbcH10
(2, 3, 6)	(6, 3, 4)	0.1111	Synch: ∼Cdc25C, Cdh1, ∼Cdc20, ∼Cdk1
		10^5	L: ∼Cdc25C, Cdh1, ∼Cdc20, ∼pAPC, ∼UbcH10, CyclinA, ∼Cdh1, UbcH10, CyclinB, pAPC, ∼CyclinA, ∼Cdk1, Cdh1, ∼CyclinB
			L: ∼Cdc25C, Cdh1, ∼Cdc20, ∼pAPC, ∼UbcH10, CyclinA, ∼Cdh1, UbcH10, CyclinB, pAPC, ∼CyclinA, Cdc20, ∼Cdk1, Cdh1, ∼Cdc20, ∼CyclinB
			L: ∼Cdc25C, Cdh1, ∼Cdc20, ∼pAPC, ∼UbcH10, CyclinA, ∼Cdh1, UbcH10, CyclinB, pAPC, ∼Cdk1, Cdc25C, ∼CyclinA, Cdh1, ∼CyclinB, ∼Cdc25C
(5, 6, 3)	(1, 4, 7) post-SAC	0.0601	Synch: Cdk1, CyclinB, pAPC, ∼CyclinA, UbcH10, Cdc20
(5, 6, 3)	(1, 6, 7) near-SAC	0.0555	Synch: Cdk1, CyclinB, pAPC, UbcH10
		10^5	L: Cdk1, CyclinB, pAPC, ∼CyclinA, Cdc20, ∼CyclinB, Cdh1, ∼Cdc20, ∼pAPC, ∼Cdc25C, CyclinA, ∼Cdh1, UbcH10, CyclinB, pAPC, Cdc25C
(2, 3, 6)	(2, 7, 6) post-G2	0.031	S: Cdh1, ∼Cdc20, ∼pAPC, ∼UbcH10, CyclinA, ∼Cdh1, CyclinB, UbcH10
			S: ∼Cdc25C, Cdh1, ∼Cdc20, ∼pAPC, ∼UbcH10, CyclinA, ∼Cdh1, UbcH10, CyclinB, Cdc25C
			S: ∼Cdk1, Cdh1, ∼Cdc20, ∼pAPC, ∼UbcH10, CyclinA, Cdk1, ∼Cdh1, CyclinB, UbcH10
		0.004	Synch: ∼Cdc25C, Cdh1, ∼Cdc20, ∼pAPC, ∼UbcH10, CyclinA, ∼Cdh1, UbcH10, CyclinB, ∼Cdk1, Cdc25C, Cdk1
			L: ∼Cdc25C, Cdh1, ∼Cdc20, ∼pAPC, ∼UbcH10, CyclinA, ∼Cdh1, UbcH10, CyclinB, pAPC, ∼Cdk1, ∼pAPC, Cdc25C, Cdk1

			L: ∼Cdc25C, Cdh1, ∼Cdc20, ∼pAPC, ∼UbcH10, CyclinA, ∼Cdh1, UbcH10, CyclinB, pAPC, ∼CyclinA, ∼Cdk1, ∼pAPC, CyclinA, Cdc25C, Cdk1
			L: Cdh1, ∼Cdk1, ∼Cdc20, ∼UbcH10, ∼pAPC, CyclinA, Cdk1, ∼Cdh1, CyclinB, UbcH10XCdh1, ∼Cdc20, ∼UbcH10, ∼pAPC, CyclinA, ∼Cdh1, CyclinB, UbcH10
(7, 4, 1)	(1, 4, 7) post-SAC	0.0300	∼Cdh1, CyclinB, Cdc25C, Cdk1, pAPC, ∼CyclinA, UbcH10, Cdc20
(7, 4, 1)	(1, 6, 7) near-SAC	0.0277	∼Cdh1, CyclinB, Cdc25C, Cdk1, pAPC, UbcH10
(5, 6, 3)	(2, 3, 6)	0.0266	Cdk1, CyclinB, pAPC, ∼CyclinA, Cdc20, ∼CyclinB, UbcH10
(2, 3, 6)	(5, 6, 3)	0.0187	S: Cdh1, ∼Cdk1, ∼Cdc20, ∼UbcH10, ∼pAPC, CyclinA, ∼Cdh1
			Synch: ∼Cdc25C, Cdh1, ∼Cdc20, ∼pAPC, ∼UbcH10, CyclinA, ∼Cdh1, ∼Cdk1, Cdc25C
(5, 6, 3)	(8, 3, 2) G0/G1	0.0138	S: Cdk1, CyclinB, pAPC, ∼CyclinA, Cdc20, ∼CyclinB, Cdh1, ∼Cdc20, ∼Cdk1, ∼pAPC, ∼Cdc25C
		0.0006	Synch: Cdk1, CyclinB, pAPC, ∼CyclinA, Cdc20, ∼CyclinB, ∼Cdc25C, UbcH10, Cdh1, ∼Cdc20, ∼pAPC, ∼UbcH10, ∼Cdk1
(7, 4, 1)	(2, 3, 6)	0.0133	∼Cdh1, CyclinB, Cdc25C, Cdk1, pAPC, ∼CyclinA, Cdc20, ∼CyclinB, UbcH10
(2, 3, 6)	(7, 4, 1)	0.0118	Synch: ∼Cdc25C, Cdh1, ∼Cdc20, ∼pAPC, ∼UbcH10, CyclinA, ∼Cdk1
		10^6	L: ∼Cdc25C, Cdh1, ∼Cdc20, ∼pAPC, ∼UbcH10, CyclinA, ∼Cdh1, CyclinB, pAPC, ∼CyclinA, ∼Cdk1, Cdh1, ∼pAPC, CyclinA, ∼CyclinB
(7, 4, 1)	(8, 3, 2) G0/G1	0.0072	S: ∼Cdh1, CyclinB, Cdc25C, Cdk1, pAPC, ∼CyclinA, Cdc20, ∼CyclinB, Cdh1, ∼Cdc20, ∼Cdk1, ∼pAPC, ∼Cdc25C
			Synch: ∼Cdh1, CyclinB, Cdc25C, Cdk1, pAPC, ∼CyclinA, Cdc20, ∼CyclinB, ∼Cdc25C, UbcH10, Cdh1, ∼Cdc20, ∼pAPC, ∼UbcH10, ∼Cdk1
(5, 6, 3)	(5, 2, 3)	0.0067	Cdk1, CyclinB, pAPC, ∼CyclinA, Cdc20, ∼CyclinB, ∼Cdc25C, UbcH10, Cdh1, ∼Cdk1
(2, 3, 6)	(1, 4, 7) post-SAC	0.0040	S: Cdh1, ∼Cdc20, ∼UbcH10, ∼pAPC, CyclinA, ∼Cdh1, CyclinB, pAPC, ∼CyclinA, UbcH10, Cdc20
			S: Cdh1, ∼Cdk1, ∼Cdc20, ∼UbcH10, ∼pAPC, CyclinA, Cdk1, ∼Cdh1, CyclinB, pAPC, ∼CyclinA, UbcH10, Cdc20
			S: ∼Cdc25C, Cdh1, ∼Cdc20, ∼pAPC, ∼UbcH10, CyclinA, ∼Cdh1, UbcH10, CyclinB, pAPC, ∼CyclinA, Cdc25C, Cdc20
			Synch: ∼Cdc25C, Cdh1, ∼Cdc20, ∼pAPC, ∼UbcH10, CyclinA, ∼Cdh1, UbcH10, CyclinB, pAPC, ∼Cdk1, Cdc20, Cdc25C, Cdk1, ∼CyclinA
			S: Cdh1, ∼Cdc20, ∼UbcH10, ∼pAPC, CyclinA, ∼Cdh1, CyclinB, pAPC, UbcH10
(2, 3, 6)	(1, 6, 7) near-SAC	0.0036	

			S: ∼Cdc25C, Cdh1, ∼Cdc20, ∼pAPC, ∼UbcH10, CyclinA, ∼Cdh1, UbcH10, CyclinB, pAPC, Cdc25C
			S: Cdh1, ∼Cdk1, ∼Cdc20, ∼UbcH10, ∼pAPC, CyclinA, Cdk1, ∼Cdh1, CyclinB, pAPC, UbcH10
			Synch: ∼Cdc25C, Cdh1, ∼Cdc20, ∼pAPC, ∼UbcH10, CyclinA, ∼Cdh1, UbcH10, CyclinB, pAPC, ∼Cdk1, Cdc25C, Cdk1
			L: ∼Cdc25C, Cdh1, ∼Cdc20, ∼pAPC, ∼UbcH10, CyclinA, ∼Cdh1, CyclinB, pAPC, ∼Cdk1, Cdc25C, ∼pAPC, Cdk1, pAPC, UbcH10
(7, 4, 1)	(5, 2, 3)	0.0034	∼Cdh1, CyclinB, Cdc25C, Cdk1, pAPC, ∼CyclinA, Cdc20, ∼CyclinB, ∼Cdc25C, UbcH10, Cdh1, ∼Cdk1
(5, 6, 3)	(6, 3, 4)	0.0005	Cdk1, CyclinB, pAPC, ∼CyclinA, Cdc20, ∼CyclinB, ∼Cdc25C, UbcH10, Cdh1, ∼Cdc20, ∼Cdk1
(5, 6, 3)	(7, 4, 1)	0.0004	S: Cdk1, CyclinB, pAPC, ∼CyclinA, Cdc20, ∼CyclinB, Cdh1, ∼Cdc20, ∼pAPC, ∼Cdc25C, CyclinA, ∼Cdk1
			Synch: Cdk1, CyclinB, pAPC, ∼CyclinA, Cdc20, ∼CyclinB, ∼Cdc25C, UbcH10, Cdh1, ∼Cdc20, ∼pAPC, ∼UbcH10, CyclinA, ∼Cdk1
(7, 4, 1)	(6, 3, 4)	0.0002	∼Cdh1, CyclinB, Cdc25C, Cdk1, pAPC, ∼CyclinA, Cdc20, ∼CyclinB, ∼Cdc25C, UbcH10, Cdh1, ∼Cdc20, ∼Cdk1

10.2.2 Supplementary Figure 10.1: The distribution of the duration of sustained ON or OFF states of each node on the asynchronous complex attractor of the Phase Switch Oscillator.

Using general asynchronous update, we sampled an extensive number of trajectories of the system on the complex attractor, where each node alternates between being ON and OFF. Each row corresponds to a node. The first figure in the row indicates the distribution of how long this node is ON (with the median in red), the second figure indicates the duration of how long this node is OFF, and the third figure indicates the distribution of the duration of a consecutive on and off period. If the complex attractor were a deterministic cycle, the duration of a consecutive on and off period for any node were 16 time steps (i.e. each of the 8 nodes turning on once and turning off once). The observed medians are very close to 16. The split between the on and off periods is even (median ON and OFF duration of 8) for five nodes and more asymmetric for three nodes, namely Cdc20, CyclinB, UbcH10. These three nodes also exhibit a slightly asymmetric pattern in the synchronous limit cycle, namely a 3 to 6 split of the nine steps as compared to the 4 to 5 split of the rest of the nodes (see Figure 6.5).

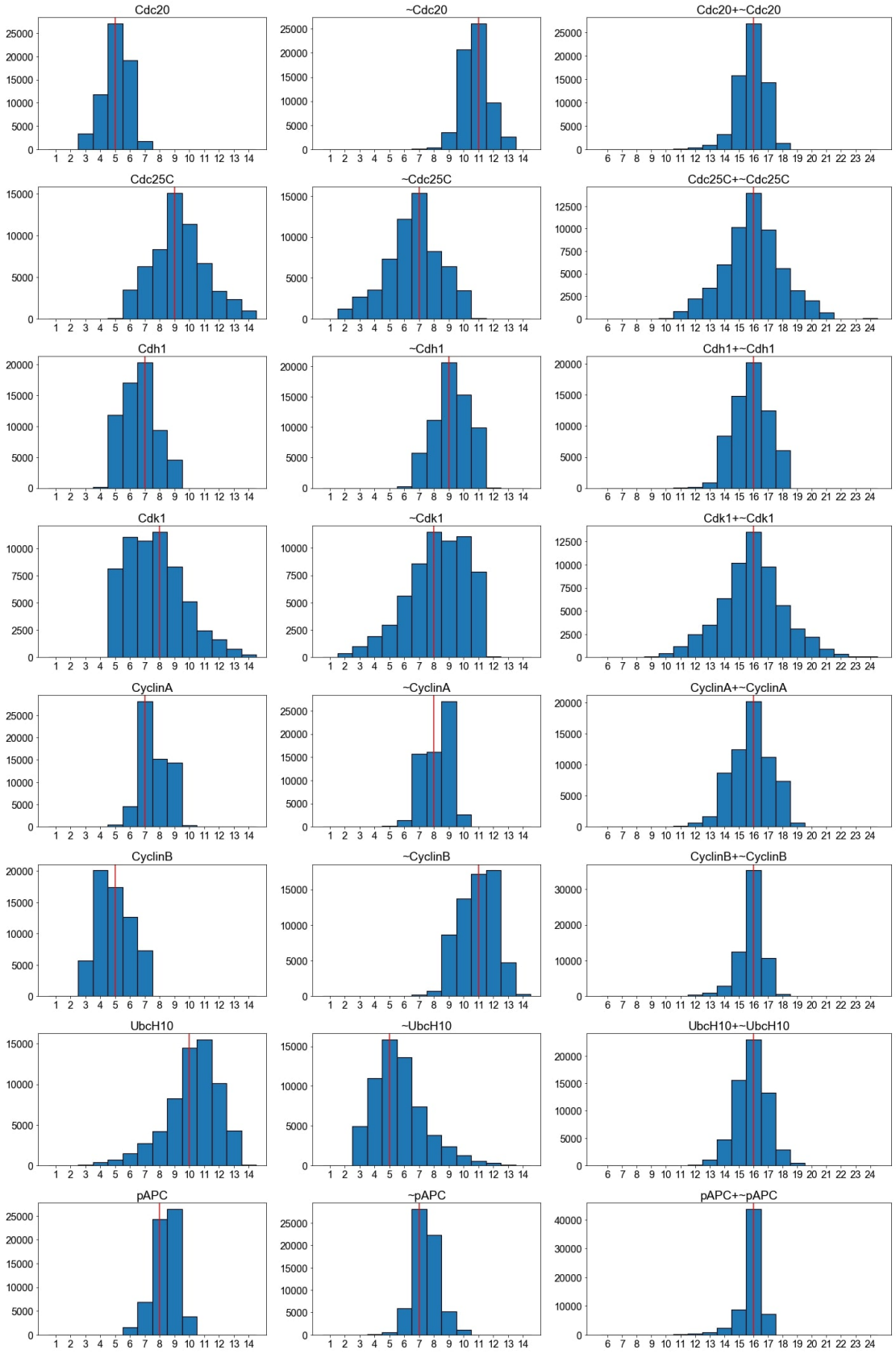

Figure 10.1. *The distribution of the duration of sustained ON or OFF states of each node on the asynchronous complex attractor of the Phase Switch Oscillator.*

10.2.3 Supplementary Table 10.2: Conditionally stable motifs of the Phase Switch Oscillator can cause the destabilization of their own conditions

Name	Virtual nodes of the conditionally stable motif	Virtual node that serves as condition
C3	∼CyclinA, Cdh1, ∼CyclinB	UbcH10
C4	∼CyclinA, ∼Cdk1, Cdh1, ∼CyclinB	UbcH10
C5	∼CyclinA, ∼Cdk1, Cdh1, ∼Cdc25C	UbcH10
C11	∼Cdh1, CyclinB, Cdk1, Cdc25C	∼Cdc20 or ∼pAPC
C13	pAPC	Cdc20
C14	pAPC, Cdc20	∼Cdh1

Table 10.2. *The conditionally CSMs of the PSO network that cause their own destabilization. The first column is the identifier of the CSM. The second column contains the node states (virtual nodes on the expanded network where refers to the 0 state) making up the CSM. The third column is the state that serves as the condition that needs to be sustained for the CSM to be stable. The opposite state is contained in the logic domain of influence of the CSM. Such destabilization does not happen in the Phase Switch because the stable motifs either stabilize, or violate, the condition of each CSM (see Figure 6.2).*

10.2.4 Supplementary Figure 10.2

Illustration of a conditionally stable motif causing its own destabilization. The conditionally stable motif C3, highlighted in green, is conditioned on UbcH10, emphasized with the dashed outline. The yellow nodes are the logical domain of influence (LDOI) of C3, i.e. states that will stabilize as long as C3 is stable. The on state of UbcH10, highlighted with orange, is also part of the LDOI but marks the destabilization of C3.

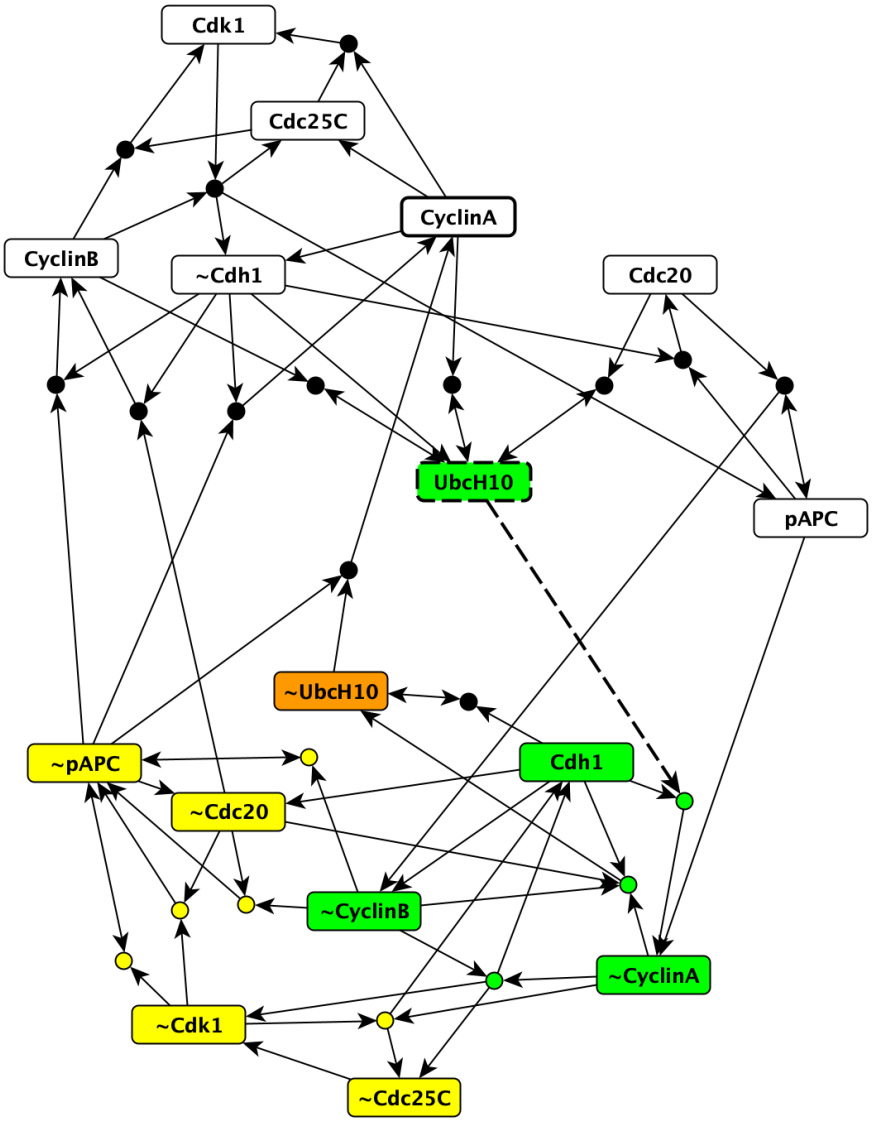

Figure 10.2. *Illustration of a conditionally stable motif causing its own destabilization.*

10.2.5 Supplementary Table 10.3

List of attractors that arise when the node state listed in the "Intervention" column is held fixed. Columns denoted by node names give the steady state value of the respective node (grey background highlights locked nodes), and the Overlap column gives the overlap of this steady state with each of the three Phase Switch attractors in the order (G0/G1, G2, SAC); see Methods a detailed definition of the overlap. The next column indicates the closest Phase Switch attractor(s). Arrows to / from phenotypes in parentheses point to other attractors with near-maximum overlap, indicating that the network is stuck close to the boundary between two Phase Switch states. The final column gives the conditionally stable motifs (as defined in Figure 6.9) for which the intervention satisfied a condition; these become stable motifs in the modified system and underlie the resulting attractor. In case there are multiple separate CSMs with the same label, e.g. C6, we refer to the specific CSM with a numeral that indicates its position in the group, e.g. C6_1 is the first in the box labeled C6 (P5) in Figure 6.9. A node state listed in the final column indicates that the intervention is a sufficient condition for setting this state. The interventions UbcH10=0, Cdc25c=1, and Cdk1=1 each result in a single complex attractor in which each remaining node oscillates; in this case no conditionally stable motif becomes a stable motif, and the steady state overlap is not well-defined.

Intervention	Attractors of the altered system								Overlap (G0/G1, G2, SAC)	Closest Phase Switch Attractor(s)	CSMs stabilized by the intervention
	Cyclin A	Cyclin B	Cdc20	Cdc25c	Cdh1	Cdk1	pAPC	UbcH10			
UbcH10=0	Osc.	Osc.	Osc.	Osc.	Osc.	Osc.	Osc.	0	N/A		None
Cdc25c=1	Osc.	Osc.	Osc.	1	Osc.	Osc.	Osc.	Osc.	N/A		None
Cdk1=1	Osc.	Osc.	Osc.	Osc.	Osc.	1	Osc.	Osc.	N/A		None
CyclinA=0	0	0	0	0	1	0	0	0	(8,3,2)	G0/G1	C0 (P3), C1 (P4), C2
pAPC=0	0	0	0	0	1	0	0	0	(7,2,3)	G0/G1	C9 (P6), Cdc20=0
UbcH10=1	0	0	0	0	1	0	0	1	(7,4,3)	G0/G1	C3, C4, C5
Cdh1=1	1	0	0	1	1	1	0	0	(5,4,3)	G0/G1 (→ G2)	C8, Cdc20=0, CyclinB=0
Cdc25c=0	1	1	0	0	0	0	0	1	(4,7,4)	G2	Cdk1=0
Cdk1=0	1	1	0	1	0	0	0	1	(3,8,5)	G2	C6_1 (P5_1)
CyclinB=0	1	0	0	1	1	1	0	1	(4,5,4)	G2	C6_2, C7_2
CyclinA=1	1	0	1	1	0	1	1	1	(1,4,5)	(G2 →) SAC	C12_1, Cdh1=0, Cdc25c=1
pAPC=1	1	1	0	1	0	1	1	1	(2,7,6)	G2 (→ SAC)	CyclinA=0
Cdc20=0	0	1	0	1	0	1	1	1	(2,5,8)	SAC	C11 (P2′)
Cdh1=0	0	0	1	0	0	0	1	1	(4,3,4)	SAC → G0/G1	C14, UbcH10=1
Cdc20=1	0	0	1	0	1	0	1	1	(5,2,3)	G0/G1	C12_3, C13
Cdc20=1	0	0	1	0	1	0	1	0	(6,1,2)	G0/G1	C13
Cdc20=1	0	0	1	0	1	0	0	1	(6,3,2)	G0/G1	C12_3
CyclinB=1	0	1	1	1	0	1	1	1	(1,4,7)	SAC	C10, C12_2
CyclinB=1	0	1	0	0	1	0	0	1	(6,5,4)	G0/G1 (→ G2)	C12_2

Oscill
Monostbl
Tri-stable
Bistable

Table 10.3. *List of attractors that arise when the node state listed in the "Intervention" column is held fixed.*

10.2.6 Supplementary Figure 10.3

The cycle graph constructed for the Phase Switch Oscillator. Each node of this graph represents a positive feedback loop of the regulatory network with node states (top row of each node label) that become self-sustaining when the state of certain other nodes (bottom row of each node label) is held fixed. As in previous figures the OFF state of a node is represented by a preceding the respective node name. An undirected edge between nodes of the cycle graph indicates that the nodes states of the two cycles and their associated conditions are mutually compatible and non-disjoint. Every node and every consistent connected subgraph of the cycle graph corresponds to a conditionally stable motif. Note that in this case, all connected subgraphs are consistent. The largest connected subgraphs correspond to the meta-nodes Cyc (a subgraph of 10 cycles in the top left), Cyc (an 8-cycle subgraph in the top right), pAPC/Cdc20 (a four-clique in the bottom right), UbcH10 (triangle in the bottom left), pAPC/Cdc20 (two cycles connected by an edge) and UbcH10 (single cycle).

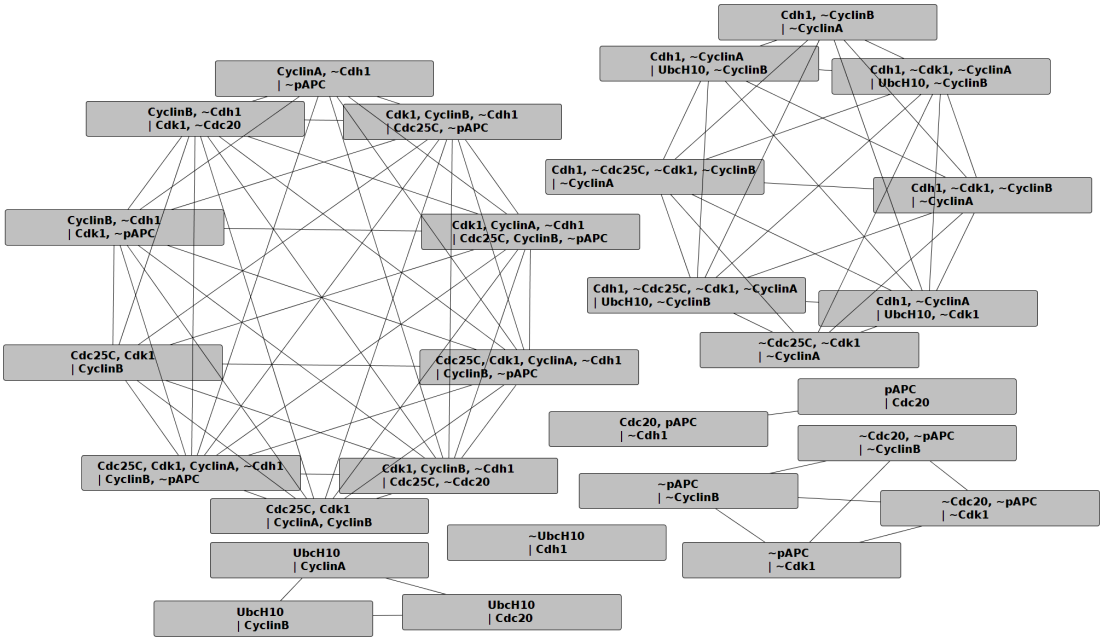

Figure 10.3. *The cycle graph constructed for the Phase Switch Oscillator*

BIBLIOGRAPHY

[1] Munos, B.: Lessons from 60 years of pharmaceutical innovation. Nature reviews Drug discovery **8**(12), 959–968 (2009)

[2] Scannell, J.W., Blanckley, A., Boldon, H., Warrington, B.: Diagnosing the decline in pharmaceutical r&d efficiency. Nature reviews Drug discovery **11**(3), 191 (2012)

[3] Meldrum, C., Doyle, M.A., Tothill, R.W.: Next-generation sequencing for cancer diagnostics: a practical perspective. The Clinical Biochemist Reviews **32**(4), 177 (2011)

[4] Geysen, H.M., Schoenen, F., Wagner, D., Wagner, R.: A guide to drug discovery: Combinatorial compound libraries for drug discovery: an ongoing challenge. Nature Reviews Drug Discovery **2**(3), 222 (2003)

[5] Mayr, L.M., Fuerst, P.: The future of high-throughput screening. Journal of biomolecular screening **13**(6), 443–448 (2008)

[6] National Cancer Act of 1971. https://dtp.cancer.gov/timeline/flash/milestones/M4_Nixon.htm. Accessed: 2020-01-20

[7] National Academic R&D Expenditures in All Fields. https://www.nsf.gov/statistics/2018/nsb20181/report/sections/academic-research-and-development/expenditures-and-funding-for-academic-r-d#national-academic-r-d-expenditures-in-all-fields. Accessed: 2019-09-24

[8] Ioannidis, J.P.: Why most published research findings are false. PLoS medicine **2**(8), 124 (2005)

[9] Baker, M.: Is there a reproducibility crisis? a nature survey lifts the lid on how researchers view the'crisis rocking science and what they think will help. Nature **533**(7604), 452–455 (2016)

[10] Peng, R.: The reproducibility crisis in science: A statistical counterattack. Significance **12**(3), 30–32 (2015)

[11] Milgram, S.: The small world problem. Psychology today **2**(1), 60–67 (1967)

[12] Heidler, R., Gamper, M., Herz, A., Eßer, F.: Relationship patterns in the 19th century: The friendship network in a german boys' school class from 1880 to 1881 revisited. Social Networks **37**, 1–13 (2014)

[13] Karinthy, F.: Chain-links (original title : Láncszemek) (1929)

[14] Erdös, P., Rényi, A.: On random graphs. I. Publ. Math. Debrecen **6**, 290–297 (1959)

[15] Watts, D.J., Strogatz, S.H.: Collective dynamics of 'small-world'networks. nature **393**(6684), 440 (1998)

[16] Albert, R., Jeong, H., Barabási, A.-L.: Internet: Diameter of the world-wide web. nature **401**(6749), 130 (1999)

[17] Barabási, A.-L., Albert, R.: Emergence of scaling in random networks. science **286**(5439), 509–512 (1999)

[18] Page, L., Brin, S., Motwani, R., Winograd, T.: The pagerank citation ranking: Bringing order to the web. Technical report, Stanford InfoLab (1999)

[19] Ferguson, N.: The Square and the Tower: Networks and Power, from the Freemasons to Facebook. Penguin Books, - (2019)

[20] Tenenbaum, J.B., Kemp, C., Griffiths, T.L., Goodman, N.D.: How to grow a mind: Statistics, structure, and abstraction. science **331**(6022), 1279–1285 (2011)

[21] Herper, M.: Bad blood: The decline and fall of elizabeth holmes and theranos. Forbes (8 October) (2016)

[22] Kauffman, S.A.: Metabolic stability and epigenesis in randomly constructed genetic nets. Journal of theoretical biology **22**(3), 437–467 (1969)

[23] Thomas, R.: Boolean formalization of genetic control circuits. Journal of theoretical biology **42**(3), 563–585 (1973)

[24] Novick, A., Weiner, M.: Enzyme induction as an all-or-none phenomenon. Proceedings of the National Academy of Sciences of the United States of America **43**(7), 553 (1957)

[25] Monod, J., Jacob, F.: General conclusions: teleonomic mechanisms in cellular metabolism, growth, and differentiation. In: Cold Spring Harbor Symposia on Quantitative Biology, vol. 26, pp. 389–401 (1961). Cold Spring Harbor Laboratory Press

[26] Albert, R., Othmer, H.G.: The topology of the regulatory interactions predicts the expression pattern of the segment polarity genes in drosophila melanogaster. Journal of theoretical biology **223**(1), 1–18 (2003)

[27] Li, S., Assmann, S.M., Albert, R.: Predicting essential components of signal transduction networks: a dynamic model of guard cell abscisic acid signaling. PLoS biology **4**(10), 312 (2006)

[28] Saez-Rodriguez, J., Alexopoulos, L.G., Epperlein, J., Samaga, R., Lauffenburger, D.A., Klamt, S., Sorger, P.K.: Discrete logic modelling as a means to link protein signalling networks with functional analysis of mammalian signal transduction. Molecular systems biology **5**(1) (2009)

[29] Zhang, R., Shah, M.V., Yang, J., Nyland, S.B., Liu, X., Yun, J.K., Albert, R., Loughran, T.P.: Network model of survival signaling in large granular lymphocyte leukemia. Proceedings of the National Academy of Sciences **105**(42), 16308–16313 (2008)

[30] Saadatpour, A., Wang, R.-S., Liao, A., Liu, X., Loughran, T.P., Albert, I., Albert, R.: Dynamical and structural analysis of a t cell survival network identifies novel candidate therapeutic targets for large granular lymphocyte leukemia. PLoS computational biology **7**(11), 1002267 (2011)

[31] Regan, E.R., Aird, W.C.: Dynamical systems approach to endothelial heterogeneity. Circulation research **111**(1), 110–130 (2012)

[32] Steinway, S.N., Zañudo, J.G., Ding, W., Rountree, C.B., Feith, D.J., Loughran, T.P., Albert, R.: Network modeling of tgfβ signaling in hepatocellular carcinoma epithelial-to-mesenchymal transition reveals joint sonic hedgehog and wnt pathway activation. Cancer research **74**(21), 5963–5977 (2014)

[33] Steinway, S.N., Zañudo, J.G.T., Michel, P.J., Feith, D.J., Loughran, T.P., Albert, R.: Combinatorial interventions inhibit tgfβ-driven epithelial-to-mesenchymal transition and support hybrid cellular phenotypes. NPJ systems biology and applications **1**, 15014 (2015)

[34] Wang, R.-S., Saadatpour, A., Albert, R.: Boolean modeling in systems biology: an overview of methodology and applications. Physical biology **9**(5), 055001 (2012)

[35] Luce, R.D., Perry, A.D.: A method of matrix analysis of group structure. Psychometrika **14**(2), 95–116 (1949)

[36] Zachary, W.W.: An information flow model for conflict and fission in small groups. Journal of anthropological research **33**(4), 452–473 (1977)

[37] Girvan, M., Newman, M.E.: Community structure in social and biological networks. Proceedings of the national academy of sciences **99**(12), 7821–7826 (2002)

[38] Ravasz, E., Somera, A.L., Mongru, D.A., Oltvai, Z.N., Barabási, A.-L.: Hierarchical organization of modularity in metabolic networks. science **297**(5586), 1551–1555 (2002)

[39] Fortunato, S.: Community detection in graphs. Physics reports **486**(3-5), 75–174 (2010)

[40] Hartwell, L.H., Hopfield, J.J., Leibler, S., Murray, A.W.: From molecular to modular cell biology. Nature **402**(6761supp), 47 (1999)

[41] Milo, R., Shen-Orr, S., Itzkovitz, S., Kashtan, N., Chklovskii, D., Alon, U.: Network motifs: simple building blocks of complex networks. Science **298**(5594), 824–827 (2002)

[42] Kashtan, N., Alon, U.: Spontaneous evolution of modularity and network motifs. Proceedings of the National Academy of Sciences **102**(39), 13773–13778 (2005)

[43] Bosco, G.: Retinoblastoma, a trip organizer. Nature **466**(7310), 1051–1052 (2010)

[44] Alberts, B., Bray, D., Hopkin, K., Johnson, A.D., Lewis, J., Raff, M., Roberts, K., Walter, P.: Essential Cell Biology - Third Edition, pp. 610–620. Garland Science, - (2010). Chap. 18

[45] Nobel Prize in Physiology and Medicine 2001. https://www.nobelprize.org/prizes/medicine/2001/press-release/. Accessed: 2019-10-04

[46] Novak, B., Tyson, J.J.: Numerical analysis of a comprehensive model of m-phase control in xenopus oocyte extracts and intact embryos. Journal of cell science **106**(4), 1153–1168 (1993)

[47] Sha, W., Moore, J., Chen, K., Lassaletta, A.D., Yi, C.-S., Tyson, J.J., Sible, J.C.: Hysteresis drives cell-cycle transitions in xenopus laevis egg extracts. Proceedings of the National Academy of Sciences **100**(3), 975–980 (2003)

[48] Li, F., Long, T., Lu, Y., Ouyang, Q., Tang, C.: The yeast cell-cycle network is robustly designed. Proceedings of the National Academy of Sciences **101**(14), 4781–4786 (2004)

[49] Chen, K.C., Calzone, L., Csikasz-Nagy, A., Cross, F.R., Novak, B., Tyson, J.J.: Integrative analysis of cell cycle control in budding yeast. Molecular biology of the cell **15**(8), 3841–3862 (2004)

[50] Novak, B., Tyson, J.J.: A model for restriction point control of the mammalian cell cycle. Journal of theoretical biology **230**(4), 563–579 (2004)

[51] Fauré, A., Naldi, A., Chaouiya, C., Thieffry, D.: Dynamical analysis of a generic boolean model for the control of the mammalian cell cycle. Bioinformatics **22**(14), 124–131 (2006)

[52] Novak, B., Tyson, J.J., Gyorffy, B., Csikasz-Nagy, A.: Irreversible cell-cycle transitions are due to systems-level feedback. Nature cell biology **9**(7), 724 (2007)

[53] Gérard, C., Goldbeter, A.: From quiescence to proliferation: Cdk oscillations drive the mammalian cell cycle. Frontiers in physiology **3**, 413 (2012)

[54] Golinelli, O., Derrida, B.: Barrier Heights in the Kauffman Model. Journal de Physique **50**(13), 1587–1601 (1989)

[55] Ribeiro, A.S., Kauffman, S.A.: Noisy attractors and ergodic sets in models of gene regulatory networks. J Theor Biol **247**(4), 743–755 (2007). doi:10.1016/j.jtbi.2007.04.020

[56] Gershenson, C.: Phase Transitions in Random Boolean Networks with Different Updating Schemes. arXiv.org:nlin/0311008 (2003)

[57] Aracena, J., Goles, E., Moreira, A., Salinas, L.: On the robustness of update schedules in Boolean networks. BioSystems **97**(1), 1–8 (2009)

[58] Saadatpour, A., Albert, I., Albert, R.: Attractor analysis of asynchronous Boolean models of signal transduction networks. Journal of Theoretical Biology **266**(4), 641–656 (2010)

[59] Zhang, Y., Qian, M., Ouyang, Q., Deng, M., Li, F., Tang, C.: Stochastic model of yeast cell-cycle network. Physica D: Nonlinear Phenomena **219**(1), 35–39 (2006)

[60] Deritei, D., Aird, W.C., Ercsey-Ravasz, M., Regan, E.R.: Principles of dynamical modularity in biological regulatory networks. Scientific reports **6**, 21957 (2016)

[61] Zañudo, J.G., Albert, R.: An effective network reduction approach to find the dynamical repertoire of discrete dynamic networks. Chaos: An Interdisciplinary Journal of Nonlinear Science **23**(2), 025111 (2013)

[62] Deritei, D., Rozum, J., Ravasz Regan, E., Albert, R.: A feedback loop of conditionally stable circuits drives the cell cycle from checkpoint to checkpoint. Scientific Reports **9**(1), 16430 (2019). doi:10.1038/s41598-019-52725-1

[63] Spencer, S.L., Cappell, S.D., Tsai, F.-C., Overton, K.W., Wang, C.L., Meyer, T.: The proliferation-quiescence decision is controlled by a bifurcation in cdk2 activity at mitotic exit. Cell **155**(2), 369–383 (2013)

[64] Yao, G., Tan, C., West, M., Nevins, J.R., You, L.: Origin of bistability underlying mammalian cell cycle entry. Molecular systems biology **7**(1) (2011)

[65] Alfieri, R., Barberis, M., Chiaradonna, F., Gaglio, D., Milanesi, L., Vanoni, M., Klipp, E., Alberghina, L.: Towards a systems biology approach to mammalian cell cycle: modeling the entrance into s phase of quiescent fibroblasts after serum stimulation. BMC bioinformatics **10**(12), 16 (2009)

[66] Pfeuty, B.: Strategic cell-cycle regulatory features that provide mammalian cells with tunable g1 length and reversible g1 arrest. PloS one **7**(4), 35291 (2012)

[67] Giunta, S., Jackson, S.P.: Give me a break, but not in mitosis: the mitotic dna damage response marks dna double-strand breaks with early signaling events. Cell Cycle **10**(8), 1215–1221 (2011)

[68] Pardee, A.B.: A restriction point for control of normal animal cell proliferation. Proceedings of the National Academy of Sciences **71**(4), 1286–1290 (1974)

[69] Thieffry, D., Romero, D.: The modularity of biological regulatory networks. Biosystems **50**(1), 49–59 (1999)

[70] Siebert, H.: Deriving behavior of boolean bioregulatory networks from subnetwork dynamics. Mathematics in Computer Science **2**(3), 421–442 (2009)

[71] Mendes, N.D., Lang, F., Le Cornec, Y.-S., Mateescu, R., Batt, G., Chaouiya, C.: Composition and abstraction of logical regulatory modules: application to multicellular systems. Bioinformatics **29**(6), 749–757 (2013)

[72] Burdon, T., Smith, A., Savatier, P.: Signalling, cell cycle and pluripotency in embryonic stem cells. Trends in cell biology **12**(9), 432–438 (2002)

[73] White, J., Stead, E., Faast, R., Conn, S., Cartwright, P., Dalton, S.: Developmental activation of the rb–e2f pathway and establishment of cell cycle-regulated cyclin-dependent kinase activity during embryonic stem cell differentiation. Molecular biology of the cell **16**(4), 2018–2027 (2005)

[74] Becker, K.A., Ghule, P.N., Therrien, J.A., Lian, J.B., Stein, J.L., Van Wijnen, A.J., Stein, G.S.: Self-renewal of human embryonic stem cells is supported by a shortened g1 cell cycle phase. Journal of cellular physiology **209**(3), 883–893 (2006)

[75] Marques-Pita, M., Rocha, L.M.: Canalization and control in automata networks: body segmentation in drosophila melanogaster. PloS one **8**(3), 55946 (2013)

[76] Li, Y., Adeyeye, J.O., Murrugarra, D., Aguilar, B., Laubenbacher, R.: Boolean nested canalizing functions: A comprehensive analysis. Theoretical Computer Science **481**, 24–36 (2013)

[77] Peters, J.-M.: The anaphase promoting complex/cyclosome: a machine designed to destroy. Nature reviews Molecular cell biology **7**(9), 644 (2006)

[78] Yang, G., Gómez Tejeda Zañudo, J., Albert, R.: Target control in logical models using the domain of influence of nodes. Frontiers in physiology **9**, 454 (2018)

[79] Pomerening, J.R., Sontag, E.D., Ferrell Jr, J.E.: Building a cell cycle oscillator: hysteresis and bistability in the activation of cdc2. Nature cell biology **5**(4), 346 (2003)

[80] He, E., Kapuy, O., Oliveira, R.A., Uhlmann, F., Tyson, J.J., Novák, B.: System-level feedbacks make the anaphase switch irreversible. Proceedings of the National Academy of Sciences **108**(24), 10016–10021 (2011)

[81] Kapuy, O., He, E., Uhlmann, F., Novák, B.: Mitotic exit in mammalian cells. Molecular systems biology **5**(1) (2009)

[82] Potapova, T.A., Daum, J.R., Byrd, K.S., Gorbsky, G.J.: Fine tuning the cell cycle: activation of the cdk1 inhibitory phosphorylation pathway during mitotic exit. Molecular biology of the cell **20**(6), 1737–1748 (2009)

[83] Novák, B., Heldt, F.S., Tyson, J.J.: Genome stability during cell proliferation: A systems analysis of the molecular mechanisms controlling progression through the eukaryotic cell cycle. Current opinion in systems biology **9**, 22–31 (2018)

[84] Sontag, E.D.: Monotone and near-monotone biochemical networks. Systems and synthetic biology **1**(2), 59–87 (2007)

[85] Novák, B., Tyson, J.J.: Design principles of biochemical oscillators. Nature reviews Molecular cell biology **9**(12), 981 (2008)

[86] Csermely, P.: The wisdom of networks: A general adaptation and learning mechanism of complex systems: The network core triggers fast responses to known stimuli; innovations require the slow network periphery and are encoded by core-remodeling. BioEssays **40**(1), 1700150 (2018)

[87] Klamt, S., Saez-Rodriguez, J., Lindquist, J.A., Simeoni, L., Gilles, E.D.: A methodology for the structural and functional analysis of signaling and regulatory networks. BMC bioinformatics **7**(1), 56 (2006)

[88] Gan, X., Albert, R.: General method to find the attractors of discrete dynamic models of biological systems. Physical Review E **97**(4), 042308 (2018)

[89] Rozum, J.C., Albert, R.: Identifying (un) controllable dynamical behavior in complex networks. PLoS computational biology **14**(12), 1006630 (2018)

[90] Sizek, H., Hamel, A., Deritei, D., Campbell, S., Regan, E.R.: Boolean model of growth signaling, cell cycle and apoptosis predicts the molecular mechanism of aberrant cell cycle progression driven by hyperactive pi3k. PLoS computational biology **15**(3), 1006402 (2019)

[91] Dutertre, S., Cazales, M., Quaranta, M., Froment, C., Trabut, V., Dozier, C., Mirey, G., Bouché, J.-P., Theis-Febvre, N., Schmitt, E., *et al.*: Phosphorylation of cdc25b by aurora-a at the centrosome contributes to the g2–m transition. Journal of cell science **117**(12), 2523–2531 (2004)

[92] Lindqvist, A., Källström, H., Lundgren, A., Barsoum, E., Rosenthal, C.K.: Cdc25b cooperates with cdc25a to induce mitosis but has a unique role in activating cyclin b1–cdk1 at the centrosome. J Cell Biol **171**(1), 35–45 (2005)

[93] Lobjois, V., Jullien, D., Bouché, J.-P., Ducommun, B.: The polo-like kinase 1 regulates cdc25b-dependent mitosis entry. Biochimica et Biophysica Acta (BBA)-Molecular Cell Research **1793**(3), 462–468 (2009)

[94] Lopez-Girona, A., Furnari, B., Mondesert, O., Russell, P.: Nuclear localization of cdc25 is regulated by dna damage and a 14-3-3 protein. Nature **397**(6715), 172 (1999)

[95] Lawlor, M.A., Alessi, D.R.: Pkb/akt: a key mediator of cell proliferation, survival and insulin responses? Journal of cell science **114**(16), 2903–2910 (2001)

[96] Raff, M.C.: Social controls on cell survival and cell death. Nature **356**(6368), 397 (1992)

[97] Foijer, F., Wolthuis, R.M., Doodeman, V., Medema, R.H., te Riele, H.: Mitogen requirement for cell cycle progression in the absence of pocket protein activity. Cancer cell **8**(6), 455–466 (2005)

[98] Bell, L., Ryan, K.: Life and death decisions by e2f-1. Cell death and differentiation **11**(2), 137 (2004)

[99] Hoffman, B., Liebermann, D.: Apoptotic signaling by c-myc. Oncogene **27**(50), 6462 (2008)

[100] Hanahan, D., Weinberg, R.A.: Hallmarks of cancer: the next generation. cell **144**(5), 646–674 (2011)

[101] Costantino, S., Paneni, F., Cosentino, F.: Ageing, metabolism and cardiovascular disease. The Journal of physiology **594**(8), 2061–2073 (2016)

[102] Lemmon, M.A., Schlessinger, J.: Cell signaling by receptor tyrosine kinases. Cell **141**(7), 1117–1134 (2010)

[103] Manning, B.D., Cantley, L.C.: Akt/pkb signaling: navigating downstream. Cell **129**(7), 1261–1274 (2007)

[104] Manning, B.D., Toker, A.: Akt/pkb signaling: navigating the network. Cell **169**(3), 381–405 (2017)

[105] Minamino, T., Miyauchi, H., Tateno, K., Kunieda, T., Komuro, I.: Akt-induced cellular senescence: implication for human disease. Cell cycle **3**(4), 447–449 (2004)

[106] Astle, M.V., Hannan, K., Ng, P., Lee, R., George, A., Hsu, A., Haupt, Y., Hannan, R., Pearson, R.B.: Akt induces senescence in human cells via mtorc1 and p53 in the absence of dna damage: implications for targeting mtor during malignancy. Oncogene **31**(15), 1949 (2012)

[107] Alvarez, B., Martínez-A, C., Burgering, B.M., Carrera, A.C.: Forkhead transcription factors contribute to execution of the mitotic programme in mammals. Nature **413**(6857), 744 (2001)

[108] Toettcher, J.E., Loewer, A., Ostheimer, G.J., Yaffe, M.B., Tidor, B., Lahav, G.: Distinct mechanisms act in concert to mediate cell cycle arrest. Proceedings of the National Academy of Sciences **106**(3), 785–790 (2009)

[109] Wang, Z., Dang, T., Liu, T., Chen, S., Li, L., Huang, S., Fang, M.: Nedd4l protein catalyzes ubiquitination of pik3ca protein and regulates pi3k-akt signaling. Journal of Biological Chemistry **291**(33), 17467–17477 (2016)

[110] Escobedo, A., Gomes, T., Aragón, E., Martín-Malpartida, P., Ruiz, L., Macias, M.J.: Structural basis of the activation and degradation mechanisms of the e3 ubiquitin ligase nedd4l. Structure **22**(10), 1446–1457 (2014)

[111] Hui, R.C.-Y., Gomes, A.R., Constantinidou, D., Costa, J.R., Karadedou, C.T., de Mattos, S.F., Wymann, M.P., Brosens, J.J., Schulze, A., Lam, E.W.-F.: The forkhead transcription factor foxo3a increases phosphoinositide-3 kinase/akt activity in drug-resistant leukemic cells through induction of pik3ca expression. Molecular and cellular biology **28**(19), 5886–5898 (2008)

[112] Petronczki, M., Lénárt, P., Peters, J.-M.: Polo on the rise—from mitotic entry to cytokinesis with plk1. Developmental cell **14**(5), 646–659 (2008)

[113] Costa, R.H.: Foxm1 dances with mitosis. Nature cell biology **7**(2), 108 (2005)

[114] Yuan, Z., Becker, E.B., Merlo, P., Yamada, T., DiBacco, S., Konishi, Y., Schaefer, E.M., Bonni, A.: Activation of foxo1 by cdk1 in cycling cells and postmitotic neurons. Science **319**(5870), 1665–1668 (2008)

[115] Spencer, S.L., Sorger, P.K.: Measuring and modeling apoptosis in single cells. Cell **144**(6), 926–939 (2011)

[116] Mai, Z., Liu, H.: Boolean network-based analysis of the apoptosis network: irreversible apoptosis and stable surviving. Journal of theoretical biology **259**(4), 760–769 (2009)

[117] Schlatter, R., Schmich, K., Vizcarra, I.A., Scheurich, P., Sauter, T., Borner, C., Ederer, M., Merfort, I., Sawodny, O.: On/off and beyond-a boolean model of apoptosis. PLoS computational biology **5**(12), 1000595 (2009)

[118] Calzone, L., Tournier, L., Fourquet, S., Thieffry, D., Zhivotovsky, B., Barillot, E., Zinovyev, A.: Mathematical modelling of cell-fate decision in response to death receptor engagement. PLoS computational biology **6**(3), 1000702 (2010)

[119] Albeck, J.G., Burke, J.M., Aldridge, B.B., Zhang, M., Lauffenburger, D.A., Sorger, P.K.: Quantitative analysis of pathways controlling extrinsic apoptosis in single cells. Molecular cell **30**(1), 11–25 (2008)

[120] Spencer, S.L., Gaudet, S., Albeck, J.G., Burke, J.M., Sorger, P.K.: Non-genetic origins of cell-to-cell variability in trail-induced apoptosis. Nature **459**(7245), 428 (2009)

[121] Legewie, S., Blüthgen, N., Herzel, H.: Mathematical modeling identifies inhibitors of apoptosis as mediators of positive feedback and bistability. PLoS computational biology **2**(9), 120 (2006)

[122] Vitale, I., Manic, G., Castedo, M., Kroemer, G.: Caspase 2 in mitotic catastrophe: the terminator of aneuploid and tetraploid cells. Molecular & cellular oncology **4**(3), 1299274 (2017)

[123] Sidi, S., Sanda, T., Kennedy, R.D., Hagen, A.T., Jette, C.A., Hoffmans, R., Pascual, J., Imamura, S., Kishi, S., Amatruda, J.F., *et al.*: Chk1 suppresses a caspase-2 apoptotic response to dna damage that bypasses p53, bcl-2, and caspase-3. Cell **133**(5), 864–877 (2008)

[124] Terrano, D.T., Upreti, M., Chambers, T.C.: Cyclin-dependent kinase 1-mediated bcl-xl/bcl-2 phosphorylation acts as a functional link coupling mitotic arrest and apoptosis. Molecular and cellular biology **30**(3), 640–656 (2010)

[125] Zhou, L., Cai, X., Han, X., Xu, N., Chang, D.C.: Cdk1 switches mitotic arrest to apoptosis by phosphorylating bcl-2/bax family proteins during treatment with microtubule interfering agents. Cell biology international **38**(6), 737–746 (2014)

[126] Weiß, L.M., Hugle, M., Romero, S., Fulda, S.: Synergistic induction of apoptosis by a polo-like kinase 1 inhibitor and microtubule-interfering drugs in e wing sarcoma cells. International journal of cancer **138**(2), 497–506 (2016)

[127] Andersen, J.L., Johnson, C.E., Freel, C.D., Parrish, A.B., Day, J.L., Buchakjian, M.R., Nutt, L.K., Thompson, J.W., Moseley, M.A., Kornbluth, S.: Restraint of apoptosis during mitosis through interdomain phosphorylation of caspase-2. The EMBO Journal **28**(20), 3216–3227 (2009)

[128] Dawar, S., Lim, Y., Puccini, J., White, M., Thomas, P., Bouchier-Hayes, L., Green, D., Dorstyn, L., Kumar, S.: Caspase-2-mediated cell death is required for deleting aneuploid cells. Oncogene **36**(19), 2704 (2017)

[129] Yuan, T.L., Wulf, G., Burga, L., Cantley, L.C.: Cell-to-cell variability in pi3k protein level regulates pi3k-akt pathway activity in cell populations. Current biology **21**(3), 173–183 (2011)

[130] Gheghiani, L., Loew, D., Lombard, B., Mansfeld, J., Gavet, O.: Plk1 activation in late g2 sets up commitment to mitosis. Cell reports **19**(10), 2060–2073 (2017)

[131] Schmit, T.L., Zhong, W., Setaluri, V., Spiegelman, V.S., Ahmad, N.: Targeted depletion of polo-like kinase (plk) 1 through lentiviral shrna or a small-molecule inhibitor causes mitotic catastrophe and induction of apoptosis in human melanoma cells. Journal of Investigative Dermatology **129**(12), 2843–2853 (2009)

[132] Choi, M., Kim, W., Cheon, M.G., Lee, C.-W., Kim, J.-E.: Polo-like kinase 1 inhibitor bi2536 causes mitotic catastrophe following activation of the spindle assembly checkpoint in non-small cell lung cancer cells. Cancer letters **357**(2), 591–601 (2015)

[133] Tandle, A.T., Kramp, T., Kil, W.J., Halthore, A., Gehlhaus, K., Shankavaram, U., Tofilon, P.J., Caplen, N.J., Camphausen, K.: Inhibition of polo-like kinase 1 in glioblastoma multiforme induces mitotic catastrophe and enhances radiosensitisation. European journal of cancer **49**(14), 3020–3028 (2013)

[134] Lu, B., Mahmud, H., Maass, A.H., Yu, B., van Gilst, W.H., de Boer, R.A., Sillje, H.H.: The plk1 inhibitor bi 2536 temporarily arrests primary cardiac fibroblasts in mitosis and generates aneuploidy in vitro. PloS one **5**(9), 12963 (2010)

[135] Petronczki, M., Glotzer, M., Kraut, N., Peters, J.-M.: Polo-like kinase 1 triggers the initiation of cytokinesis in human cells by promoting recruitment of the rhogef ect2 to the central spindle. Developmental cell **12**(5), 713–725 (2007)

[136] Lindon, C., Pines, J.: Ordered proteolysis in anaphase inactivates plk1 to contribute to proper mitotic exit in human cells. The Journal of cell biology **164**(2), 233–241 (2004)

[137] Burkard, M.E., Randall, C.L., Larochelle, S., Zhang, C., Shokat, K.M., Fisher, R.P., Jallepalli, P.V.: Chemical genetics reveals the requirement for polo-like kinase 1 activity in positioning rhoa and triggering cytokinesis in human cells. Proceedings of the National Academy of Sciences **104**(11), 4383–4388 (2007)

[138] Rudner, J., Jendrossek, V., Lauber, K., Daniel, P.T., Wesselborg, S., Belka, C.: Type i and type ii reactions in trail-induced apoptosis–results from dose–response studies. Oncogene **24**(1), 130 (2005)

[139] Matsuzaki, H., Schmied, B.M., Ulrich, A., Standop, J., Schneider, M.B., Batra, S.K., Picha, K.S., Pour, P.M.: Combination of tumor necrosis factor-related apoptosis-inducing ligand (trail) and actinomycin d induces apoptosis even in trail-resistant human pancreatic cancer cells. Clinical cancer research **7**(2), 407–414 (2001)

[140] Flusberg, D.A., Roux, J., Spencer, S.L., Sorger, P.K.: Cells surviving fractional killing by trail exhibit transient but sustainable resistance and inflammatory phenotypes. Molecular biology of the cell **24**(14), 2186–2200 (2013)

[141] Kim, M., Liao, J., Dowling, M.L., Voong, K.R., Parker, S.E., Wang, S., El-Deiry, W.S., Kao, G.D.: Trail inactivates the mitotic checkpoint and potentiates death induced by microtubule-targeting agents in human cancer cells. Cancer research **68**(9), 3440–3449 (2008)

[142] Maurer, U., Charvet, C., Wagman, A.S., Dejardin, E., Green, D.R.: Glycogen synthase kinase-3 regulates mitochondrial outer membrane permeabilization and apoptosis by destabilization of mcl-1. Molecular cell **21**(6), 749–760 (2006)

[143] Romorini, L., Coso, O.A., Pecci, A.: Bcl-xl mediates epidermal growth factor dependent cell survival in hc11 mammary epithelial cells. Biochimica et Biophysica Acta (BBA)-Molecular Cell Research **1793**(3), 496–505 (2009)

[144] Wagner, B., Natarajan, A., Grünaug, S., Kroismayr, R., Wagner, E.F., Sibilia, M.: Neuronal survival depends on egfr signaling in cortical but not midbrain astrocytes. The EMBO journal **25**(4), 752–762 (2006)

[145] Dobles, M., Liberal, V., Scott, M.L., Benezra, R., Sorger, P.K.: Chromosome missegregation and apoptosis in mice lacking the mitotic checkpoint protein mad2. Cell **101**(6), 635–645 (2000)

[146] Nagy, Z., Esiri, M., Cato, A.-M., Smith, A.: Cell cycle markers in the hippocampus in alzheimer's disease. Acta neuropathologica **94**(1), 6–15 (1997)

[147] Nagy, Z., Esiri, M., Smith, A.: Expression of cell division markers in the hippocampus in alzheimer's disease and other neurodegenerative conditions. Acta neuropathologica **93**(3), 294–300 (1997)

[148] Yang, Y., Mufson, E.J., Herrup, K.: Neuronal cell death is preceded by cell cycle events at all stages of alzheimer's disease. Journal of Neuroscience **23**(7), 2557–2563 (2003)

[149] Fallik, D.: Pfizer ends funding to alzheimer's and parkinson's research—the fallout for neurology. Neurology Today **18**(4), 1–22 (2018)

[150] Alon, U.: An Introduction to Systems Biology: Design Principles of Biological Circuits. Chapman and Hall/CRC, - (2006)